

Live-cell imaging reveals subcellular
localization of plant membrane compartments
during oomycete infections and quantitative
high-throughput imaging identifies endocytic
trafficking mutants

Inaugural-Dissertation

zur

Erlangung des Doktorgrades

der Mathematisch-Naturwissenschaftlichen Fakultät

der Universität zu Köln

vorgelegt von

Yi-Ju Lu

aus Taipei, Taiwan

Köln, February 2012

Die vorliegende Arbeit wurde am Max-Planck-Institut für
Pflanzenzüchtungsforschung in Köln in der Abteilung für Molekulare Phytopathologie
(Direktor: Prof. Dr. P. Schulze-Lefert) angefertigt.



MAX-PLANCK-GESELLSCHAFT



Max Planck Institute for
Plant Breeding Research

Berichterstatter: Prof. Dr. Jane Parker

Prof. Dr. Martin Hülskamp

Prüfungsvorsitzender: Prof. Dr. Ute Hökcer

Tag der mündlichen Prüfung: 11.04.2012

PUBLICATIONS

Lu, Y.-J., Schornack, S., Spallek, T., Geldner, N., Chory, J., Schellmann, S., Schumacher, K., Kamoun, S., and Robatzek, S. (2012). Patterns of plant subcellular responses to successful oomycete infections reveal differences in host cell reprogramming and endocytic trafficking. Cellular Microbiology doi: 10.1111/j.1462-5822.2012.01751.x.

TABLE OF CONTENTS

PUBLICATIONS.....	III
TABLE OF CONTENTS.....	IV
ABBREVIATIONS	VII
SUMMARY.....	XI
ZUSAMMENFASSUNG	XIII
Zusammenfassung	XIII
1. INTRODUCTION.....	1
1.1 Plant-pathogen interactions	1
1.2 Membrane trafficking in plant cell.....	2
1.3 Membrane trafficking in PTI	4
1.4 Membrane trafficking upon pathogen penetration.....	5
1.5 Membrane trafficking in haustorial accommodation	7
1.6 Arabidopsis-Hpa interaction: a good model to study membrane trafficking in a pathosystem	11
1.7 Tools to study membrane trafficking in plants	11
1.8 Aims of the thesis.....	14
2. MATERIALS AND METHODS	16
2.1 Materials	16
2.1.1 Plant materials	16
2.1.2 Pathogens.....	16
2.1.3 Oligonucleotides	16
2.1.4 Enzymes	16
2.1.5 Chemicals	17
2.1.6 Antibiotics	17
2.1.7 Media	17

2.2	Methods.....	18
2.2.1	Growth conditions	18
2.2.2	Generation of Arabidopsis F1 and F2 progeny.....	18
2.2.3	Seed sterilization	18
2.2.4	Pathogen inoculation	18
2.2.5	Staining leaf tissues.....	19
2.2.6	Microscopy.....	19
2.2.7	Molecular biological methods	20
2.2.8	Software	22
3.	RESULTS.....	26
3.1	Membrane trafficking in Arabidopsis- <i>Hpa</i> interactions.....	26
3.1.1	The plant cell cytoplasm surrounds the haustorium	27
3.1.2	Nuclear migration towards the haustorium	28
3.1.3	PM proteins differentially label the EHM	28
3.1.4	Secretory vesicles and Golgi stacks localized around the haustorium	30
3.1.5	Endosomal vesicles accumulated around the haustorium	31
3.1.6	MVBs dynamics in the infected plant cell.....	34
3.1.7	The tonoplast envelopes the haustorium.....	35
3.1.8	Haustorial encasements comprise membrane components.....	35
3.2	Genetic dissection of endocytosis in Arabidopsis.....	41
3.2.1	<i>Fel</i> mutant candidates screen	42
3.2.2	Mutant <i>fel2</i> and <i>fel9</i> exhibit cellular phenotypes.....	44
3.2.3	FYVE endosome levels differ significantly between Ler/GFP-2xFYVE and Col-0/YFP-2FYVE progenies for generating mapping populations	48

3.2.4	<i>Fel</i> mutants showed different genetic inheritances	51
3.2.5	Map-based cloning of <i>fel</i> mutant plants.....	55
3.2.6	Genetic characterization of <i>fel2</i> and <i>fel9</i>	60
4.	DISCUSSION.....	66
4.1	Imaging the Arabidopsis- <i>Hpa</i> interaction	66
4.1.1	PM-residing proteins are excluded from the EHM selectively	66
4.1.2	Vesicle trafficking in haustoria containing cells	68
4.1.3	Membrane compartments around the encasement	70
4.2	A genetic screen to identify membrane trafficking components using a quantitative microscopic platform.....	73
4.2.1	Identification of <i>fel</i> mutants	73
4.2.2	FYVE endosomal levels in <i>Ler</i> and <i>Col-0</i> ecotypes - A fluorescent reporter issue.....	75
4.2.3	Genetic characterization of <i>fel</i> mutants	76
4.2.4	Map-based cloning of <i>FEL2</i> and <i>FEL9</i>	76
5.	REFERENCES	79
	APPENDIX.....	XV
	Appendix A- Supplementary data	XV
	Appendix B – Figure and table lists	XXIX
	List of figures.....	XXIX
	List of tables	XXX
	List of supplementary figures.....	XXX
	List of supplementary tables.....	XXX
	ACKNOWLEDGEMENTS	XXXII
	ERKLÄRUNG	XXXIII
	LEBENS LAUF	XXXIV

ABBREVIATIONS

°C	degree Celsius
μ	micro
35S	Cauliflower mosaic virus 35S promoter
ABC	ATP-binding cassette
ACA8	Arabidopsis-autoinhibited Ca(2+)-ATPase
ADP	Adenosine diphosphate ribose
AGP	arabinogalactan protein epitopes
ARA	<i>Arabidopsis</i> Rab-like GTPase
ARF	ADP-ribosylation factor
<i>Arabidopsis</i>	<i>Arabidopsis thaliana</i>
ATP	adenosine triphosphate
Ax21	Activator of XA21-mediated immunity
BAK1	BRI1-associated receptor kinase
BEN1	BFA-visualized endocytic trafficking defective1
BFA	Brefeldin A
<i>Bgh</i>	<i>Blumeria graminis f. sp. hordei</i>
CCP	clathrin coated pit
CASP	Casparian strip membrane domain protein
CCV	clathrin coated vesicles
cDNA	complementary DNA
CERK	CHITIN ELICITOR RECEPTOR KINASE
CFP	Cyan fluorescent protein
CLSM	Confocal laser scanning microscopy
cm	centimeter
Col-0	Columbia-0
CSD	Casparian strip domain
ddH ₂ O	double-distilled water
DMSO	dimethyl sulfoxide
DNA	deoxyribonucleic acid
dNTP	deoxyribonucleotide triphosphate
dpi	days post infection
EDTA	Ethylenediaminetetraacetic acid
EE	early endosomes
EHM	Extrahaustorial membrane

EHM	Extrahaustorial matrix
EIX	ETHYLENE INDUCED XYLANASE
EFR	ELONGATION FACTOR-TU RECEPTOR
EF-TU	ELONGATION FACTOR-TU
EMS	ethyl methane sulfonate
ER	endoplasmatic reticulum
ES1	ensosidin 1
et al.	et alii
ETI	effector triggers immunity
F ₁	first filial generation after crossing two different parental lines
F ₂	second filial generation after crossing two different parental lines
F ₃	third filial generation after crossing two different parental lines
<i>fel</i>	FYVE endosomal levels
FLS2	FLAGELLIN SENSITIVE 2
FP	fluorescent protein
<i>f. sp</i>	<i>Forma specialis</i>
g	gram
Gb	gigabyte
GEF	Guanine-nucleotide exchange factor
GFP	green fluorescent protein
GTP	guanosine triphosphate
Ha	<i>Hyaloperonospora arabidopsidis</i>
<i>Hpa</i>	<i>Hyaloperonospora arabidopsidis</i>
HR	hypersensitive response
kb	kilo base pair
LCSM	Leica confocal scanning microscopy
Le	Landsberg <i>erecta</i>
LE	late endosome
<i>Ler</i>	Landsberg <i>erecta</i>
m	milli
m	meter
M	molar
M ₃	third filial generation after mutagenesis
M ₄	fourth filial generation after mutagenesis
Mb	mega bases
MAMP	Microbe-associated molecular patterns

min	minutes
mL	micro liters
<i>Mlo</i>	<i>mildew resistance locus o</i>
MS	Murashige and Skoog
Ms	milli seconds
MTI	MAMPs-triggered immunity
MVB	Multivesicular body
Nb-LRR	nucleotide binding leucine rich repeats
<i>N. benthamiana</i>	<i>Nicotiana benthamiana</i>
nm	nano meter
NPSP12	Novel plant SNARE 12
p	promotor fragment
p35S	promoter of Cauliflower mosaic virus promoter 35S
PAMP	Pathogen-associated molecular pattern
PCR	polymerase chain reaction
PEN1	PENETRATION 1
pH	negative logarithm of proton concentration
<i>Pi</i>	<i>Phytophthora infestans</i>
PIP1; 4	Plasma membrane intrinsic protein1; 4
PI3K	Phosphatidylinositol-3-kinase
PI3P	Phosphatidylinositol-3-phosphate
PM	plasma membrane
PMR/GSL	powdery mildew resistance/glucan synthase-like
PRR	Pattern Recognition Receptor
PTI	PMAPs-triggered immunity
<i>Pto</i> DC3000	<i>Pseudomonas syringae</i> pv. <i>syringae</i> DC3000
pv.	pathovar
RFP	red fluorescent protein
R	resistance protein
PVC	Prevacuolar compartment
RxLR	arginine, any amino acid, leucine, arginine
RLK	Receptor Like Kinase
RLP	Receptor Like Protein
RNA	ribonucleic acid
ROR2	REQUIRED FOR MLO SPECIFICED RESISTANCE
RPW8	RESISTANCE TO POWDERY MILDEW8

RT-PCR	Reverse transcription polymerase chain reaction
SA	salicylic acid
SD	standard deviation
SDS	sodium dodecyl sulfate
sec	seconds
SERK	SOMATIC-EMBRYOGENESISRECEPTOR-LIKE KINASE
SNAP	soluble N-ethylmaleimide-sensitive factor adaptor protein
SNARE	soluble N-ethylmaleimide-sensitive factor adaptor protein receptor
SNP	single nucleotide polymorphisms
SSLP	single sequence length polymorphism
SYP	SYNTAXIN OF PLANTS
TBE	Tris-Borate-EDTA
TEM	transmission electron microscopy
TGN	Trans-Golgi Network
V	volume
VAMP	Vesicle-associated membrane protein
W	weight
X	fold
YFP	yellow fluorescent protein

SUMMARY

To successfully infect plants, filamentous pathogens such as the oomycete *Hyaloperonospora arabidopsidis* (*Hpa*) are able to penetrate host tissues and form haustoria, a feeding structure, inside the host cell. Reorganization of the host cell is required to accommodate the haustoria. Formation of haustoria is accompanied by the biogenesis of the extrahaustorial membrane (EHM) which surrounds the haustorium and separates the host cell from the pathogen. In this study, available fluorescent marker protein fusions were used to monitor the re-distribution of membrane compartments at the interface between *Arabidopsis* and *Hpa*. The aquaporin PIP1;4, the ATPase ACA8, and the plasma membrane (PM) intrinsic protein NPSN12 were excluded from the EHM while the syntaxin PEN1 and the receptor-like kinase FLS2 labelled the EHM. This suggests PM-resident proteins are recruited to the EHM selectively. The nucleus is always observed adjacent to haustoria, suggesting that the presence of haustoria causes migration of the nucleus. Secretory vesicles and endosomal compartments localize around the haustoria, implicating secretory and endocytic pathways in the biogenesis of the EHM. Upon *Hpa* infection, haustorial encasements develop around mature haustoria. All examined plant proteins accumulate at haustorial encasements, indicating that formation of encasements is derived by default redirection of vesicle trafficking pathways.

With the aim to genetically dissect endosomal trafficking regulators, I took advantage of quantitative high throughput confocal imaging system and transgenic plants containing the fluorescent biosensor GFP-2xFYVE to perform a forward genetic screen. Different numbers of GFP-2xFYVE positive endosomes were found in two reference lines, *Ler*/GFP-2xFYVE and *Col-0*/YFP-2xFYVE suggesting the endosomal levels may vary in different ecotypes of *Arabidopsis*. Mutants with altered numbers of FYVE Endosomal Levels (*fel*) have been previously identified and were re-confirmed in this study. *fel1*, *fel2*, *fel3*, *fel6*, *fel9*, and *fel12* revealed genetically recessive mutations while *fel10* could not reveal its genetic inheritance. Two mutants, *fel2* and *fel9* exhibited more GFP-2xFYVE compartments than wild-type reference plants. These two mutants are affected in endosome trafficking and *fel2* is likely tissue

specific. We identified gene loci by classical mapping and whole genome sequencing. *Fel2* co-segregated with the lower arm of chromosome 4. *Fel9* was mapped to two chromosome loci. Investigation of genes in the rough mapping region will unravel regulators of endocytosis or multivesicular bodies (MVBs) biogenesis. Because only few mutant phenotypes recovered in the F₂ of backcrossed *fel2* and *fel9*, identification of *FEL2* and *FEL9* was hampered. Additionally, basal differences of endosomal numbers in the reference lines lead to the limitation for genetic screen based on quantitative changes in endosomal numbers.

Altogether, these results show that there are common elements in the subcellular changes associated with biotrophic oomycete between different pathogens. For *Hpa* and other fungal/oomycete pathogens, reprogramming host cell vesicle trafficking occurs to accommodate haustorial structures. A genetic screen for novel endocytosis mutants, based on quantitative measurements of endosomal numbers, was performed with advanced microscopy technology. *Fel* mutant plants may be further used to study molecular mechanisms for membrane trafficking, as well as subcellular rearrangement in plant-pathogen interactions.

ZUSAMMENFASSUNG

Zusammenfassung

Um Pflanzen erfolgreich zu infizieren, bilden filamentöse Pathogene, zu denen der Oomycet *Hyaloperonospora arabidopsidis* (*Hpa*) zählt, sogenannte Haustorien, spezialisierte Hyphen, die ins Wirtsgewebe eindringen und dort der Nährstoffaufnahme dienen. Die zelluläre Aufnahme des Haustoriums führt zu einer intrazellulären Umorganisation der Wirtszelle, die von der Biogenese einer Wirtszell-spezifischen Membran, der äusseren haustoriellen Membran (EHM) begleitet ist, welche das Haustorium umschliesst und somit die Wirtszelle vom Pathogen abgrenzt. In dieser Arbeit wurden bekannte zelluläre Markerproteine fusioniert mit Fluoreszenzproteinen verwendet, um die Umverteilung von Membrankompartimenten an der Grenzfläche zwischen Arabidopsis und *Hpa* zu untersuchen. Das Aquaporin PIP1,4, die ATPase ACA8 und das Plasmamembran intrinsische Protein NPSN12 sind abwesend von der EHM, wohingegen das Syntaxin PEN1 und die Rezeptorkinase FLS2 die EHM klar markieren. Dies lässt den Schluss zu, dass Plasmamembran lokalisierte Proteine selektiv zur EHM rekrutiert werden können. Der Zellkern wurde meist angrenzend zum Haustorium detektiert. Dies zeigt, dass das Vorhandensein des Haustoriums in der Wirtszelle die Migration des Nucleus bewirkt. Sekretorische Vesikel und endosomale Kompartimente lokalisieren um das Haustorium herum. Somit scheinen sekretorische und endozytische Transportwege an der Biogenese der EHM beteiligt zu sein. Zu späteren Stadien einer *Hpa* Infektion bildet sich eine Verkapselung um das ausgereifte Haustorium. Alle untersuchten Pflanzenproteine wurden an dieser haustoriellen Verkapselung detektiert, welches darauf hindeutet, dass die Verkapselung mit einer generellen Umverteilung der vesikulären Transportwege einhergeht.

Endosomale Vesikel lassen sich anhand von fluoreszenzierenden Biosensoren wie GFP-2xFYVE markieren. Um genetische Komponenten zu finden, die den endosomalen Vesikeltransport regulieren, wurden Arabidopsis Pflanzen einer mit Ethylmethylsulfonat (EMS) mutagenisierten *Ler*/GFP-2xFYVE Linie mittels

automatisierter konfokaler Mikroskopie im Detail untersucht. Hierfür wurden bereits zuvor isolierte Kandidaten mit veränderter FYVE Endosomen Anzahl, so genannte *fel* (FYVE Endosomal Levels) Mutanten, in ihrem Phänotyp bestätigt und genetisch weiter analysiert. Während sich die *fel1*, *fel2*, *fel3*, *fel6*, *fel9*, und *fel12* Loci rezessiv vererbten, konnte hinsichtlich *fel10* keine eindeutige Aussage getroffen werden. *Fel2* und *fel9* Mutanten zeigten signifikant mehr FYVE-Endosomen als die parentale *Ler/GFP-2xFYVE* Linie. Interessanterweise scheint dieser Phänotyp gewebespezifisch zu sein, da er sich nicht in Wurzeln ausprägte. Mittels klassischer genetischer Kartierung konnten die *fel2* und *fel9* Loci dem unteren Arm von Chromosom 4 zu geordnet werden. Zudem ko-segregierte der *fel9* Phänotyp ebenfalls mit genetischen Marken auf Chromosom 3. Mit Hilfe einer Illumina basierenden Genomsequenzierung wurden genetische Sequenzvariationen in diesen Bereichen untersucht, konnte jedoch nicht spezifisch einer Mutante zu geordnet werden und wurden stattdessen ebenfalls in der parentalen Linie gefunden. Erschwerend kam hinzu, dass sowohl die Rückkreuzungen von *fel2* als auch die von *fel9*, auf eine komplexe genetische Struktur hinweisen, die vermutlich auf jeweils mehr als ein Mutantenloкус zurückzuführen ist. Zudem zeigte die zur Auskreuzung verwendete *Col-0/YFP-2xFYVE* Linie qualitative und quantitative Unterschiede zur *Ler/GFP-2xFYVE* Linie auf, was auf eine Ökotypen-spezifische Regulierung von FYVE markierten Endosomen hindeuten könnte.

Zusammenfassend zeigen diese Ergebnisse, dass *Hpa* und andere pilzliche/oomyzischen Pathogene eine Umprogrammierung der vesikulären Transportwege innerhalb der Wirtszelle erzwingen, welches mit der Aufnahme des Haustoriums einhergeht. Um neue Endozytose Mutanten zu identifizieren wurde ein genetischer Screen mittels quantitativer Messungen der Anzahl von Endosomen mit neuester Mikroskopie Technologie durchgeführt. Die *fel* Mutanten können in Zukunft für weitergehende Studien der Membran Transport Wege in Pflanzen, als auch für eine weitere Charakterisierung der subzellulären Umprogrammierung während der Interaktion zwischen Pflanzen und Pathogenen genutzt werden.

1. INTRODUCTION

Plants are frequently exposed to various pathogenic microbes such as viruses, bacteria, fungi, and oomycetes that lead to disease and eventually cause economic loss in agriculture. However, not all microbes cause disease on all plant species – many plants are resistant to specific pathogens. Resistant plants have evolved a multilayered immune system to detect and respond to microbial invasion (Jones and Dangl, 2006). These responses are complex and involve many molecular and cellular components. There is increasing evidence that membrane trafficking within plant cells is a crucial regulatory component of several aspects of defence responses. The mechanisms and consequences of subcellular membrane re-organization during plant-pathogen interactions are not yet fully understood and thus remain a question that must be addressed in order to clearly understand the spectrum of plant defence responses.

1.1 Plant-pathogen interactions

Plant defence responses are complex and multilayered. The first layer of active plant defence is based on the perception of pathogen/microbe-associated molecular patterns (PAMPs/MAMPs) by pattern-recognition receptors (PRRs). PRRs are proteins that are tethered to or anchored in the plasma membrane and expose ligand-binding domains extracellularly (Zipfel 2009). Upon perception of a ligand, PRRs mediate a host of intracellular responses that are aimed at obstructing pathogen invasion. PAMPs/MAMPs are typically conserved components of pathogens, such as flagellin in bacteria or chitin in fungi. Perception of PAMPs/MAMPs, which enables self/non-self discrimination, leads to PAMPs/MAMPs-triggered immunity (PTI/MTI). Examples of PRRs involved in plant defence are FLAGELLIN SENSITIVE 2 (FLS2), which detects bacterial flagellin (Gómez-Gómez and Boller, 2000); ELONGATION FACTOR-TU RECEPTOR (EFR), which recognizes bacterial EF-Tu (Zipfel et al., 2006); CHITIN ELICITOR RECEPTOR KINASE1 (CERK1), which is a fungal chitin receptor (Miya et al., 2007). Tomato LeEIX2 binds the fungal elicitor, ETHYLENE-INDUCED-XYLANASE (EIX)

(Ron and Avni, 2004). In rice, XA21 recognizes a sulfated peptide, Ax21 (activator of XA21-mediated immunity), which exists in all *Xanthomonas* and *Xylella* species (Lee et al., 2009).

Successful pathogens have evolved effectors that are delivered into the host cells to suppress PTI/MTI, causing effector-triggered susceptibility. Recognition of effectors by nucleotide binding leucine rich repeats (NB-LRR) proteins provides a second layer of defence, leading to the so-called effector-triggered immunity (ETI). Effectors vary between different strains of a given species; matched by a diverse array of NB-LRR genes in host plant species. ETI results from the specific recognition of effectors by NB-LRRs and leads to hypersensitive responses (HR). HR causes programmed host cell death to avoid invasion of pathogens to neighbouring cells. This host-pathogen arms-race, represents evolutionary molecular interactions between plants and pathogens (Chisholm et al., 2006; Jones and Dangl, 2006). The complex relationship between plant resistance and pathogen virulence through co-evolution can also be described as a 'zig-zag' model (Jones and Dangl, 2006).

1.2 Membrane trafficking in plant cell

To prevent penetration of oomycete and fungal pathogens, plants build up physical and chemical barriers such as formation of cell wall depositions (Jacobs et al., 2003; Nishimura et al., 2003), secretion of unknown cargoes by vesicles (Collins et al., 2003; Kwon et al., 2008) and delivery of toxic secondary metabolites (Bednarek et al., 2009) to sites of pathogen invasion. These events involve rearrangement and redistribution of membrane compartments.

There are different membrane compartments and the movement of membranes between these compartments allows the transport and exchange of proteins and other molecules, maintaining many basic cellular functions (Figure 1). The secretory pathway is one such membrane trafficking pathway that allows the delivery of proteins from the endoplasmic reticulum (ER) to their final destination, which may be the plasma membrane (PM), the extracellular space or the vacuole. Proteins

destined for secretion are translated in the cytosol, and then imported into the ER where maturation, assembly and folding occurs (Jürgens 2004). Proteins can be directly exported from the ER to the protein storage vacuole, while other secretory proteins are transported to the Golgi apparatus (Hanton et al., 2005). The plant Golgi apparatus comprises membrane stacks and is defined as having cis- and trans-cisternae. Proteins are modified and glycosylated in the Golgi apparatus, sorted to the trans Golgi network (TGN). The TGN is a specialized compartment only found in plant cells, acting as the junction between the secretory and endocytic pathways (Robinson et al., 2008). From the TGN proteins can be delivered to intracellular compartments like the vacuole via the multivesicular bodies (MVBs)/prevacuolar compartment (PVC) (Hanton and Brandizzi, 2006; Otegui and Spitzer, 2008; Viotti et al., 2010), addressed to the PM via fusions of exosomes with the PM, or are released in the extracellular space (Robinson et al., 2008).

Endocytosis is a process of uptake of the PM. It involves the transport of extracellular molecules or proteins to the vacuole, or recycling back to the PM. In general, endocytosis starts from invagination of the PM. Endocytic vesicles are formed by internalization of PM components and extracellular materials. Clathrin-mediated endocytosis is used by all known eukaryotic cells and clathrin-coated pits (CCPs) associated with the PM have been reported in plant cells (Robinson and Hiller, 1990; Dhonukshe et al., 2007). It begins at the PM with the recruitment of cargo and the coat machinery. This leads to the formation of CCPs that eventually mature and scission off to form clathrin coated vesicles (CCVs) (McMahon and Boucrot, 2011). Uncoated vesicles fuse with the early endosome (EE) where the cargo is further sorted for recycling back to the PM or to the vacuole (Chen et al., 2011). Cargo that is taken up from the PM can either be recycled back to the PM or EEs can mature to late endosomes. Materials are sorted to the vacuole via MVBs. MVBs originate from the maturation of the TGN and eventually fuse to the tonoplast. Proteins could also be retrograded from MVBs to the TGN. In both secretory and endocytic pathways, the TGN and the MVBs play as intermediate sorting compartments that are important to determine membrane compositions of the PM, vacuole and endosomes (Robinson et al., 2008; Scheuring et al., 2011).

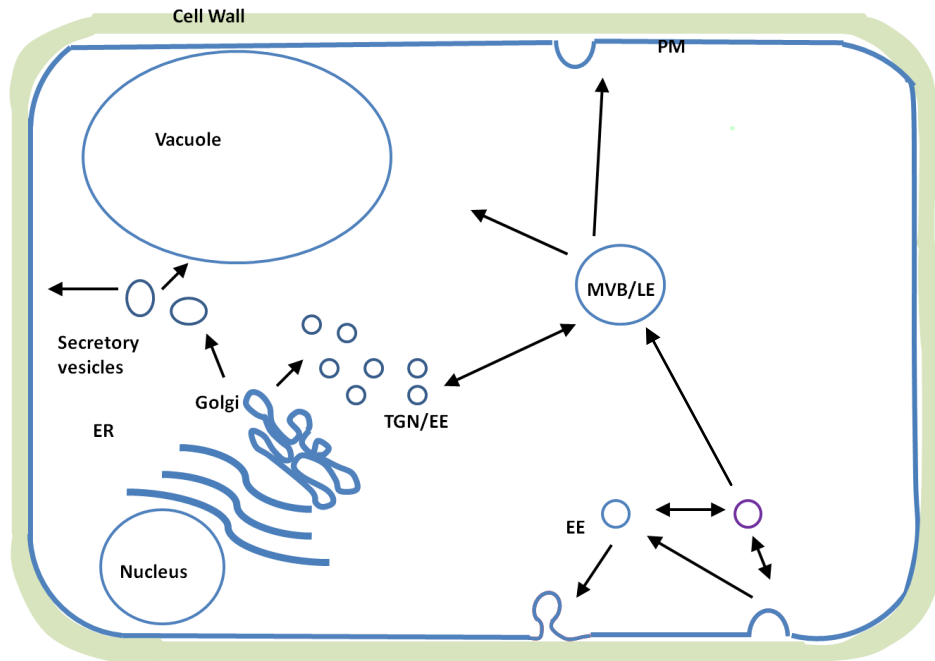


Figure 1. Membrane compartment and membrane trafficking in plant cells. Secretory trafficking to the cell surface begins at the endoplasmic reticulum (ER), transits the Golgi apparatus and into trans-Golgi network (TGN). The TGN is a station for secretion to the PM. Endocytosis begins at the PM and early endosomes (EE/TGN) is formed. EEs mature and cluster into multivesicular bodies (MVBs), and subsequently traffic to the vacuole. EEs can recycle to the PM.

1.3 Membrane trafficking in PTI

Multiple subcellular changes have been described to occur in plant cells upon pathogen attack. One of the best studied PRR receptors in plants is Flagellin Sensitive 2 (FLS2). It encodes a LRR receptor like kinase (LRR-RLK) and is responsible for the detection of bacterial flagellin, through its elicitor-active peptide flg22 (Gomez-Gomez and Boller 2002; Chinchilla *et al.* 2007). The FLS2 receptor resides at the PM and becomes internalized into highly mobile vesicles specifically upon addition of its ligand flg22, the first example of ligand-induced receptor-mediated endocytosis in plants (Robatzek *et al.* 2006). Interfering with FLS2 internalization leads to impaired downstream signalling of specific PTI responses (Robatzek *et al.*,

2006, Salomon and Robatzek, 2006, Chinchilla et al, 2007) and shows the importance of membrane trafficking for plant defence responses. Recent data provide evidence for elicitor-induced changes in the membrane compartmentalization of PAMP signaling components and suggest the role of PM microdomains in pathogen recognition (Keinath et al., 2010). LeEIX2 provides another example of ligand-induced endocytosis and signalling in plant defence responses. The 22-kD fungal protein EIX induces ethylene biosynthesis, electrolyte leakage, pathogenesis-related protein expression, and hypersensitive response (HR) in specific plant species and/or varieties (Bailey et al., 1993). The receptor of EIX, LeEIX2, is identified and contains of the internalization motif, YxxØ for endocytosis (Ron and Avni, 2004). The localization of GFP-tagged LeEix2 receptor changes from the PM to LEs 10 to 15 min after EIX treatment. A mutation in the endocytosis motif of LeEix2 resulted in abolishment of HR induction in response to EIX, suggesting that endocytosis plays a key role in mediating the signal generated by EIX (Ron and Avni, 2004). The role of membrane trafficking in PTI is stressed in *Pto* DC3000-Arabidopsis interactions. The effector HopM1 targets and destabilizes the ADP ribosylation factor guanine nucleotide exchange factor, AtMIN7, which is associated to TGN (Nomura et al., 2011). The requirement of AtMIN7 for plant innate immunity suggests that the TGN/EE is an important membrane compartment for plant immune pathways (Nomura et al., 2011).

1.4 Membrane trafficking upon pathogen penetration

Thickening of callose-rich cell wall depositions called papillae is reported at sites of pathogen penetration. For a long time, papillae were thought to reinforce the call wall at attempted fungal entry sites and act as physical and chemical barriers against pathogen invasion (O'Connell and Panstruga, 2006). However, the biogenesis of papillae does not absolutely enhance resistance to adapted pathogens. Arabidopsis mutants in the callose synthase gene *PMR4/GSL5*, which are reduced in the formation of papillary callose, are more resistant to *Hyaloperonospora arabidopsidis* (*Hpa*) and *Golovinomyces orontii* (Jacob et al., 2003; Nishimura et al., 2003; Vogel

and Somerville, 2000). The susceptibility could be restored in *pmr4/gsl5* when blocking the salicylic acid (SA) pathway, which suggests that callose or callose synthase negatively regulates defence responses mediated by SA (Nishimura et al., 2003).

The *Arabidopsis* PENETRATION1 (PEN1) syntaxin is recruited to papillae when challenged by compatible or incompatible powdery mildew *Golovinomyces cichoracearum* and *Blumeria graminis f.sp. hordei* (*Bgh*) (Assaad et al., 2004). In *Arabidopsis*, PEN1, together with SNAP33 and vesicle-associated membrane proteins721/722 (VAMP721/722), form a ternary soluble N-ethylmaleimide-sensitive factor adaptor protein receptor (SNARE) complex. This ternary SNARE complex is associated with secretory vesicles (Kwon et al., 2008). Mutation in PEN1 decreases penetration resistance of non-host *Arabidopsis* against *Bgh* and *Erysiphe pisi*, indicating a role of vesicle trafficking in non-host resistance (Collins et al., 2003; Lipka et al., 2005). In barley (*Hordeum vulgare*), an ortholog of PEN1 syntaxin, REQUIRED FOR MLO-SPECIFIED RESISTANCE3 (ROR2), forms a SNARE complex with SNAP34 (Collins et al., 2003; Douchkov et al., 2005). The ADP-ribosylation factor, ARFA1b/1c, is required for ROR2-mediated penetration resistance and localizes to MVBs. Membrane compartments containing ARFA1b/1c are recruited beneath fungal entry sites before formation of callose deposition. This study points at the possibility that MVBs are involved in callose deposition between penetration sites (Böhlenius et al., 2010).

Pre-invasion resistance also relies on PEN2 and PEN3 and their directed secretion. Peroxisomes containing PEN2 accumulate at fungal entry sites (Lipka et al., 2005). PEN2-encoded myrosinase contributes to defence against a broad-spectrum of fungal pathogens (Bednarek et al., 2009). PEN3, a PM residing ABC transporter, is thought to deliver PEN2-derived toxic metabolites to the apoplast under *Bgh* appressoria (Bednarek et al., 2009; Stein et al., 2006).

There are many examples of the redistribution of subcellular components during plant-pathogen interactions illustrating that plant-pathogen interactions involve complex cell biological responses. Another example of a membrane protein that

re-localises during pathogen attack is barley *mildew resistance locus o* (*Mlo*)-encoded protein which relocates from the cell periphery to the site beneath the appressorium during *Bgh* challenges to Arabidopsis and barley, inducing the proliferation of PM microdomains (Bhat et al., 2005). Cytoplasmic aggregation and the accumulation of actin microfilaments, the ER, peroxisomes and Golgi bodies occurs at the infection site in all non-host, compatible and incompatible interactions (Takemoto et al., 2003). Additionally, the nucleus has been observed to relocate in response to pathogen invasion. The list of subcellular components that are affected by pathogen attack identifies that plant-pathogen interactions involve dramatic changes to subcellular structure, as plants mount multiple defence responses. The regulation of these re-arrangements is poorly understood but, as illustrated by the membrane trafficking mutants listed above, is likely to be crucial to the success of defence responses.

1.5 Membrane trafficking in haustorial accommodation

Successful pathogens overcome the first layer of defence and form specialized intracellular hyphae called haustoria inside the host cells. The haustorium is expanded from the haustorial neck, which is surrounded by callose-like deposits. The intracellular body of the haustorium is separated from the host cell by the extrahaustorial matrix (EHMx) and the extrahaustorial membrane EHM (Figure 2). To prevent leaking of EHMx to the apoplast, the haustorial neck and the EHM are conjugated at the haustorial neckband (O'Connell and Panstruga, 2006). The EHMx is an electron-dense material dividing the EHM and the haustorial cell wall (Mims et al., 2004). Moreover, the EHMx and the EHM are thought to be the site where pathogen uptake of nutrients and water from the plant cell occurs, as well as delivery of effectors to the plant cell (Voegelé and Mendgen 2003). Accordingly, a role of haustoria in sugar transport has been reported: HXT1 from the rust *Uromyces fabae* is a transporter localized to the haustorial plasma membrane and probably functions in hexose uptake (Voegelé et al., 2001). Additionally, the transcript levels of Arabidopsis sugar transporter genes are elevated after the inoculation of powdery

mildew *G. cichoracearum* and the fungus *Botrytis cinerea*, suggesting sugar transporter alters during pathogen infection (Chen et al., 2010).

The subcellular localization of *Hpa* RxLR effector candidates (HaRxLs) in planta were investigated (Caillaud et al., 2012). This screening leads to the identification of an effector, HaRxL17 that enhanced plant susceptibility to *Hpa* during compatible and incompatible interactions when stably expressed in Arabidopsis. HaRxL17 is strongly localized to the membrane around haustoria, probably to the EHM. Both C- or N-terminal fluorescent-tagged HaRxL17 localizes around *Hpa* haustoria, in early and in late stages of infection (Caillaud et al., 2012). The host-translocated RXLR-type effector protein AVRblb2 of *Phytophthora infestans* (*Pi*) is identified to focally accumulate around haustoria and promotes virulence by interfering with the execution of host defences (Bozkurt et al., 2011).

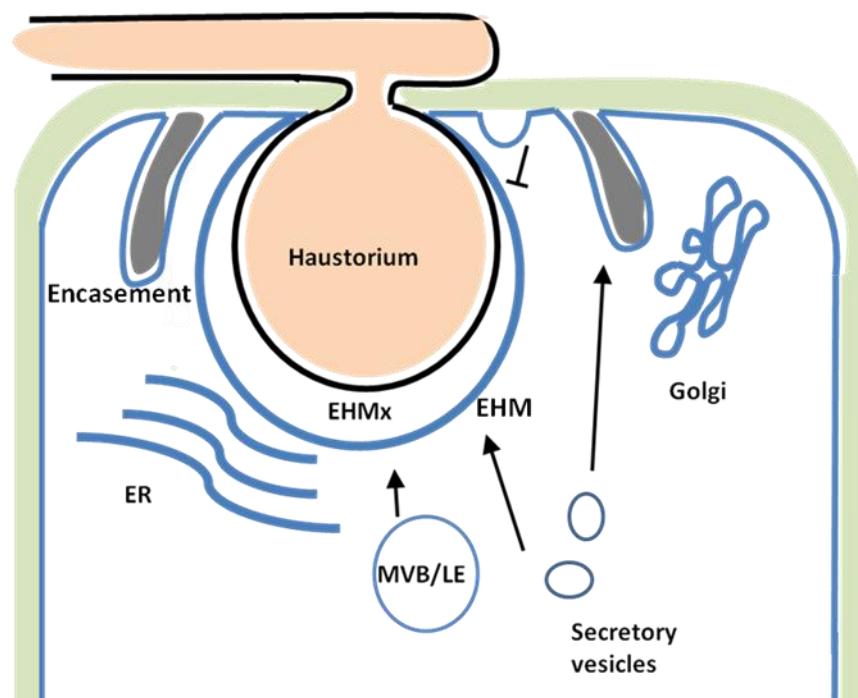


Figure 2. Schematic diagram depicting putative vesicle dynamics at the plant–fungal/oomycetes interaction site. On the plant side, vesicles originating from Golgi and MVBs fuse with the EHM to deliver their cargo. Secretory vesicles and MVBs are also trafficked to the haustorial encasement.

Several plant PM proteins are excluded from the EHM in *G. cichoracearum* and Arabidopsis interactions (Koh et al., 2005). The EHM of *G. orontii* lacks arabinogalactan protein epitopes (AGPs) and non-AGP glycoproteins that reside in the PM (Micali et al., 2011). In Arabidopsis-*Hpa* interactions, PEN1-GFP localized to the callose ring present at the neck of the developing haustorium and labelled the encasement (Caillaud et al., 2012). Based on these results, it has been hypothesized that biogenesis of the EHM could result from rapid differentiation of the plant PM, or by de novo synthesis by targeted secretory vesicles (Koh et al., 2005). These data also implied that diffusion between the PM and the EHM has to be prevented or controlled.

An Arabidopsis resistance (R) protein, RPW8.2, localizes to the EHM of *G. cichoracearum* UCSC1. Secretory vesicles containing RPW8.2 move toward and fuse to the peripheral layer of the haustorium, suggesting secretion of components from the host to the EHM (Wang et al., 2009b). The composition of the EHM may change during development - the presence or absence of RPW8.2 in *G. orontii* EHM depends on the maturation state of the haustorium. This result raises the possibility that *G. orontii* is able to postpone the expression of RPW8.2 or delay the movement of RPW8.2 to the EHM (Micali et al., 2011).

Redistribution of plant ER and Golgi bodies is reported in different plant-pathogen interactions (Leckie et al., 1995; Koh et al., 2005). Additionally, some small vesicles in the host cytoplasm are localized near the EHM (Mims et al., 2004). Besides secretory vesicles, host ER is found to distribute close to the EHM of *G. orontii* and *G. cichoracearum* (Micali et al., 2011; Koh et al., 2005). These data could support the idea that the host ER may directly transfer lipids and proteins to form the EHM without the need of transportation via vesicles (Leckie et al., 1995). The central vacuole of mesophyll cells accommodating haustoria resembled the vacuole in a non-infected mesophyll cell (Caillaud et al., 2012).

At a later stage of haustorial development, the haustorium is enveloped by a layer of

a callose-containing structure known as the haustorial encasement (Soylu EM and Soyly S, 2003). In Arabidopsis, encasements around the haustoria of the compatible pathogens *G. orontii* and *Hpa* have been reported (Donofrio and Delaney, 2001; Jacobs et al., 2003). The encasement is proposed to function in restricting growth of the haustorium. In incompatible Arabidopsis-*Hpa* interactions, the inhibition of growth is associated with the encasement (van Damme et al., 2009).

Membrane compartments are associated with the encasement. In Arabidopsis, Green Fluorescent Protein (GFP) tagged PEN1 (GFP-PEN1) and membrane lipids stained by FM4-64 are entrapped in the encasements of both incompatible *E. pisi*, *Bgh* and compatible *G. orontii* (Meyer et al., 2009). In cells containing *Hpa* encasements, GFP-PEN1 not only labels the encasements but is also distributed in the cytoplasm (Meyer et al., 2009). Notably, SNAP33, VAMP722 and PEN3 incorporation into the encasement with different frequency suggests that defence-related plasma membrane proteins are selectively recruited (Meyer et al., 2009). It has been shown that the composition of *G. orontii* encasements is not different to that of the papillae and collars: these deposits possess similar vesicles or MVBs. This finding may support extracellular transportation and entrapment of secretory vesicles at the growth site of the encasement. Additionally, transmission electron microscopy (TEM) shows that Golgi bodies and vesicles locate around the encasement, suggesting conventional exocytosis is involved in the formation of the encasement (Figure 2; Micali et al., 2011).

The mechanisms by which plant membranes remodel to accommodate and/or mount defence responses against haustoria are not yet understood. It is clear that the EHM is a specialized membrane interface between host and pathogen but, as for the haustorial encasement, the specific details of its biogenesis and function have not yet been determined.

1.6 Arabidopsis-Hpa interaction: a good model to study membrane trafficking in a pathosystem

Most successful filamentous biotrophic and hemibiotrophic plant pathogens such as oomycetes or fungi penetrate and develop specialized structures inside host tissues to sustain their growth and development (O'Connell and Panstruga, 2006). *Hpa* is an obligate biotrophic oomycete that completes its asexual life cycle in living host tissues. After landing on the surface of the leaf, conidiospores germinate and produce a penetration hypha that allows it to enter the leaf tissue between two neighboring epidermal cells. While the hypha develops and branches in the intercellular spaces, a feeding structure named haustorium is formed and inserted into host cells. In incompatible interactions haustoria formation triggers cell death. Whether pathogens are able to penetrate, feed and grow in turn determines their host range.

In *Arabidopsis*, *Hpa* is able to establish a compatible interaction, developing successful feeding haustoria that are eventually encased (Coates and Beynon, 2010; Soylyu EM and Soylyu S, 2003); considering all the advantages that working with the model plant *Arabidopsis* offers, the *Hpa/Arabidopsis* pathosystem provides a nice framework to study plant-pathogen interactions from subcellular and pathogenicity perspectives.

1.7 Tools to study membrane trafficking in plants

Advanced imaging techniques facilitate the investigation of how plants and pathogens interact with each other at subcellular levels. TEM provides high resolution images to study ultrastructure of plant cells or the pathogen itself at the nanometer scale. Moreover, with successful expression of stable and bright fluorescent proteins (FPs) in plant cells, together with confocal laser scanning microscopy (CLSM), live cell imaging enables the study of the dynamics of proteins fused to FPs or their targeting components (Cutler et al., 2000; Ehrhardt 2003). So far,

many endosomal markers have been generated and facilitate further understanding of plant cell biology. For example, the Rab GTPases Rab F1/ ARA6 and Rab F2b/ARA7 are identified to localize in endosomes (Ueda et al., 2004). Stably transformed plants expressing membrane proteins tagged by distinct FPs provide markers for a variety of membrane compartments such as the PM, EE/TGN, Golgi stacks, and the vacuole (Geldner et al., 2009).

Beside GFP, Yellow FP (YFP), and Red FP (RFP), styryl FM4-64 staining serves as a tool to study the nature of endosomes. FM4-64 is an amphiphilic dye and integrates in the outer layer of the PM where it anchors to the PM and is taken up into the endocytic pathway and stains EEs. Therefore, MVBs and the TGN can be labelled in a time-dependent manner, making FM4-64 a useful marker for analyzing endocytosis and vesicle trafficking (Bolte et al, 2004).

The FYVE domain is a zinc finger protein domain that binds specifically to phosphatidylinositol-3-phosphate (PI3P) that is abundant on the surface of EEs and MVBs/LEs. Subcellular inspection confirmed that in Arabidopsis, DsRed-2xFYVE is colocalized with ARA6-GFP, members of Rab GTPases residing in MVBs (Voigt et al., 2005). For this reason, GFP-2xFYVE is an excellent marker to study trafficking of endosomes in plants. It has been reported that the amount of GFP-2xFYVE compartments is altered when plants are exposed to biological and environmental stresses. The number of GFP-2xFYVE compartments increase upon *Pto* DC3000 infection and cold treatment but is reduced upon dark incubation (Salomon et al., 2010). Interestingly, previous work from our lab showed that two mutants with altered endosomal numbers, *fel4* and *fel5* mutants (for FYVE Endosome Levels) containing either increased or decreased levels of GFP-2xFYVE compartments exhibit slightly enhanced susceptibility to *Pseudomonas syringae* pv. *tomato* (*Pto*) DC3000 (Salomon, 2009), a finding that stresses a role of MVBs in plant immunity. Internalization of the GFP-tagged LeEix2 receptor to FYVE-positive endosomes 10–15 min after EIX application was reported (Bar and Avni, 2009). These results indicate that the study of MVBs could be not only relevant from a cell biology perspective, but also crucial for gaining insight into the cellular changes underlying

plant-pathogen interactions and how membrane trafficking may affect plant defence.

One can dissect the role of endosomal compartments by application of chemicals that interfere with different trafficking processes. The most frequently used drugs to study vesicle trafficking are Brefeldin A (BFA) and wortmannin. BFA is a fungal lactone compound that targets GNOM, a member of the guanine-nucleotide exchange factors (GEFs) for ADP-ribosylation factor (ARF) in the plant cell. BFA blocks the recycling of endosomes to the PM, causing the aggregation of recycling endosomes and TGN/EEs into 'BFA-bodies'. Following removal of BFA, PM residing proteins are redirected to the PM (Geldner et al., 2001; Grunewald and Friml, 2010). Wortmannin inhibits PI3-kinase (PI3K), which is required for the synthesis PI3P, an abundant component of plant LEs (Robinson et al., 2008). Moreover, Wortmannin treatment causes vacuolation by the fusion of MVB/PVC. Thus, Wortmannin treatment allows the identification of components of MVBs/PVCs (Wang et al., 2009a). The observation that uptake of the dye FM1-43 (a chemical relative of FM4-64) is blocked by Wortmannin treatment indicates that Wortmannin blocks endocytosis (Emans et al., 2002). Other chemicals that are applied to study different endocytic processes include filipin, a compound that binds to polyene sterol and interferes with sterol dependant endocytosis. Endosidin 1 (ES1), that traps TGN/EEs into "Endosidin-bodies" and affects brassinosteroid signalling; tyrphostin A23, an inhibitor of tyrosin kinases and interferes with clathrin dependent endocytosis (Beck and Robatzek, 2011). These compounds form a comprehensive toolbox that can be used to dissect various aspects of the dynamics of membrane trafficking under different conditions.

The combination of specific inhibitors and dyes, used together with confocal imaging and genetic screening, has proven useful to identify regulators of the endocytic pathway: *Arabidopsis BEN1/MIN7* was identified and mapped as a protein important for internalization of proteins from the PM (Tanaka et al., 2009). A mutant in this gene fails to form proper "BFA-bodies" upon treatment with this inhibitor. Interestingly, mutation of *BEN1/MIN7* also affects plant immunity, indicating a link exists between membrane trafficking and plant defence (Nomura et al., 2006). A mutant screen for abnormal endomembrane structure within the cells identified the Golgi membrane protein *KATAMARI1/MURUS3* is required for endomembrane

organization (Tamura et al., 2005). These qualitative screens, aimed at identifying important components of membrane trafficking, are usually challenging. On one hand, mutations in crucial regulators of intracellular traffic will most likely be lethal (Tanaka et al., 2009). On the other hand, mutations with a milder effect lead to difficulties in the collection of robust quantitative information of membrane compartments at the subcellular level. This can be addressed by a high number of repetitions for the measurement of membrane compartments, but this is a laborious process. The recent development of a high-throughput imaging method has allowed automation of this process and made quantitative detection of membrane compartments feasible (Salomon et al., 2010).

1.8 Aims of the thesis

Membrane trafficking is essential for plant adaptation to different stresses, including pathogen attack. However, little is known about molecular components regulating membrane trafficking or its reprogrammed trafficking during pathogen infection. This thesis aims at providing new insight into these questions through two different approaches.

The aim of first project is to gain insights into the role of membrane trafficking in the *Arabidopsis-Hpa* interaction. A number of studies have observed subcellular rearrangement beneath pathogen penetration sites and membrane proteins have been found at these sites. However, this information relates to different pathogens and different plant species and thus we do not have a complete understanding of these interactions. To comprehensively characterize the redistribution of membranous compartments around haustoria in a single plant-pathogen interaction this study will examine the re-localization of multiple membrane compartments at the interface between *Arabidopsis* and *Hpa*.

The aim of the second project is to shed light on the regulation of membrane trafficking in plants through the identification of *Arabidopsis* mutants with altered endosome levels. For this purpose, I have continued a high-throughput fluorescence

imaging-based forward genetic screen previously developed in our lab. In contrast to previous qualitative screens, this screen monitors quantitative differences in endosome numbers of the chemically mutagenized population of *Ler*/GFP-2xFYVE, with the potential for identifying mutants with both dramatic and subtle phenotypes to be detected. This study expands on a previous genetic screen and further characterizes two of the isolated candidates, *fel2* and *fel9*.

2. MATERIALS AND METHODS

2.1 Materials

2.1.1 Plant materials

The transgenic *Arabidopsis* plants in the genetic background of the *Arabidopsis thaliana* ecotypes Columbia-0 (Col-0), Landsberg erecta (*Ler*) and Nd (Niederzenz) are listed in Supplementary Table 1.

2.1.2 Pathogens

Hyaloperonospora arabidopsidis (*Hpa*) isolate Cala 2 (Parker et al., 1993) was provided by Jane Parker, (MPIMZ, Cologne, Germany) and isolate Waco 9 (Fabro et al., 2011) was provided by Jonathan Jones (The Sainsbury Laboratory, Norwich, UK).

2.1.3 Oligonucleotides

Oligonucleotides were synthesized by Sigma-Aldrich (St. Louis, MI, USA), diluted with ddH₂O to 100 µM stock solutions and 10 µM working solution. Supplementary Table 2 lists used oligonucleotides and their corresponding targets.

2.1.4 Enzymes

PCRs were performed with Taq DNA polymerase from New England Biolabs (Ipswich MA, USA). RT-PCRs were carried out with Superscript II (Invitrogen Carlsbad, CA, USA). Restriction enzymes were commonly purchased from New England Biolabs (Ipswich MA, USA).

2.1.5 Chemicals

If not stated otherwise, standard chemicals were purchased from Sigma-Aldrich (St. Louis, MI, USA), Merck (Whitehouse Station, NJ, USA), Invitrogen (Carlsbad, CA, USA), VWR (Radnor, PA, USA) or Helena Bioscience (Gateshead, UK).

2.1.6 Antibiotics

Kanamycin (Kan) 50 mg/ml in ddH₂O

Phosphimothricin (PPT) 15 mg/ml in ddH₂O

Hygromycin (Hyg) 100 mg/ml in DMSO

Stock solutions (1000x) were stored at -20° C. Aqueous solutions were sterile filtered.

2.1.7 Media

Media were sterilized by autoclaving at 121° C for 20 min. The solution or media were cooled down to 50° C for the addition of antibiotics.

MS (Murashige and Skoog) medium

MS powder including vitamins 4.4 g/l

Sucrose 10.0 g/l

pH 5.8

For MS plates 0.8 % (w/v) phytogel (Becton, Dickinson and Company, LePont de Claix, France) was added.

2.2 Methods

2.2.1 Growth conditions

Arabidopsis seeds were grown on soil (Arabidopsis mix, John Innes Centre, Norwich) or sterile on Murashige and Skoog medium. Seeds were stratified for two days at 4°C in darkness. Then pots or plates were transferred to growth chamber with a 12 hours light period and 60% humidity. If required for setting seed, plants were transferred to long day conditions (16 h photoperiod) to allow early bolting and setting of seed. To collect seed, mature siliques were wrapped and dried before harvest. Progenies were harvested and keep in a dry condition.

2.2.2 Generation of Arabidopsis F₁ and F₂ progeny

Flowers that had a well-developed stigma but immature stamen were used as a recipient. Donor stamens were picked to touch each stigma for three to four times. Siliques containing F₁ hybrids were packed and harvested when they get ripen. Seedlings of F₁ were genotyped by PCR or tested by antibiotics. F₂ seeds were generated by self pollinate from F₁.

2.2.3 Seed sterilization

Arabidopsis seeds were incubated with 70% ethanol with 0.05% SDS (Sodium dodecyl sulfate) for 2 minutes. The liquid was discarded. Seeds were washed by 100% ethanol for 5 minutes and were dried in room temperature.

2.2.4 Pathogen inoculation

Hpa isolates were maintained on leaves of their susceptible Arabidopsis ecotypes over a 7 day cycle (Cala2 on ecotype *Ler* and Waco 9 on ecotype *Col-0*). Leaves containing *Hpa* sporangia and spores were cut into a 50 ml Falcon tube containing 15mL sterile water. Conidiospores were collected by vortexing harvested leaves. Two weeks-old plants were inoculated by *Hpa* via spraying. Inoculated plants were

kept in the hood for 5 min to allow drying and transferred to trays and covered with lids to maintain the humidity. Inoculated plants were grown in a growth chamber with 21°C and were prepared for microscopy studies at 3 or 4 days after infection.

2.2.5 Staining leaf tissues

Arabidopsis leaves were incubated with FM4-64 or aniline blue in a 1.5 mL tube. Leaves were subsequently imaged by confocal microscopy at 30 min after staining.

2.2.6 Microscopy

2.2.6.1 Confocal laser scanning microscopy

Detached leaves were examined with Leica SP5 confocal microscope (Leica Microsystems, Wetzlar, Germany). Images were taken by HCX PL APO CS 63.0 x 1.20 water objective, 2 scans per line, 2 scans per frame.

The microscope is equipped with an Argon/Helium-Neon laser and diode laser of 405 nm. Excitations of the samples were performed at 488 nm for GFP, at 514 nm for YFP and 405 nm for CFP. Emission spectra were taken from 490 to 560 nm for GFP, at 518 to 578 nm for mYFP, and 435 to 500 nm for cCFP. Aniline blue stained samples were excited using the 495 nm diode laser and the emission was taken from 410 to 480 nm. For FM4-64 stained samples the excitation was set to 561 nm and fluorescence emission was measured from 570 to 630 nm.

2.2.6.2 Opera, semi-automated confocal laser microscopy

Cotyledons of 2 weeks-old plants were detached and put upside up on a 96 pins stamp that fits 96 well sensoplates with glass bottom (Greiner Bio-One GmbH, Essen, Germany). Both cotyledons of each plant were imaged. Due to technical reasons the

pins at the margins were left free, resulting in 60 leaves from 30 plants on the stamp. The fully loaded stamp was then turned upside down and inserted into 96 well sensoplates that contain 100µL sterile ddH₂O. After 5 min the plate was put into the Opera platform for imaging and imaged with a water immersion 40x objective.

2.2.7 Molecular biological methods

2.2.7.1 Genomic DNA isolation from Arabidopsis

Genomic DNA was isolated from Arabidopsis leaves according to protocols for REExtract-N-Amp™ Plant PCR Kit (Sigma-Aldrich, Deisenhofen, Germany). 2 µL genomic DNA was used in subsequent PCR reactions for map based cloning. Genomic DNA for sequencing analysis was isolated following Edward's isolation protocol (Sambrook and Russel, 2001).

2.2.7.2 Polymerase Chain Reaction (PCR)

PCR reactions were performed using Taq DNA polymerase (New England Biolabs) according to the manufacturer's instructions. All PCR reactions were carried out with a Peltier Thermal Cycler PTC-225 (GMI Inc., Ramsey, USA). A typical PCR condition is shown below,

94°C 4 minutes

20-40 cycles of 94°C 30 seconds

55°C 30 seconds

72°C 30 seconds (1 kb / minute)

1cycle of 72°C 5 minutes

16°C hold

2.2.7.3 Gel-electrophoresis

Agarose gel electrophoresis were to separate PCR amplified DNA fragments were in gels consisting of 1% to 3.5% (w/v) agarose (80-110 V, Biorad, UK) in TBE buffer. 10 µl of PCR product was mixed with 2.5µl of 5x DNA-loading dye. The mixture was loaded to wells in agarose gels containing 1 µl/ml ethidium bromide (Sigma-Aldrich St. Louis, MI, USA). The electrophoresis was performed with 80 to 110 V for 30 to 60 minutes (Biorad, UK). Ethidium bromide stained gels were visualized by UV excitation (ChemiDOC XRS, Bio-Rad Laboratories, Hercules, CA, USA). 2-log DNA ladder (New England Biolabs) was used as a reference for the size of DNA fragments.

2.2.7.4 DNA sequencing

2.2.7.5 Sanger sequencing

Reactions were carried out in final volumes of 10 µl containing 5.5 µL PCR product (100 to 250 ng) , 1 µL of 10 mM primer, 0.5 µL of DMSO, 2 µl of 5x sequencing buffer and 1 µl Big Dye Terminator Ready Reaction Mix (PerkinElmer, Waltham, MA, USA).

The PCR condition is

96°C for 1 minute,

35 cycles of 96°C for 10 seconds,

50°C for 5 seconds

60°C for 4 minutes

Read analysis was carried out with Dye-Deoxy Terminator Cycle Sequencer (PerkinElmer, Waltham, MA, USA) in the The Genome Analysis Centre (TGAC, Norwich, UK).

2.2.7.6 Illumina-Sequencing

DNA was isolated with protocol adapted from McKinney et al., 1995 (McKinney et al., 1995). 2 g fresh weight of two-week-old *Arabidopsis* was grinded in liquid nitrogen, incubated at 37°C for 30 minutes in 10 ml extraction buffer (50 mM Tris-HCl, pH 8.0, 200 mM NaCl, 2 mM EDTA, 0.5 % SDS (v/v), 100 mg/ml Proteinase K, Invitrogen (Carlsbad, CA, USA). 10 ml of saturated phenol-chloroform-isoamyl alcohol was added, and centrifuged (SS-34 rotor, Beckman Thermo Fisher Scientific, Waltham, MA, USA) at 16,000 g for 10 minutes (10°C). The top layer was transferred into a new tube and mixed with 10 ml of chloroform-24 isoamyl alcohol (24:1). After centrifugation at 16,000g for 10 minutes (10 °C) the upper layer was transferred into a new tube and mixed with 900 µl of 3M sodium acetate (pH 5) and 2.5 volumes ethanol (98 % (v/v)). Precipitated DNA was pelleted for 20 minutes at 8,000g (10 °C), washed twice with 70 % (v/v) ethanol, air dried and resuspended 200 µl of TE buffer (20 mM Tris-HCl, pH 7.5, 1 mM EDTA). DNA was stored at 4°C. Library preparation and sequencing was carried out by Jodie Pike, followed by bioinformatics analysis in collaboration with Dr. Dan MacLean (The Sainsbury Laboratory, Norwich, UK).

2.2.8 Software

2.2.8.1 Sequence Alignments

Alignments of sequenced DNA fragments were performed by Clustal W and assemblies were generated with Vector NTI Advanced version 11 (Invitrogen, Carlsbad, CA, USA).

2.2.8.2 Primer designation

Primer designs are according to NCBI database (National Centre for Biotechnology, Bethesda, MA, USA). Mapping primers were designed according to the *Arabidopsis*

Mapping Platform (AMP, Peking University, Beijing, China).

2.2.8.3 Image processing

2.2.8.3.1 CLSM

Confocal images were processed using the Leica LAS AF, Adobe PHOTOSHOP 9.0, and ImageJ (National Institutes of Health, MA, USA).

2.2.8.3.2 Image processing and data analysis

The image processing and automate analysis methods were used as described before (Salomon et al., 2010). Briefly, for the automated screen five areas per leaf were defined. Because two leaves per plant were processed, up to ten images per plant could be analyzed. Due to the curvature of the leaves, images of a consecutive series of 21 planes (z-stack) with a distance of 1 μm were taken per area. 105 images were taken per leaf. The images were automatically analyzed with the Acapella Software. A projection of images was performed to merge the three-dimensional stack of 21 optical planes into a two-dimensional pseudo image. The pseudo-image was analyzed Acapella script (Salomon et al., 2010), specifically identifying GFP-2xFYVE labeled membrane compartments. The number and size of epidermal leaf cells were analyzed and manual inspection was performed for the images of interests. To facilitate and fasten the analysis of the output results, a script for graphical presentation of the output data with respect to the different parameters was generated. Six parameters including average width to length ratio of spots, average roundness of spots, average contrast of spots, average number of spots per 100 % image area, average number of found spots per image and average number of spots per cell.

2.2.8.3.3 Sequence data analysis

To analyse output of whole genome sequencing, 76 bp paired-end reads generated by Illumina Solexa GA2 platform (Illumina, Cambridge, UK) was used for whole-genome sequencing. Paired reads were removed prior to alignment if either of the pair contained an ambiguous nucleotide (I.E an 'N' was called). Illumina scaled quality scores (ASCII offset 64) were converted to Sanger scaled quality scores (ASCII offset 33) using the equations found in Cock PJ, Fields CJ, Goto N, Heuer ML, Rice PM. The Sanger FASTQ file format for sequences with quality scores, and the Solexa/Illumina FASTQ variants. Nucleotide distributions and Quality score distributions after filtering were calculated using the FASTQ Information tool in the FASTX-Toolkit version 0.0.13 (http://hannonlab.cshl.edu/fastx_toolkit/). Quality score distributions revealed that the reads had median quality scores of at least 25 across the length of the reads so no further pre-filtering was carried out. Paired reads were mapped to the TAIR10 Arabidopsis thaliana reference sequence using BWA version 0.5.8c. The TAIR 10 Fasta sequence was indexed with the 'index' command and paired reads mapped with 'sampe'. Resulting SAM format files were filtered to remove reads that appeared to be optical or PCR duplicates and converted to BAM format using SAMTools version 0.0.12a. In order to identify candidate SNPs, positions polymorphic to the reference genome were identified using the bcftools software in the SAMTools 0.0.12a package. Pileups were generated using SAMTools mpileup as 'mpileup -Q 13 -q 20 -C 50 -uf' (-Q = minimum base quality for a read nucleotide to be included in the pileup; -q = minimum mapping quality for a read to be included in the pileup; -C = filter to remove effects of reads with very large number of mismatches). Pileups were converted to bcf format with the bcftools 'view' command and SNPs called using 'vcfutils.pl -D 100 -d 10' (-D = maximum coverage depth for SNP calling; -d = minimum coverage depth for SNP calling). Candidate SNPs were removed from the list if they appeared in candidate lists generated in an identical pipeline from *Ler-FYVE*, *fel2*, *fel4* or *fel9* mutants given that *fel2*, *4*, *9* are not allelic (Salomon, 2009) or if they appeared in the list of *Ler-1/Col-0* SNPs generated by the 1001 genomes project (Assembly dated 26-04-2011). SNP positions within genes (including UTRs, CDS, Exon and Intron) as

described in the TAIR 10 annotation were marked with information as to which gene contained the SNP and whether it caused a synonymous or non-synonymous mutation in the gene using a custom Perl script. All bioinformatic analyzes were carried out in The Sainsbury Laboratory's compute cluster, a 22 node cluster composed of IBM blade server machines with AMD 64 processors running Debian GNU/Linux version 5.0.8 'Lenny' and with 4Gb to 32Gb RAM.

3. RESULTS

3.1 Membrane trafficking in *Arabidopsis-Hpa* interactions

Subcellular rearrangement occurs at the site of pathogen attack and in the infected cells that accommodate formation of the feeding structure- the haustorium (Koh et al., 2005). However, we have little information pertaining to how *Arabidopsis* interacts with the oomycete *Hpa* at the subcellular level. To study the role of membrane trafficking in the *Arabidopsis-Hpa* interaction, two-week old transgenic *Arabidopsis* marker lines for different subcellular components were inoculated with *Hpa* isolate Waco 9 and live-cell imaging by confocal microscopy was performed at three and four days after inoculation (Table 1).

Table 1. Summary of marker lines used in investigation of *Arabidopsis-Hpa* interaction.

Subcellular compartment	Marker	References
Cytoplasm	Free GFP	Caillaud et al., 2012
PM	YFP-PIP1;4	Geldner et al., 2009
	GFP-ACA8	Lee et al., 2007
	YFP-NPSN12	Geldner et al., 2009
	GFP-PEN1	Meyer et al., 2009
	FLS2- GFP	Goehre et al., 2009
Golgi	YFP-SYP32	Geldner et al., 2009
	YFP-Got1p	Geldner et al., 2009
	YFP-Rab A5d	Geldner et al., 2009
	YFP-Rab E1d	Geldner et al., 2009
	RPW8.2-YFP	Wang et al., 2009
TGN/EE	YFP-VTI12	Geldner et al., 2009
	YFP-Rab A1e	Geldner et al., 2009
LE	ARA7- RFP	Kindly provided by Karin Schumacher, U. Heidelberg, Germany
	RFP-ARA6	Kindly provided by Karin Schumacher, U. Heidelberg, Germany
	GFP-2xFYVE	Voigt et al., 2005
	YFP-Rab G3f	Geldner et al., 2009
Vacuole	Rab G3f	Geldner et al., 2009;
	YFP-VAMP711	Geldner et al., 2009

3.1.1 The plant cell cytoplasm surrounds the haustorium

In *Arabidopsis*, the cytoplasm is aggregated at the penetration site when infected by *E. cichoracearum* indicating rearrangement of subcellular compartments upon pathogen infection (Koh et al., 2005). Transgenic *Arabidopsis* expressing 35S::GFP that marks the cytoplasm and the nucleus were examined after *Hpa* infection. The cytoplasm was observed around the haustorium, consistent with recently published data (Figure 3 A) (Caillaud et al., 2012). This suggests at this stage of the infection, the host cells are already responding with subcellular changes and therefore we used this time point for further study. FM4-64 stained the lipid bilayers of the haustorium (Figure 3 C) and was also found to stain the encasement of older haustoria (Figure 9) revealed projection of *Hpa* haustoria inside host cells.

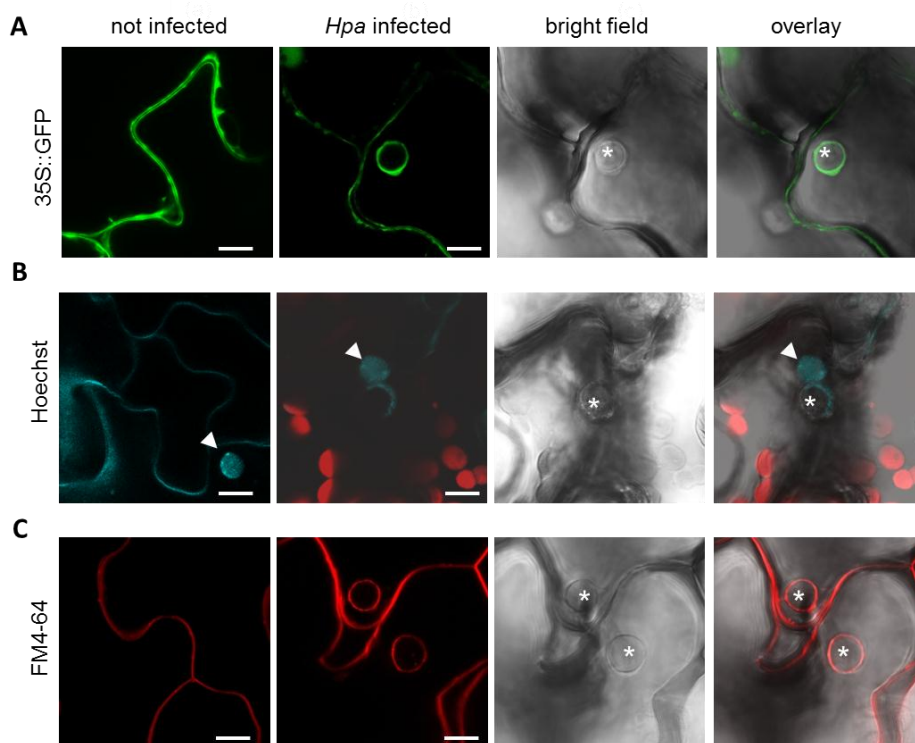


Figure 3. The cytoplasm and the nucleus are detected at the haustorium. CLSM images of haustorial projections in epidermal cells of transgenic *Arabidopsis* (Col-0) lines after *Hpa* inoculation (3 dpi). *Hpa* haustoria are presented in bright field images and indicated by asterisks. (A) 35S::GFP labelled cytoplasm localizes around the *Hpa* haustorium. (B) The nucleus is localized around the *Hpa* haustorium could be labelled by Hoechst stain. (C) FM4-64 stains the lipid bilayers of the *Hpa* haustorium. Bar=10 μ m.

3.1.2 Nuclear migration towards the haustorium

Hoechst dye staining marked the nucleus in infected cells. The nucleus was frequently observed adjacent to the haustorium (Figure 3 B). This indicates subcellular reorganization occurs not only at the sites of penetration but also at stages when the haustorium is projected in to the host cell and later when the encasement is developed. This is consistent with previous study of host nucleus localization in *Arabidopsis-Hpa* interactions (Caillaud et al., 2012).

3.1.3 PM proteins differentially label the EHM

Formation of haustoria causes expansion and modification of the plant's plasma membrane. Previous studies showed that several PM proteins such as glycoprotein, aquaporin and RLKs are excluded from the EHM of fungal or oomycete haustoria, suggesting that the composition of the EHM is different from the plant PM (Koh et al., 2005; O'Connell and Panstruga, 2006; Caillaud et al., 2012). To investigate the nature of the EHM of *Hpa*, five PM marker lines were used to examine their localization in compatible interactions. *Arabidopsis* PM intrinsic protein 2a (PIP2a), PIP1b, and PIP1;4 were absent from the EHM of *E. cichoracearum* and *Hpa* (Koh et al., 2005; Caillaud et al., 2011). In this study, PIP1;4, was localised in the PM of infected cells and found to be excluded from the EHM of *Hpa* - the fluorescent signal remained discrete at the PM as shown in uninfected cell (Figure 4). Auto-inhibited Ca^{2+} -ATPase isoform 8 (ACA8) did not accumulate at the EHM (Figure 4). The novel plant SNARE 12 (NPSN12) also did not label the EHM indicating this protein is not utilized by *Hpa* in forming the EHM (Figure 4). These PM-localized proteins remained at the PM as shown before (Koh et al., 2005; O'Connell and Panstruga, 2006; Caillaud et al., 2011). However, not all PM residing proteins examined in this study were excluded from the EHM of *Hpa*. GFP-PEN1 localized around the haustorium and labelled vesicle-like structures along the boundary of the haustorium containing cell (Figure 4). Also, the GFP fusion protein of the PM-localized RLK FLS2 clearly labelled the haustorium (Figure 4). These results suggest that there is a selective mechanism for recruitment

of PM proteins at the EHM.

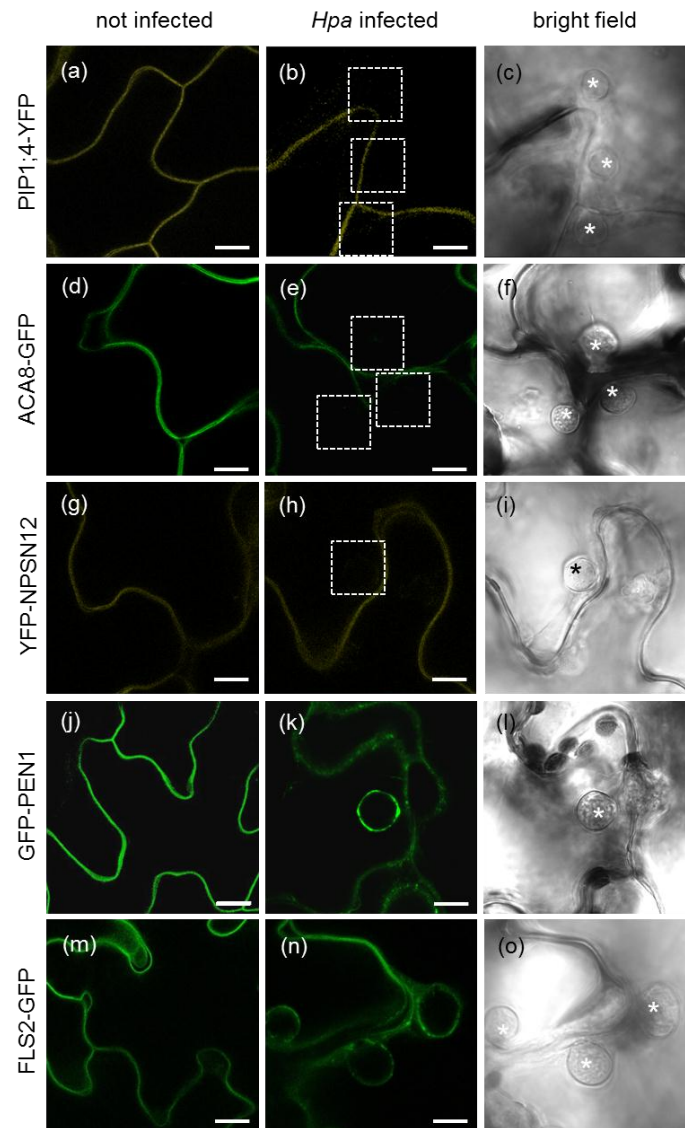


Figure 4. PM proteins selectively label the *Hpa* EHM. CLSM images of haustorial projections in epidermal cells of transgenic Arabidopsis (Col-0) lines after *Hpa* inoculation (3 dpi). *Hpa* haustoria are presented in bright field images and indicated by asterisks. YFP-PIP1;4, ACA8-GFP, YFP-NPSN12 are localized at the PM but excluded around the haustoria (dashed boxes). GFP-PEN1 and FLS2-GFP are localized at the PM and the EHM. Bar=10 μ m.

3.1.4 Secretory vesicles and Golgi stacks localized around the haustorium

Penetration resistance to filamentous plant pathogens relies on focal accumulation of secretory vesicles and active protein secretion (Lipka et al., 2005; Kwon et al., 2008). However, whether the redirection and contents of secretory vesicles contribute to the biogenesis of the EHM has not been determined. In order to characterise the role of secretory vesicles in the formation and development of this structure we investigated the localisation of secretory compartments. Golgi stacks labelled by syntaxin SYP32-YFP, YFP-Rab GTPase E1d and A5d, and vesicle transport protein Got1p-YFP localized around the haustorium (Figure 5). The shape and number of fluorescently labelled Golgi stacks was similar in uninfected and infected cells for each marker line (Figure 5). There was clear accumulation of SYP32-YFP labelled compartments around the haustorium indicating pathogen-induced changes to the distribution of Golgi stacks.

RPW8.2 is a resistance protein and provides a broad spectrum of resistance against powdery mildew and oomycetes (Wang et al., 2007; Wang et al., 2009). It is inducibly expressed in infected cells and targeted to the EHM of *G. cichoracearum* UCSC1 and *G. orontii* (Wang et al., 2009; Micali et al., 2011). Trafficking of RPW8.2 containing vesicles to the haustorium suggests that maturation of the EHM may need proteins or lipids secreted from host cell. In the compatible interaction between *Hpa* and Arabidopsis, RPW8.2-YFP was expressed in infected cells rather in uninfected cells (Figure 5) under its endogenous promoter and vesicles containing RPW8.2-YFP were localized around the haustorium (Figure 5). This supports previous studies that the expression of RPW8.2-YFP is triggered upon infection and constitutively expressed RPW8.2-YFP labels ER/Golgi compartments (Wang et al., 2007; Wang et al., 2010). It is also interesting that RPW8.2 did not label the EHM of *Hpa* uniformly as it is shown in powdery mildew interactions. This indicates RPW8.2 functions and behaves differently in different pathosystem.

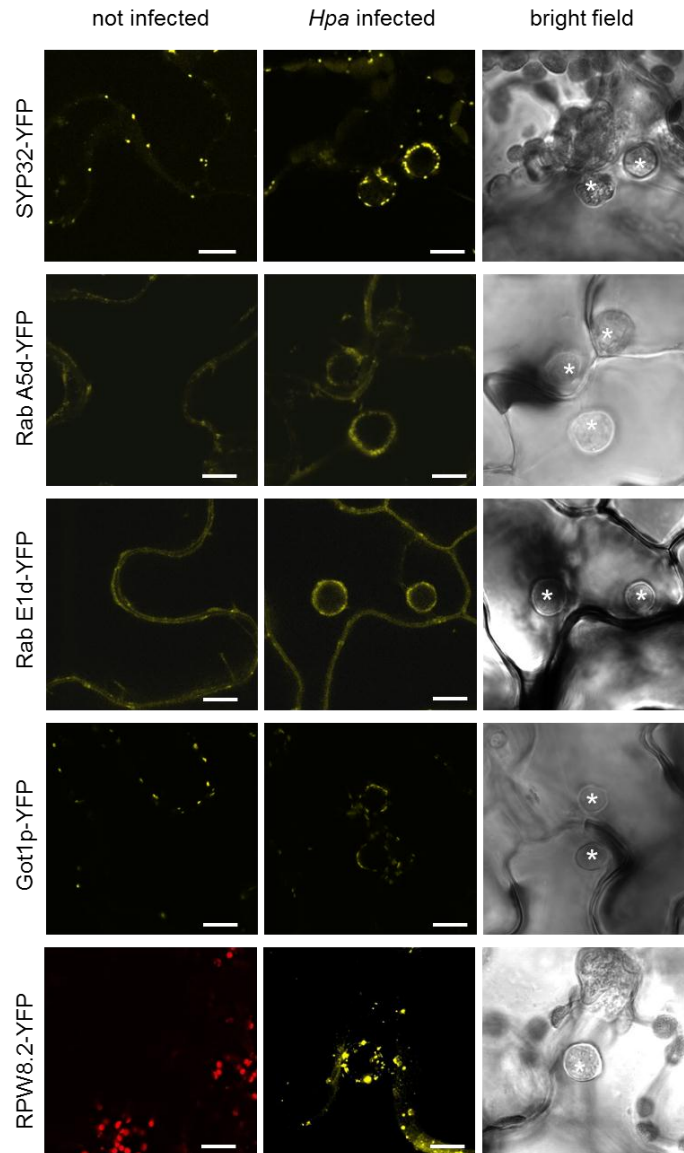


Figure 5. Secretory vesicles localize around the *Hpa* haustoria. CLSM images of haustorial projections in epidermal cells of transgenic Arabidopsis (Col-0) lines after *Hpa* inoculation (3 dpi). *Hpa* haustoria are presented in bright field images and indicated by asterisks. YFP-SYP32, YFP-Rab A5d, YFP-Rab E1d, YFP-Got1p and YFP-RPW8.2 labelled compartments are around the *Hpa* haustoria. The red colour corresponds to chloroplast autofluorescence. Bar=10 μ m.

3.1.5 Endosomal vesicles accumulated around the haustorium

The components of the EHM have been investigated using markers for the PM and secretory vesicles in various pathosystems (Koh et al., 2005; Micali et al., 2011). Endocytosis seems to play a role in plant-pathogen interactions since endocytic

trafficking regulates the PM composition and may mediate effectors trafficking from the pathogen to the host cell (Dhonukshe et al., 2008). To understand distribution of endosomal vesicles upon *Hpa* infection, different transgenic Arabidopsis expressing fluorescently-tagged markers that label the TGN and MVBs in the route of endocytic pathways were monitored.

YFP-VTI12 labelled vesicles localized around the haustorium in the infected cell and the vesicular structure remained similar to uninfected status (Figure 6 A). Vesicles containing YFP-Rab A1e localized around the haustorial projection, although fluorescence from this marker was diffuse around the whole haustorium rather than in punctate associated with discrete vesicles (Figure 6 A). To investigate the activity of endosomal recycling in the infected cell, BFA was applied to block recycling and FM4-64 was used to trace endosomal vesicles. “BFA-bodies” stained by FM4-64 are present in *Hpa* infected cell (Figure 7 C) suggesting early and recycling endosome trafficking is functional in infected cells. Late endosomal compartments labelled by YFP-Rab C1, RFP-ARA7, ARA6-RFP, and GFP-2xFYVE localized around the haustorium (Figure 6 B). There were more vesicles localizing around the haustorium than residing in the distal sites of the plant cell. This indicates polarization of MVBs in the infected cell. GFP-2xFYVE labels LEs and to some extent the PM through the association with PI3P (Vermeer et al., 2006). GFP-2xFYVE was also expressed around the haustorium uniformly (Figure 6 B). This indicates the EHM likely contains PI3P. PI3P might act as binding sites for oomycete effectors, providing means for effector entry into host cells and/or the sites for or effector activities (Rafiqi et al., 2010; Gan et al., 2010, Yaeno et al., 2011).

Taken together, distribution of endosomal compartments reveals not only secretory vesicles but also TGNs, and MVBs surrounded the haustorium in infected cells. This suggests a functional endocytic and recycling trafficking at the interface between Arabidopsis and *Hpa*.

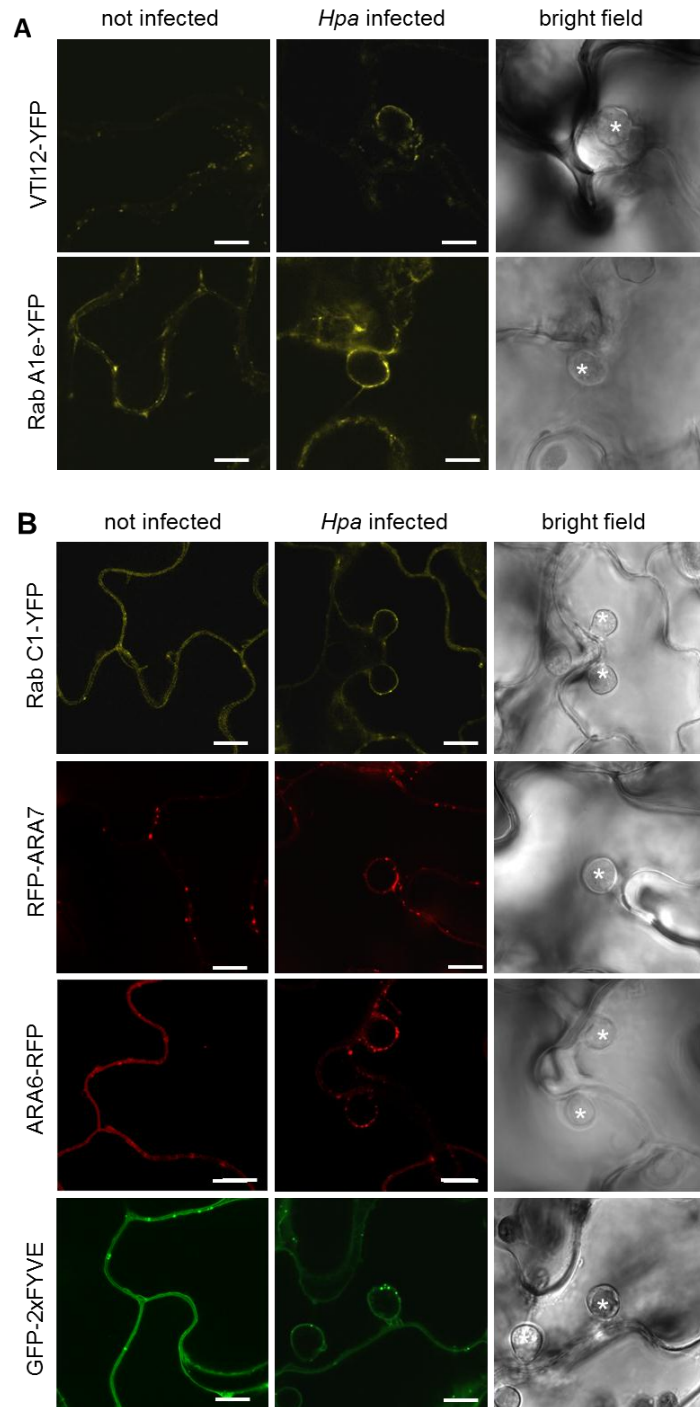


Figure 6. Endosomal compartments localize around the *Hpa* haustoria. CLSM images of haustorial projections in epidermal cells of transgenic Arabidopsis (Col-0) lines after *Hpa* inoculation (3 dpi). *Hpa* haustoria are presented in bright field images and indicated by asterisks. (A) YFP-VTI12 and YFP-Rab A1e labelled early endosomes/TGN. (B) RFP-ARA7, ARA6-RFP and GFP-2xFYVE labelled LEs/MVBs. Bar=10 μ m.

3.1.6 MVBs dynamics in the infected plant cell

In Arabidopsis, actin microfilaments build a dense network around the penetration site after inoculation with *Hpa* (Takemoto et al., 2003). YFP-2xFYVE labeled endosomes are transported by the actin cytoskeleton that participates in cytoplasmic streaming (Vermeer et al., 2006). To examine the dynamics of GFP-FYVE labelled endosomes in infected plants, live-cell imaging of in time series was performed. In the infected cell, GFP-FYVE residing vesicles moved toward the haustorial neck and some of them departed from the site of infection via cytoplasmic strands (Figure 7 A and B). MVBs around the haustoria were dynamic and the observation that they can move towards and away from the haustoria raises the possibility that MVBs may play a role in transporting molecules or proteins between host cells and haustoria.

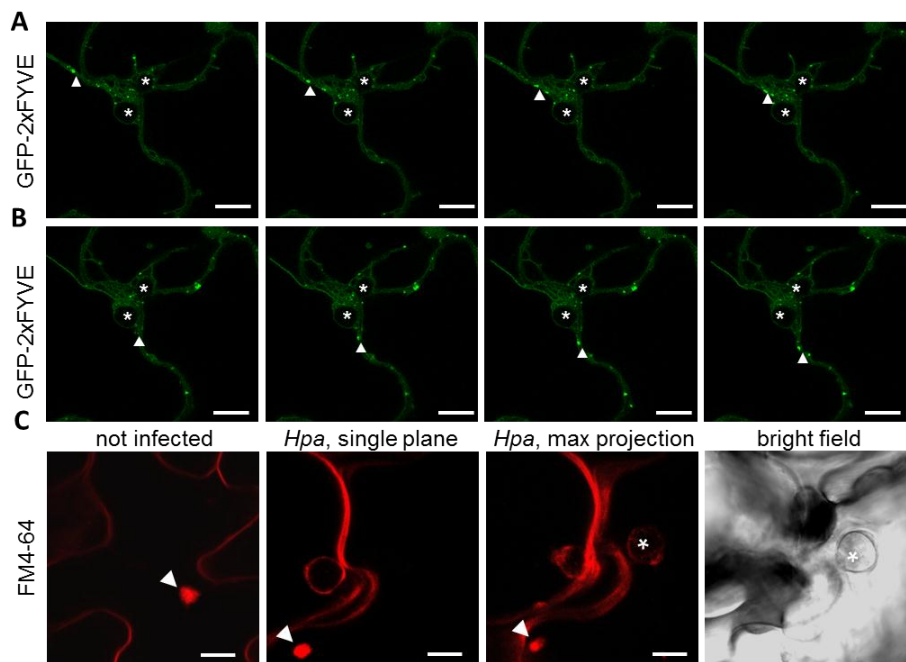


Figure 7. MVBs move bi-directional and recycling occurs in the *Hpa* infected cells. CLSM images of haustorial projections in epidermal cells of transgenic Arabidopsis (Col-0) lines after *Hpa* inoculation (3 dpi). *Hpa* haustoria are presented in bright field images and indicated by asterisks. (A) MVBs move toward and (B) MVBs move away the *Hpa* haustorium. Time-frame between single images is 815ms. (C) BFA bodies are stained by FM4-64 indicating recycling occurs in *Hpa* infected cell. Bar=10 μ m.

3.1.7 The tonoplast envelopes the haustorium

In plant cells, the large central vacuole occupies a most of the intracellular space and is a final destination for many proteins that have trafficked through the secretory and endocytic pathways. In infected cells, the tonoplast membrane was visualised using the Rab G3f and VAMP711 YFP tagged markers. The tonoplast was observed surrounding the haustorium (Figure 8). The vacuolar markers Rab G3f and VAMP711 were not observed in vesicle-like structures.

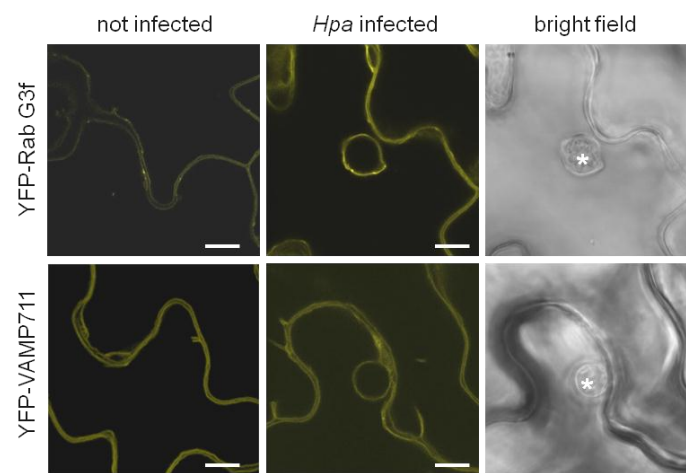


Figure 8. The vacuole envelopes the *Hpa* haustoria. CLSM images of haustorial projections in epidermal cells of transgenic Arabidopsis (Col-0) lines after *Hpa* inoculation (3 dpi). *Hpa* haustoria are presented in bright field images and indicated by asterisks. YFP-Rab G3f and YFP-VAMP711 labelled vacuole encompass the haustoria. Bar=10 μ m.

3.1.8 Haustorial encasements comprise membrane components

The mature haustorium is often enveloped by a callose-containing encasement (Meyer et al., 2009). The encasements could restrict uptake of nutrient from host cells and provide a defence mechanism for plants. The biogenesis of the encasement is mediated by exosomal secretion (Meyer et al., 2009). To study the Arabidopsis encasement of *Hpa* haustoria, localization of different membrane components were examined in plant cells at four days after *Hpa* inoculation. FM4-64 stained the encasement (Figure 9) again indicating entrapment of membrane lipids into this

callose-containing structure. In *35S::GFP* expressing plant GFP not only surrounded the encasement but also appeared at the inner and outer surface (Figure 9). This suggests there are membranous and cytoplasmic material between the EHM and the encasements.

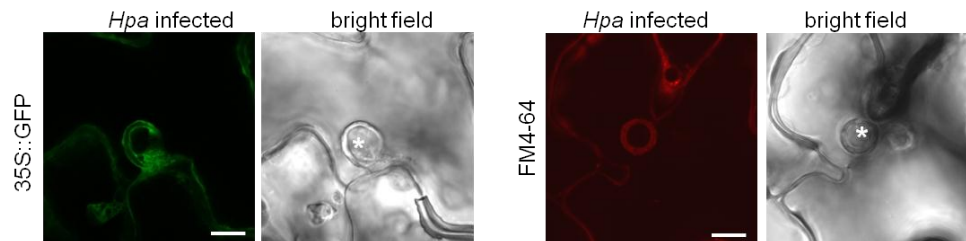


Figure 9. The cytoplasm and the nucleus are detected at the encasement. CLSM images of haustorial projections in epidermal cells of transgenic Arabidopsis (Col-0) lines after *Hpa* inoculation (4 dpi). Free GFP is localized around the encasement and is detected between the encasement and the haustorium. FM4-64 stains encased *Hpa* haustorium. Bar=10 μ m.

PIP1;4, ACA8-GFP, YFP-NPSN12 and GFP-PEN1, were distributed throughout the encasement (Figure 10). The observation that PM markers such as ACA8-GFP, YFP-NPSN12 and YFP-PIP1;4 were excluded from the EHM but were present in the encasement suggests different nature and biogenesis pathway of the encasement from the EHM.

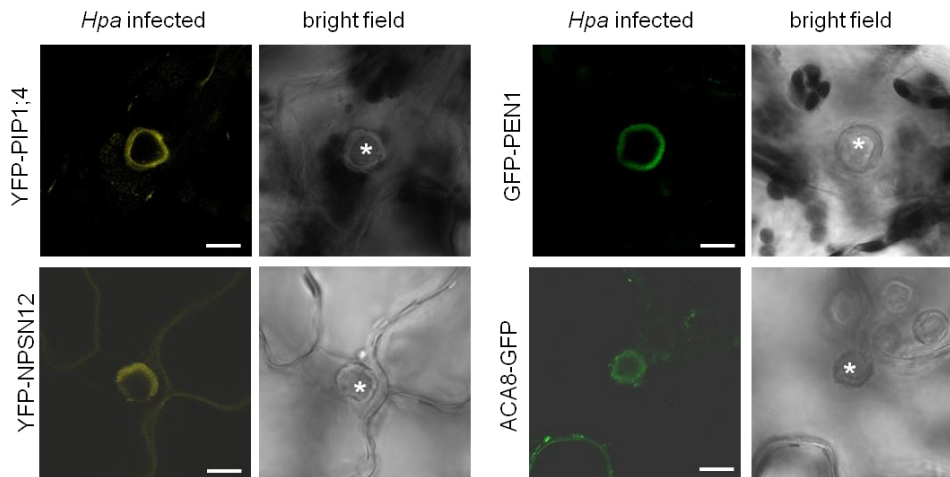


Figure 10. The PM proteins constitute the encasement. CLSM images of haustorial projections in epidermal cells of transgenic Arabidopsis (Col-0) lines after *Hpa* inoculation (4 dpi). Haustoria are presented in bright field images and indicated by asterisks. YFP-PIP1;4, YFP-NPSN12, GFP-PEN1 and ACA8-GFP localize at the PM and the encasement. Bar=10 μ m.

Markers for secretory vesicles labelled the encasement. At the outer surface of the encasement, YFP-SYP32, Got1p-YFP and Rab A5d labelled Golgi located closely to the encasement (Figure 11). YFP-SYP32 signal was also observed as diffuse signal inside the encasement. There was stronger accumulation of YFP-SYP32 at the interface between the haustorium and the encasement (Figure 11). RPW8.2-YFP was detected in the encasement of *G. orontii* and immunolocalization assays show RPW8.2 vesicles on the encasement of *G. cichoracearum* UCSC1 (Micali et al., 2011; Wang et al., 2009). In this study, RPW8.2-YFP labelled both the inner and outer surface of the encasement. Interestingly, vesicular-like structures at the EHM did not appear in or around the encasement. There was uniformed expression of RPW8.2-YFP at the encasement indicating fusion of vesicles at this structure. Only weak or diffused signal was inside the encasement (Figure 11).

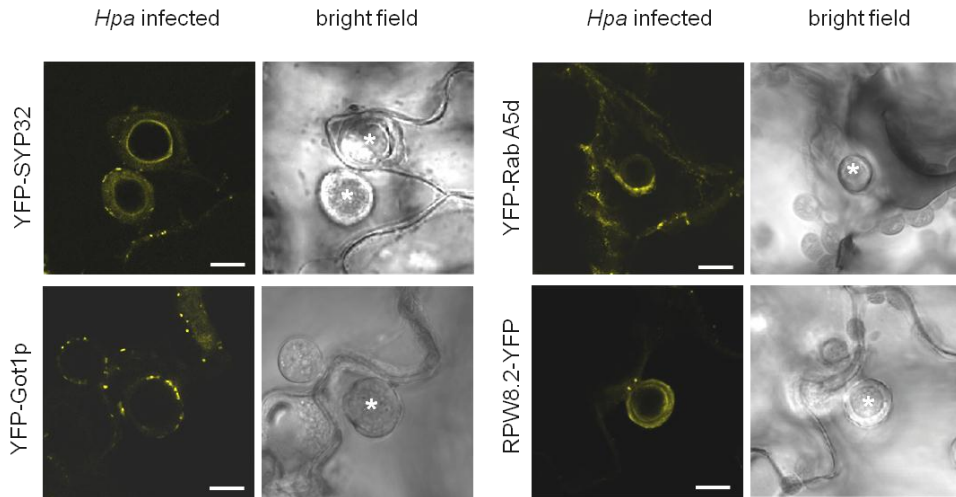


Figure 11. Secretory proteins surround the *Hpa* encasement. CLSM images of haustorial projections in epidermal cells of transgenic Arabidopsis (Col-0) lines after *Hpa* inoculation (4 dpi). *Hpa* haustoria are presented in bright field images and indicated by asterisks. Proteins YFP-SYP32, YFP-Got1p, YFP-Rab A5d and YFP-RPW8.2 are recruited in the *Hpa* encasements. Secretory vesicles are visible around the *Hpa* encasement. Bar=10µm.

All endosomal markers used in this study labelled the haustorial encasement. The TGN marker YFP-VTI12 localized at the encasement but distinct vesicular structure did not appear at the outer surface of the encasement (Figure 12). YFP-Rab A1e was diffusely distributed in the encasements (Figure 12).

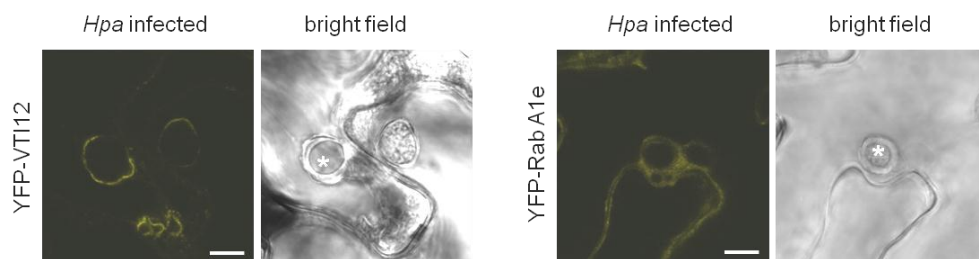


Figure 12. Early endosomal proteins are detected at the *Hpa* encasement. CLSM images of haustorial projections in epidermal cells of transgenic Arabidopsis (Col-0) lines after *Hpa* inoculation (4 dpi). *Hpa* haustoria are presented in bright field images and indicated by asterisks. YFP-VTI12 and YFP-Rab A1e localizes diffusely around the *Hpa* encasement. Bar=10µm.

RFP-ARA7 was similarly present as diffuse label in the encasement, additionally RFP-ARA7 labelled vesicles localized around the encasement (Figure 13). There was

weak ARA6-RFP signal in the encasement but no vesicular structures were observed around the encasement, suggesting fusion of vesicles (Figure 13). Vesicles containing GFP-2xFYVE were present around the encasement (Figure 13). Moreover, RFP-ARA7, ARA6-RFP and GFP-2xFYVE clearly defined the inner and outer surface of the encasement (Figure 13). This indicates a distinct localization of endosomal proteins at the membrane of the encasement.

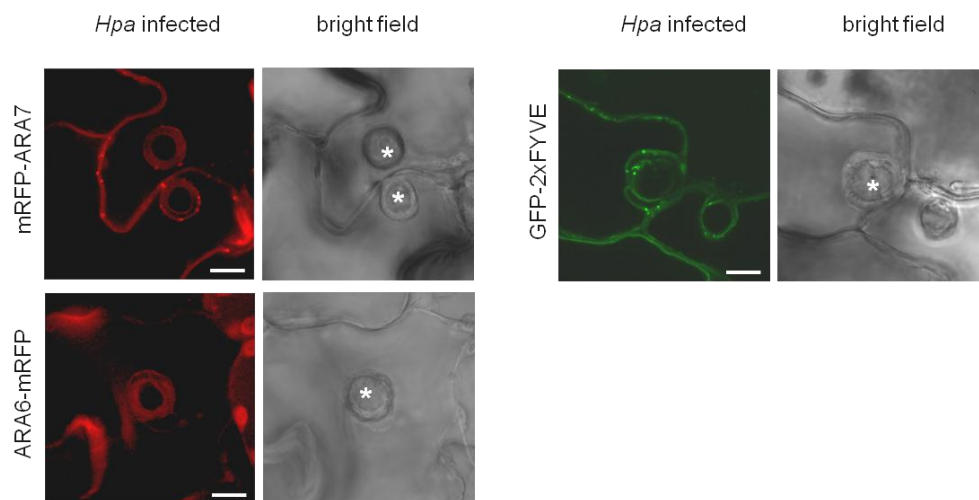


Figure 13. Proteins marking LEs label the *Hpa* encasement. CLSM images of haustorial projections in epidermal cells of transgenic Arabidopsis (Col-0) lines after *Hpa* inoculation (4 dpi). *Hpa* haustoria are presented in bright field images and indicated by asterisks. RFP-ARA7, ARA6-RFP, and GFP-2xFYVE positive vesicles are visible around the *Hpa* encasement. Bar=10 μ m.

The localization of the vacuole markers VAMP711 and Rab G3f appeared similar, surrounding the encasement (Figure 14). In both marker lines, no discrete vesicles were observed as for un-encased haustoria. These data suggested the large central vacuole maintained close association with the encased haustoria.

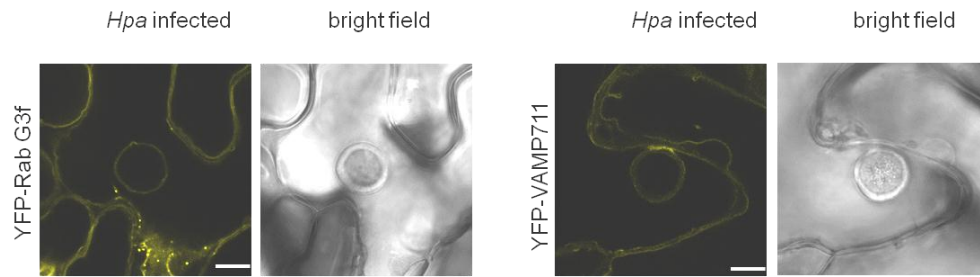


Figure 14. The vacuole envelopes the encased haustoria. CLSM images of haustorial projections in epidermal cells of transgenic Arabidopsis (Col-0) lines after *Hpa* inoculation (4 dpi). *Hpa* haustoria are presented in bright field images and indicated by asterisks. YFP-Rab G3f and YFP-VAMP711 labelled tonoplast are detected around the encasement. Bar=10 μ m

3.2 Genetic dissection of endocytosis in Arabidopsis

MVBs play an important role in both the endocytic and the secretory pathways, since they act as central sorting centres in the release of exosomes and recycling endosomes to the PM, the delivery of endocytosed cargoes to the lytic vacuole, and the retrogradation of vesicles to the TGN (Robinson et al., 2008). Consequently, the function of the MVBs is closely connected to cell signalling and transport of cargoes, as well as to the determination of the protein composition of the PM, vacuole and endosomes. Our data showed that MVBs accumulated and move dynamically around the *Hpa* haustoria raising a possibility of their role for transporting materials (Figure 6 B and 7).

In Arabidopsis, GFP-2xFYVE has been identified to localize in MVBs (Voigt et al., 2005). Interestingly, previous work from our lab showed that two mutants, *fel4* and *fel5* mutant plants, containing increased or decreased levels of GFP-2xFYVE compartments respectively exhibit slightly enhanced susceptibility to *Pto* DC3000 (Salomon, 2009), a finding that stresses a role of MVBs in plant immunity. Internalization of the GFP-tagged LeEix2 receptor to FYVE-positive endosomes 10–15 min after EIX application was reported (Bar and Avni, 2009). These results indicate that the study of MVBs could be not only relevant from a cell biology perspective, but also crucial for gaining insight into the cellular changes underlying plant-pathogen interactions and how membrane trafficking may affect plant defence.

To identify possible regulators of the biogenesis of MVBs, *Ler*/GFP-2xFYVE (Voigt et al., 2005) was selected. Cotyledons of two week-old plants were detached and the amounts of GFP-2xFYVE compartments in leaf epidermal cells were measured. Averagely, *Ler*/GFP-2xFYVE contains 479 ± 162 GFP-2xFYVE compartments/image areas and there are 37 ± 8 cells/image area with 10 ± 4 GFP-2xFYVE compartments/cell (Figure 15). Ethyl methanesulfonate (EMS) mutagenized *Ler*/GFP-2xFYVE lines were generated (Salomon, 2009). Numbers of GFP-2xFYVE compartments were measured in the M_2 generation and putative mutants with fewer than 200 or more than 800 GFP-2xFYVE compartments were selected for further genetic studies (Salomon, 2009).

Previously, 13 600 M_2 plants of the EMS-mutagenized *Ler*/GFP-2xFYVE line were inspected (Salomon, 2009). 228 putative mutants (at least 97 individual mutants) out of 8100 informative M_2 plants were initially selected (Salomon, 2009). Up to date, 12 *fel* mutants were identified and confirmed in the M_3 generation on the basis of quantitative differences (Salomon, 2009).

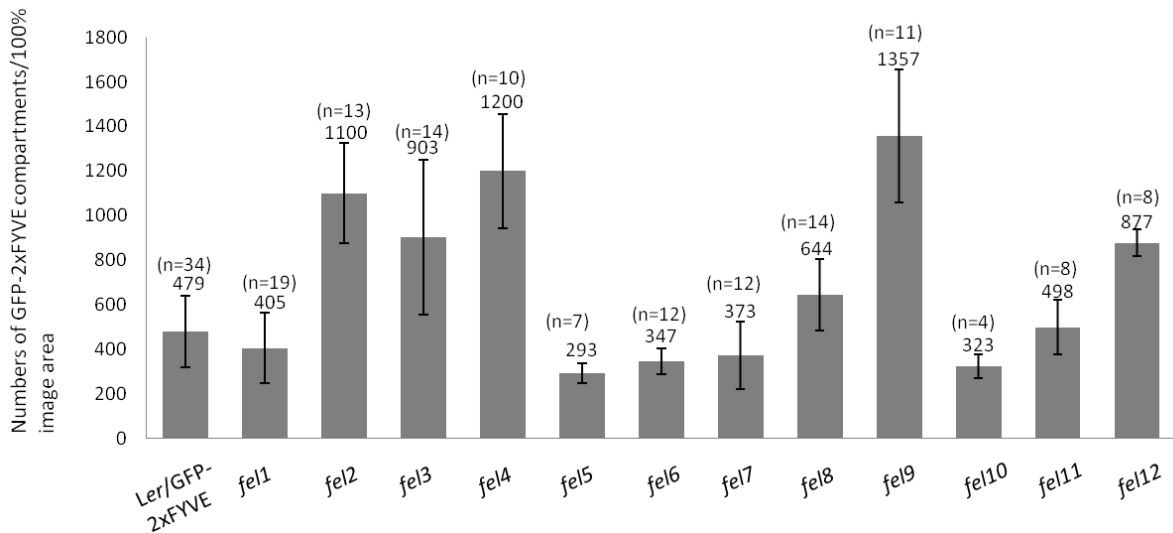


Figure 15. Quantification of GFP-2xFYVE compartments *fel* mutants (M_3). Cotyledons of two-week-old *fel* mutant plants and the reference line were measured. Average numbers of GFP-2xFYVE compartments per 100% image area were calculated. Bars and error bars indicate average number (indicated above bars) of GFP-2xFYVE compartments and standard deviation. Number of individual measured plant is indicated in brackets.

3.2.1 *Fel* mutant candidates screen

In order to identify more *fel* mutant candidates, 120 pools of EMS-mutagenized plants in M_2 were screened. The previous study carried out in our lab (Salomon, 2009) indicates around 40% silencing in these EMS-mutagenized plants. In this study, only 4809 out of 9862 EMS-mutagenized plants (49%) showed GFP signals (51% silencing). This low amount of GFP-expressing plants may be due to EMS-mutagenesis of GFP-2xFYVE and/or silencing of the transgene. The *fel* mutants found in this screen could be divided into three classes according to the numbers of GFP-2xFYVE compartments (Figure 16; Table 2). Mutants containing more than 1000 GFP-2xFYVE compartments/image area are grouped in class I, while mutants with 800 to 1000 GFP-2xFYVE compartments/image area are categorized in class II and those with less than 200 GFP-2xFYVE compartments/image area are contained in class III. In total, 444 M_2 candidates with altered endosome levels were selected and re-screened at the M_3 generation. At the M_3 stage, 30 plants from each independent line were rescreened for endosomal phenotypes. The numbers of GFP-2xFYVE compartments were averaged from individual plants in the M_3 stage but no mutant was confirmed. Notably, there is a 20%, 14% and 13% loss of mutant candidates in these three classes of mutants, respectively, because these plants are either not viable or cannot produce progenies. Also, the ratio of loss of progeny is higher in class I than in class II. This difference suggests that mutants exhibiting stronger endosomal phenotypes may cause more striking defects in development or fertility. Moreover, the criteria of screening was based on the numbers of

GFP-2xFYVE compartments per image area, the output results could only represent total amount of GFP-2xFYVE compartments but not how many GFP-2xFYVE compartments per cell. Therefore, we should carefully consider about the robustness of the output result.

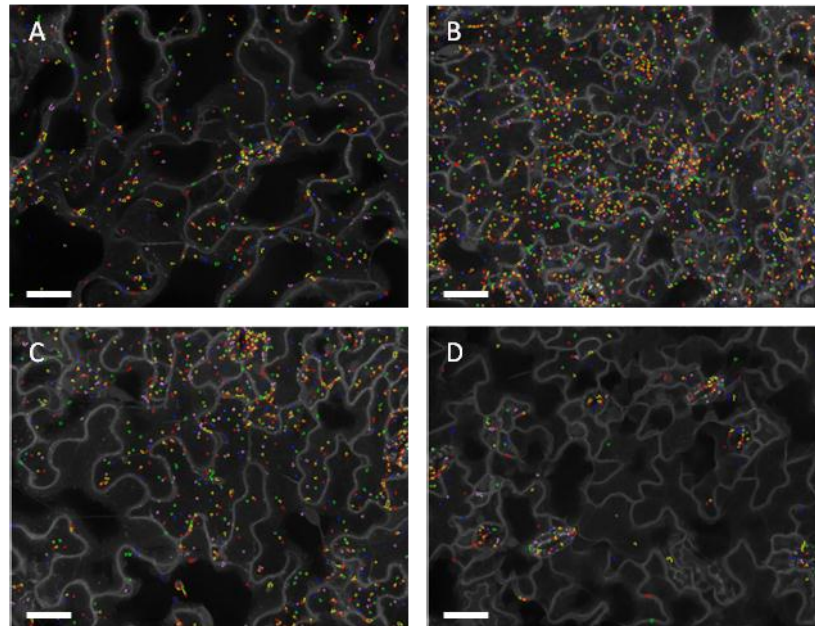


Figure 16. Detection of GFP-2xFYVE compartments in leaf epidermal tissues. Merged confocal microscopy images were taken from epidermal cells of *Arabidopsis* cotyledons expressing GFP-2xFYVE. Images were taken with the Opera microscope and analyzed with the Endomembrane script (Salomon et al., 2010). Recognized GFP-2xFYVE compartments are shown by coloured circles (scale bar=50 mm). (A) *Ler*/GFP-2xFYVE containing around 500 GFP-2xFYVE compartments/image area. (B) Class I mutant (increased numbers) containing more than 1000 GFP-2xFYVE compartments/image area. (C) Class II mutant (increased numbers) containing between 800 to 1000 GFP-2xFYVE compartments/image area. (D) Class III mutant (reduced numbers) containing fewer than 200 GFP-2xFYVE compartments/image area.

Table 2. Classification of *fel* candidates in M₂ plants and endosomal phenotype in M₃ plants. Numbers of *fel* mutant candidates together with developmental phenotypes in M₂ and M₃ are indicated. Mutant candidates were grouped into three different classes according to the numbers of GFP-2xFYVE compartments/image area.

Mutant class	M ₂ candidates				M ₃ re-screened plants			
	Total number of plants	Healthy	Lethal	Sterile	Total number of plants	Wild type	Mutant	No GFP signal
I: Increased endosomes (> 1000)	192	154	20	18	45	44	0	1
II: Increased endosomes (800-1000)	222	191	18	13	55	55	0	0
III: Reduced endosomes (< 200)	30	26	2	2	2	2	0	0
Total numbers of plant	444	371	40	33	102	101	0	1

3.2.2 Mutant *fel2* and *fel9* exhibit cellular phenotypes

Among the 12 *fel* mutants isolated in the previously screening (Salomon, 2009), *fel2* and *fel9* were selected for further characterization. Because both *fel2* and *fel9* showed strikingly increased endosomal numbers with an average number of 1100 ± 224 and 1357 ± 300 GFP-2xFYVE compartments/image area respectively ($n = 8$ and $n = 11$), while 479 ± 162 GFP-2xFYVE compartments/image area are found in the reference line *Ler*/GFP-2xFYVE (Figure 15; Figure17). The average number of GFP-2xFYVE compartments/cell is 13 ± 1 and 33 ± 9 in *fel2* and *fel9*, respectively, while it is 10 ± 4 in the reference line. The average number of cells/image is 37 ± 8 in the reference line, and 65 ± 6 and 47 ± 6 in *fel2* and *fel9*. *Fel2* contained roughly the same number of endosomes/cell but more cells than the reference line per image area. In contrast *fel9* exhibited 3 times more endosomes/cell with only a 25% increase in cell number per image area. This reveals *fel2* and *fel9* contain not only more GFP-2xFYVE compartments in individual cells but also more epidermal cells than *Ler*/GFP-2xFYVE.

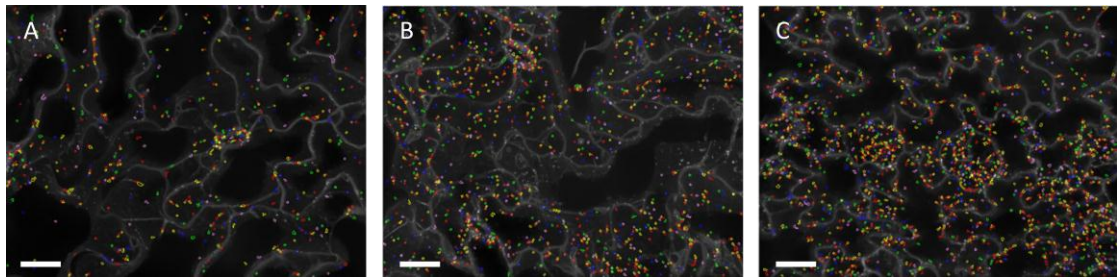


Figure 17. Comparison of GFP-2xFYVE compartments in leaf epidermal tissues. Merged confocal microscopy images were taken from epidermal cells of *Arabidopsis* cotyledons expressing GFP-2xFYVE. Images were taken with the Opera microscope and analyzed with the Endomembrane script (Salomon et al., 2010). Recognized GFP-2xFYVE compartments are shown by coloured circles (scale bar=50 mm). Both *fel2* and *fel9* are in the M₃ generation. Representative images of (A) *Ler*/GFP-2xFYVE. (B) *Fel2*. (C) *Fel9*.

In leaf epidermal cells of cotyledons in the M₃ generation, the endosomal phenotypes of *fel2* and *fel9* could be confirmed by conventional confocal microscopy (Figure 19 A). There were also more GFP-2xFYVE compartments in true leaves of *fel2* and *fel9* than *Ler*/GFP-2xFYVE (data not shown). Moreover, *fel9* exhibited stronger GFP signals than *fel2* and *Ler*/GFP-2xFYVE. In root epidermal cells, *fel9* contained more GFP-2xFYVE compartments while the endosomal level of *fel2* was similar to *Ler*/GFP-2xFYVE (Figure 18 B). This suggests that *fel2* and *fel9* are different mutants because they have different phenotypes in cotyledon and root. Phenotypes in *fel2* indicate that the alteration of FYVE-endosomal levels is specifically happening in leaves, raising the enticing idea that the regulation of membrane trafficking processes in plants is tissue-specific. Interestingly, *fel4* and *fel5* phenotypes could be confirmed in epidermal leaf cells but remain wild type-like in root epidermis cells (Salomon, 2009). This support the possibility that *fel* phenotypes maybe tissue-specific.

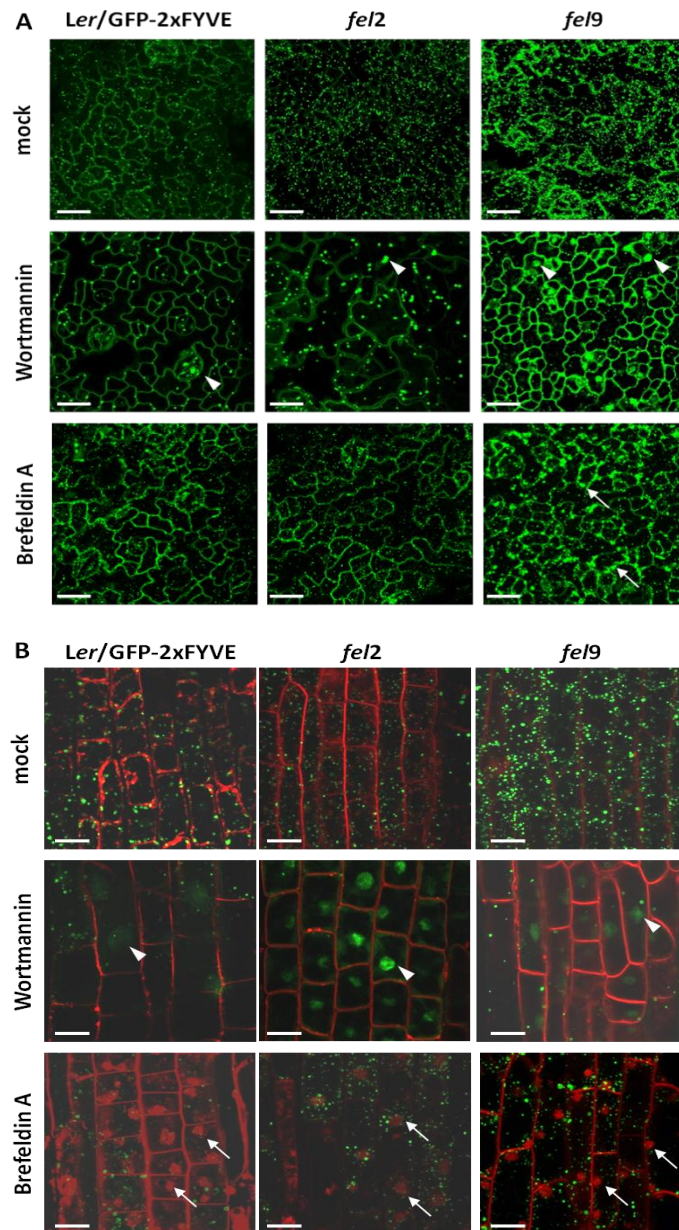


Figure 18. Subcellular phenotypes of *Ler/GFP-2xFYVE*, M₃ of *fel2* and M₃ of *fel9*. Cotyledons and roots of two-week-old plants were treated with 30 μ M BFA for 2 hours or 33 μ M Wortmannin for 1 hour. Images were taken with a confocal laser scanning microscopy (Leica). The green signal is GFP-2xFYVE. (A) Single stack image of a cotyledon. Mock-, Wortmannin- and BFA-treated samples are indicated. Wortmannin treatment results in a reduction of the GFP-2xFYVE signal and the formation of large vesicles (arrow heads). Aggregations of GFP-2xFYVE positive compartments (arrows) appear in *fel9* after BFA treatment. (B) Single stack image of root epidermal cells. Mock-, Wortmannin- and BFA-treated samples are indicated. Roots were stained with FM4-64 (red). Arrow heads indicate the nucleus. BFA bodies are indicated by arrows.

Increased GFP-2xFYVE compartments may result from mislocalization of GFP-2xFYVE, labelling vesicles other than LEs/MVBs. With the aim of further characterizing *fel2* and *fel9*, different drugs/inhibitors were tested for their effect on *fel2* and *fel9*. In all cases, the reference line *Ler*/GFP-2xFYVE was used as a control. Treatment with Wortmannin reduced GFP-2xFYVE endosomal levels in *fel2*, *fel9* and the reference line in both cotyledons and roots (Figure 18). In cotyledons, larger GFP-2xFYVE vesicles were found in *fel2* and the reference line. On the contrary, in *fel9*, GFP-2xFYVE signals accumulated in the nucleus and the cytosol. These results highlight a differential response of *fel9* to Wortmannin, which suggests that *fel2* and *fel9* are likely independent mutants. In root cells, GFP-2xFYVE redistributed to the nucleus in all the tested plants (Figure 18 B). When the effect of BFA was tested in the reference line *Ler*/GFP-2xFYVE as well as in *fel2* and *fel9* mutants, we found that GFP-2xFYVE signals remained in endosomes upon BFA treatment (Figure 18 A). Interestingly, aggregations of GFP-2xFYVE compartments were present in cotyledons of *fel9* (Figure 18 A). BFA showed different effects in *fel2* and *fel9* mutants, again suggesting that they likely carry different mutations. Taking together these results of inhibitor treatment, we can conclude that GFP-2xFYVE compartments in mutant plants are endocytic components, since they are sensitive to Wortmannin. Since BFA treatment did not recruit them into BFA-bodies, we can conclude that the GFP-2xFYVE labelled compartment in the *fel2* and *fel9* mutants still possess late endosomal properties. The appearance of BFA-bodies in root cells observed from *fel2* and *fel9* suggests that endocytic recycling is occurring in these mutants.

The stronger GFP signals in *fel9* could be due to overexpression of the GFP-2xFYVE transgene. To exclude this possibility, semi-quantitative RT-PCR analysis comparing the GFP-2xFYVE mRNA levels of *Ler*/GFP-2xFYVE, M₃ of *fel2* and M₃ of *fel9* was performed. The data revealed similar transcript levels in *Ler*/GFP-2xFYVE and *fel9* but fewer in *fel2* meaning that there is probably no positive correlation between transcript levels and endosome numbers (Figure 19). This suggests phenotypes of *fel2* and *fel9* are caused by EMS-mutagenesis but not overexpression of the GFP-2xFYVE transgene. Besides, we also investigate the development of *fel2* and *fel9*. In M₃ and M₄ generation, only a small portion of *fel9* is viable and germinating. Mature *fel2* and *fel9* could only produce short siliques and low seed production (data not shown).

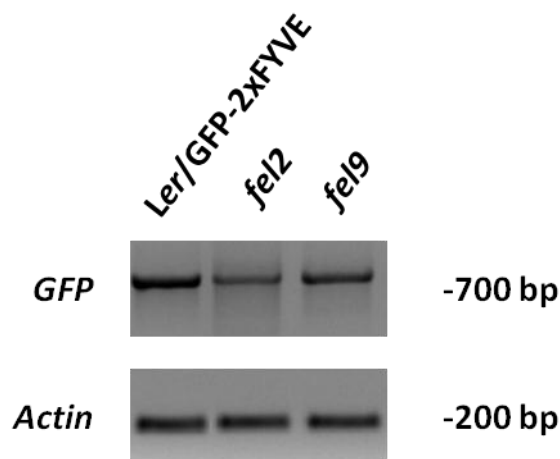


Figure 19. Transcript levels of GFP in *Ler/GFP-2xFYVE*, *M₃* of *fel2* and *M₃* of *fel9*. Semi-quantitative RT-PCR analysis of *GFP* expression in the reference line and mutant plants. Actin is shown as control. True leaves and cotyledons of two-week-old plants were used. This experiment was performed twice with similar results.

3.2.3 FYVE endosome levels differ significantly between *Ler/GFP-2xFYVE* and *Col-0/YFP-2FYVE* progenies for generating mapping populations

In order to identify the loci responsible for the altered endosomal numbers in the previously identified *fel* mutants, we generated mapping populations between *fel* mutants and *Col-0/YFP-2xFYVE*. *Col-0/YFP-2xFYVE* plants were generated by Vermeer et al., 2006. To gain insights into the variance of *GFP-2xFYVE* levels between *Col-0/YFP-2xFYVE* and the parental *Ler/GFP-2xFYVE* used for EMS mutagenesis, we evaluated *YFP-2xFYVE* endosomes in *Col-0* under screening conditions. We observed a significant decrease in *YFP-2xFYVE* levels compared to *GFP-2xFYVE* levels observed in *Ler/GFP-2xFYVE*. Whereas 479 ± 162 ($n=20$) endosomes were detected in *Ler/GFP-2xFYVE*, only 363 ± 24 ($n=16$) were detected in *Col-0/YFP-2xFYVE* (Figure 20 A; Supplementary Table 3). In addition, *Col-0/YFP-2xFYVE* showed frequently enlarged endosomal compartments (Figure 20 B), which were absent in *Ler/GFP-2xFYVE* as reported previously (Salomon et al., 2009).

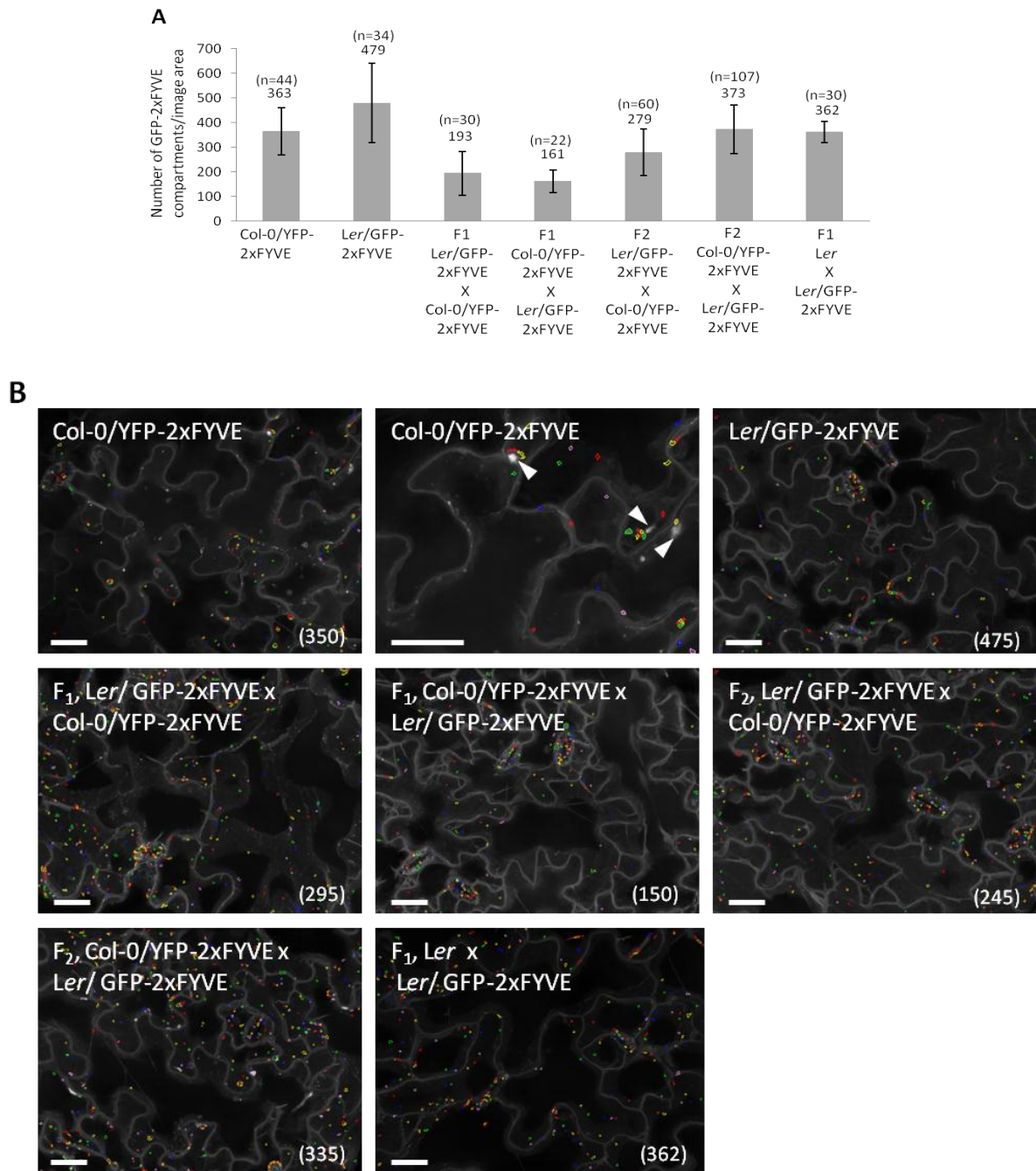


Figure 20. Quantification of YFP-2xFYVE and GFP-2xFYVE compartments in reference lines. Cotyledons of two-week-old reference lines and the reference line were measured. Representative images of (A) Average numbers of YFP-2xFYVE or GFP-2xFYVE compartments per 100% image area were calculated in reference lines. Bars and error bars indicate average and standard deviation. (B) Merged confocal microscopy images of Arabidopsis cotyledons expressing YFP-2xFYVE and GFP-2xFYVE. Number of recognized GFP/YFP-2xFYVE FYVE compartments is indicated in brackets. Recognized GFP/YFP-2xFYVE compartments are shown by coloured circles (scale bar = 50 mm).

The appearance of YFP-2xFYVE accumulates may be correlated with higher expression of YFP-2xFYVE in Col-0/YFP-2xFYVE compared to GFP-2xFYVE expression in Ler/GFP-2xFYVE and was also reflected by higher protein levels (Figure 21).

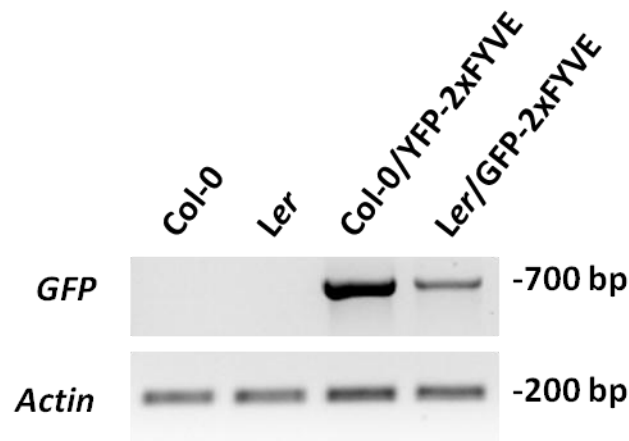


Figure 21. Transcript levels of GFP and YFP in Ler/GFP-2xFYVE and Col-0/YFP-2xFYVE. Semi-quantitative RT-PCR analysis of GFP and YFP expression in the reference lines. Actin is shown as control. This experiment was performed twice with similar results.

These quantitative and qualitative differences could potential influence the phenotypic analysis in mapping populations of *fel* mutants crossed to Col-0/YFP-2xFYVE. Therefore we generated bidirectional crosses between Ler/GFP-2xFYVE and Col-0/YFP-2xFYVE and evaluated GFP/YFP-2xFYVE endosome levels in the F₁ progenies. The F₁ progenies of Ler/GFP-2xFYVE crossed to Col-0/YFP-2xFYVE had 193 ± 90 (n=9) and 161 ± 47 (n=17) compartments/image area, respectively (Figure 20 A and B). This significant reduction in GFP/YFP-2xFYVE endosome levels is likely not only due to the heterocosity of *GFP-2xFYVE* transgene, since Ler/GFP-2xFYVE backcrosses to Ler wild type showed 362 ± 43 (n = 30) GFP-2xFYVE compartments/image area in F₁ progeny (Figure 20 A and B). It is rather possible that the co-existence of the *YFP-2xFYVE^{Col}* gene negatively influence the levels GFP-2xFYVE^{Ler}. This is supported by analyses of Ler/GFP-2xFYVE and Col-0/YFP-2xFYVE F₂ progenies. The average number of endosomes increased to 279 ± 95 (n=24) and 373 ± 99 (n=95) compartments/image area (Figure 20 A and B). These results indicate that the F₂ progenies of crossed reference lines recover the endosomal levels. If this is dependent on absence of YFP-2xFYVE^{Col-0} transgenes needs to be further analysed. It also suggest that endosomal numbers segregate dependent on the copy number variation of the two different transgenes, which could influence the phenotypic and segregation analyses in *fel* plants crossed to Col-0/YFP-2xFYVE F₂ mapping populations. To validate the assumption, analyses of endosomal levels in F₂ are in progress. It is still possible that endosomal levels are various

in different *Arabidopsis* ecotypes carrying the same GFP-2xFYVE transgene. To test the assumption, as well as to provide a tool for genetic dissection, introgression of GFP-2xFYVE from *Ler*/GFP-2xFYVE to Col-0 was generated to make the same transgenic construct at the same locus in these two ecotypes. *Ler*/GFP-2xFYVE was crossed to Col-0 to generate F₁ progenies. The F₁ progenies then served as one of the parent and were crossed to Col-0 again to generate F₂ seeds. This procedure was continued for eighth generation. At the eighth generation, the F₈ seeds were selfed to obtain homozygous GFP-2xFYVE in Col-0 background. So far, we finished the introgression in the eighth crosses and the GFP-2xFYVE level in Col-0 containing homozygous GFP-2xFYVE would be measured. The number of GFP-2xFYVE compartments was not analyzed yet but there was no enlarged GFP-2xFYVE compartment in the heterozygous line (Supplementary Figure 2).

3.2.4 *Fel* mutants showed different genetic inheritances

In order to investigate the genetic inheritances of *fel* mutants and to reduce mutations unlinked to the *fel* endosomal phenotypes, *fel* mutants were backcrossed to the reference line *Ler*/GFP-2xFYVE and *Ler* wild type. The backcross for *fel1* was attempted, but the resulting siliques did not contain any seed (Table 3). In F₁ progenies of backcrossed *fel9* to *Ler*, most siliques contain no seeds inside. In the F₁ backcross progenies of *fel2*, *fel6* and *fel9*, GFP-2xFYVE endosomal levels were restored to wild type levels (Figure 22; Table 3; Supplementary Table 4). This suggests that the mutations underlying the *fel* endosomal phenotypes are inherited in a recessive manner. Notably, *fel10* backcross lines contained similar endosomal levels to those detected in the M₃ generation (323 ± 52 GFP-2xFYVE compartments/image area) (Table 3 and Figure 15). *Fel10* x *Ler*/GFP-2xFYVE progenies showed similar endosome levels as *fel10* parental line, indicating a dominant inheritance of the *fel10* mutant locus.

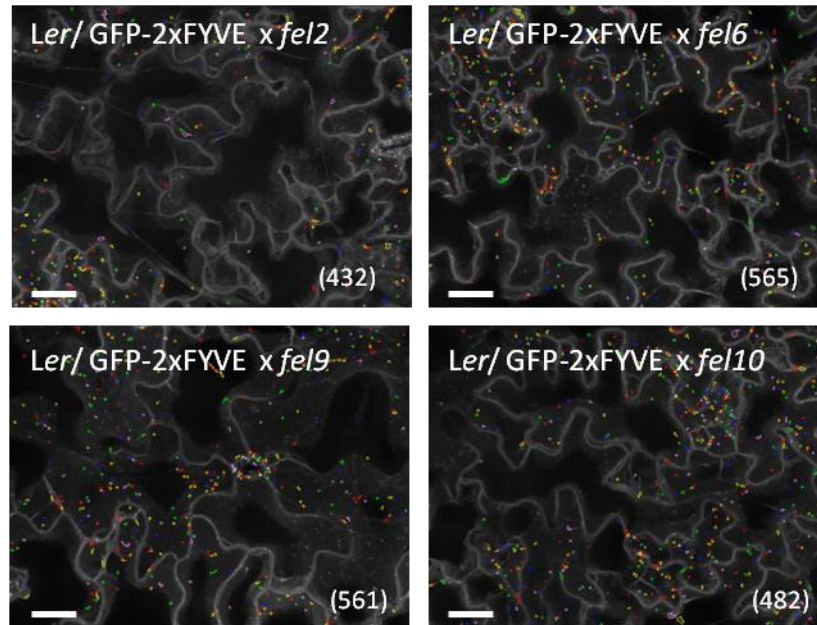


Figure 22. Detection of GFP-2xFYVE compartments in the F₁ *fel* mutants backcrossed to Ler/GFP-2xFYVE. Merged confocal microscopy images were taken from epidermal cells of *Arabidopsis* cotyledons expressing GFP/YFP-2xFYVE. Images were taken with the Opera microscope and analyzed with the Endomembrane script (Salomon et al., 2010). Recognized GFP/YFP-2xFYVE compartments are shown by coloured circles in representative images (scale bar=50 mm). Number of recognized GFP/YFP-2xFYVE compartments is indicated in brackets.

Table 3. Quantification of GFP-2xFYVE compartments in the F₁ of *fel* mutants backcrossed to Ler/GFP-2xFYVE. The average numbers and standard deviation (SD) of GFP-2xFYVE compartments/image area are indicated. Numbers of GFP-2xFYVE compartments/image area in individual plants are listed in Supplementary Table 4.

Cross (Female x Male)	Number of independent crosses	Number of plants displaying a wild type phenotype (200 to 800 compartments)	Number of plants displaying a mutant phenotype (<200 or >800 compartments)	Average Number of endosomes/image area ± SD
<i>Ler</i> /GFP-2xFYVE		34		479 ± 161
<i>Ler</i> /GFP-2xFYVE x <i>fel1</i>	3	No seeds production		N. D. ^a
<i>Ler</i> /GFP-2xFYVE x <i>fel2</i>	4	38	0	534 ± 102
<i>fel6</i> x <i>Ler</i> /GFP-2xFYVE	2	2	0	433 ± 48
<i>Ler</i> /GFP-2xFYVE x <i>fel9</i>	3	15	0	450 ± 85
<i>fel10</i> x <i>Ler</i> /GFP-2xFYVE	2	22	0	312 ± 58
<i>Ler</i> /GFP-2xFYVE x <i>fel10</i>	2	13	0	314 ± 63

^aN. D.=not detected

Endosomal levels in F₂ progenies of backcrossed *fel2*, *fel9*, and *fel10* were detected (Figure 23; Table 4). The F₂ of *fel2* backcrossed lines indicates recessive monogenic inheritance (Table 4). The F₁ progenies of *Ler* crossed to *fel2* are supposed to carry heterozygous GFP-2xFYVE transgene and FEL genes. Therefore, endosomal levels were measured in the F₂. In F₂ generation, the ratio of *fel2* phenotype was still low (Figure 23; Table 4). This again suggests homozygosity of GFP-2xFYVE transgene is correlated to endosomal levels and indicates the complexity of genetic screen for these endosomal mutants. Only a few mutant plants could be confirmed from F₂ backcrossed progenies of *fel9*. Only 5 out of 100 mutants were detected from F₂ of backcrossed *fel9* (Table 4). This indicates that *fel9* phenotypes are most likely associated with the effects of multiple genes. From *fel10* backcrossed F₂ lines, none of plants carried fewer than 200 GFP-2xFYVE compartments/image area. However, whether these F₂ progenies show true *fel* phenotype needs to be confirmed in the F₃ generation or needs to repeat the backcross.

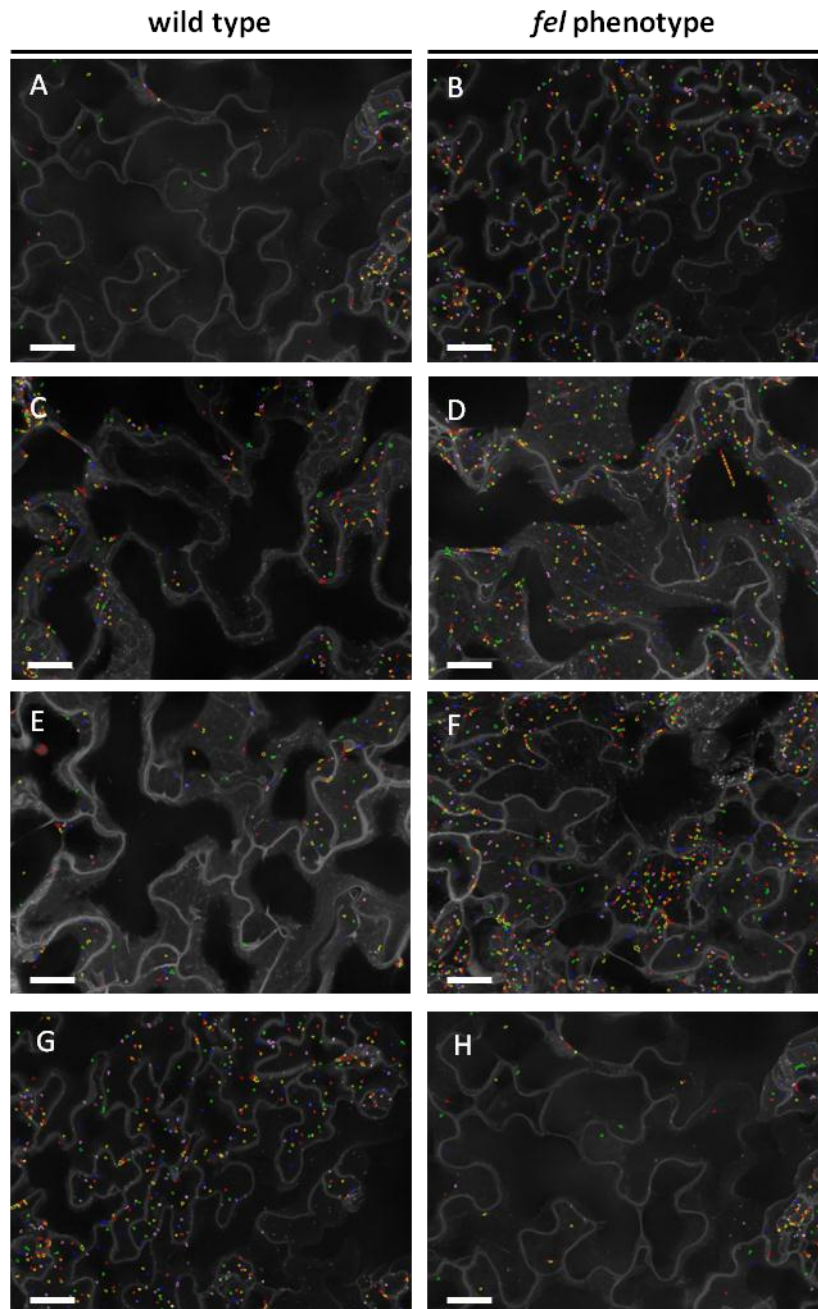


Figure 23. Detection of GFP-2xFYVE compartments in the F₂ of *fel* mutants backcrossed to Ler/GFP-2FYVE. Merged confocal microscopy images were taken from epidermal cells of Arabidopsis cotyledons expressing GFP/YFP-2xFYVE. Images were taken with the Opera microscope and analyzed with the Endomembrane script (Salomon et al., 2010). Recognized GFP/YFP-2xFYVE compartments are shown by coloured circles in Representative images (scale bar=50 mm). (A), (E), (G) *Fel2*, *fel9* and *fel10* crossed to Ler/GFP-2FYVE and (C) *fel2* crossed to Ler showed wild type phenotypes. (B), (F), (H) *Fel2*, *fel9*, and *fel10* crossed to Ler/GFP-2FYVE and (D) *fel2* crossed to Ler showed increased or reduced endosomal phenotypes.

Table 4. Quantification of GFP-2xFYVE compartments in the F₂ of *fel* mutants crossed to Ler/GFP-2xFYVE. The average numbers and standard deviation (SD) of GFP-2xFYVE compartments/image area are indicated.

Cross	Number of crosses	Wild type (200 to 800 compartments)		Mutant phenotype (<200 or >800 compartments)		Ratios of segregation
		Number of plants	Average Number of endosomes /image area	Number of plants	Average Number of endosomes /image area	
			± SD		± SD	
<i>Ler</i> /GFP-2xFYVE x <i>fel2</i>	2	51	609 ± 239	22	975 ± 164	2.31 : 1
		33	542 ± 142	12	955 ± 147	2.75 : 1
<i>Ler</i> x <i>fel2</i>	2	200	510 ± 105	3	1011 ± 7	66.6 : 1
<i>Ler</i> /GFP-2xFYVE x <i>fel9</i>		150	468 ± 133	4	1039 ± 170	37.5 : 1
<i>Ler</i> x <i>fel9</i>	2	No seeds production				
<i>fel10</i> x <i>Ler</i> /GFP-2xFYVE	2	37	482 ± 96	0	N. D. ^a	N. D. ^a
		37	396 ± 110	0	N. D. ^a	N. D. ^a
<i>Ler</i> /GFP-2xFYVE x <i>fel10</i>	1	36	441 ± 97	0	N. D. ^a	N. D. ^a

^aN. D.=not detected

3.2.5 Map-based cloning of *fel* mutant plants

Given the complex genetic behaviour of the *fel* mutations, we decided to use next generation sequencing techniques, in combination with a classical map-based cloning strategy as previously described in Ashelford et al., 2011. In this study, *Arabidopsis* Col-0 carrying YFP-2xFYVE transgene (Vermeer et al., 2006) was used to generate a mapping population. The genetic inheritances of outcrossed F₁ progenies were investigated. The numbers of GFP/YFP-2xFYVE compartments were like those in the wild type plants in the F₁ outcross progenies of *fel1*, *fel2*, *fel3*, *fel6*, *fel9* and *fel12* (Figure 24; Table 5; Supplementary Table 5). In the F₁ of *fel10* outcrossed progenies, there are fewer than 200 GFP/YFP-2xFYVE compartments/image area indicating a dominant inheritance (Figure 24; Table 5). However, the F₁ of *fel10* x Col-0/YFP-2xFYVE have similar endosome levels to the F₁ control plants (*Ler*/GFP-2xFYVE crossed to Col-0/YFP-2xFYVE), making it difficult to distinguish between wild type and mutant phenotype and not suitable for further mapping.

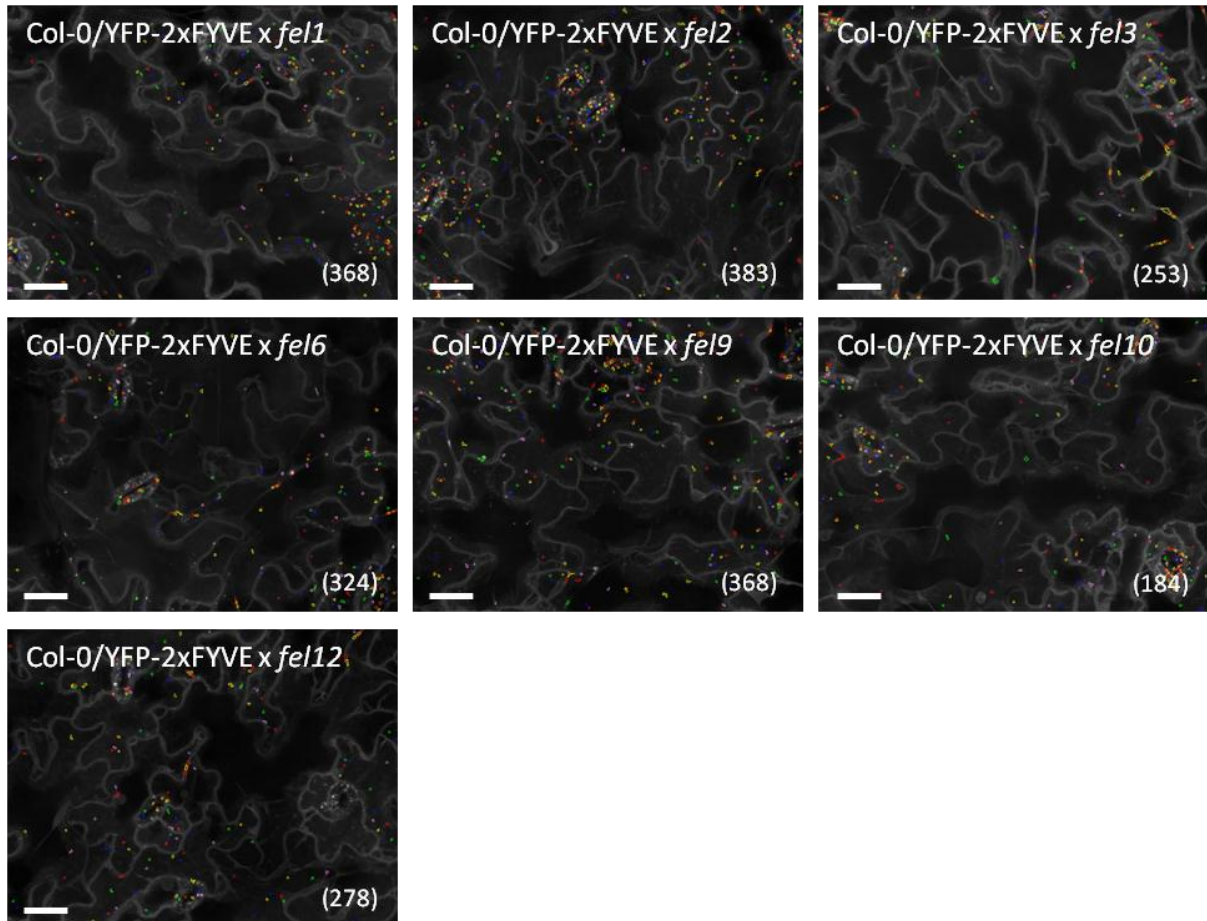


Figure 24. Detection of GFP-2xFYVE compartments in the F₁ of *fel* mutants outcrossed to Col-0/YFP-2FYVE. Merged confocal microscopy images were taken from epidermal cells of Arabidopsis cotyledons expressing GFP/YFP-2xFYVE. Images were taken with the Opera microscope and analyzed with the Endomembrane script (Salomon et al., 2010). Recognized GFP/YFP-2xFYVE compartments are shown by coloured circles in representative images of (scale bar=50 mm). Number of recognized GFP/YFP-2xFYVE FYVE compartments is indicated in brackets.

Table 5 Quantification of GFP-2xFYVE compartments in the F₁ of *fel* mutants crossed to Col-0/YFP-2xFYVE. The average numbers and standard deviation (SD) of GFP-2xFYVE compartments/image area are indicated. Numbers of GFP/YFP-2xFYVE compartments/image area in individual plants are listed in Supplementary Table5.

Cross	Number of crosses	Wild type phenotype (200 to 800 compartments)		Mutant phenotype (<200 or >800 compartments)	
		Number of plants	Average Number of endosomes /image area ±	Number of plants	Average Number of endosomes /image area ±
Col-0/YFP-2xFYVE x <i>fel1</i>	2	2	334 ± 48	0	N. D. ^a
Col-0/YFP-2xFYVE x <i>fel2</i>	4	14	306 ± 88	0	N. D. ^a
<i>fel3</i> x Col-0/YFP-2xFYVE	1	2	206 ± 51	0	N. D. ^a
Col-0/YFP-2xFYVE x <i>fel3</i>	1	3	214 ± 16	0	N. D. ^a
<i>fel6</i> x Col-0/YFP-2xFYVE	1	7	348 ± 68	0	N. D. ^a
Col-0/YFP-2xFYVE x <i>fel6</i>	1	8	283 ± 57	0	N. D. ^a
Col-0/YFP-2xFYVE x <i>fel9</i>	2	2	341 ± 39	0	N. D. ^a
<i>fel10</i> x Col-0/YFP-2xFYVE	1	0	N. D. ^a	4	147 ± 28
Col-0/YFP-2xFYVE x <i>fel10</i>	1	0	N. D. ^a	12	156 ± 26
<i>fel12</i> x Col-0/YFP-2xFYVE	1	4	147 ± 19	0	N. D. ^a
Col-0/YFP-2xFYVE x <i>fel12</i>	3	16	214 ± 40	0	N. D. ^a

^aN. D.=not detected

Phenotypic segregation of F₂ progenies of *fel* mutants outcrossed to Col-0/YFP-2xFYVE was investigated. Out of 3 independent F₂ families, we did not recover any plants showing the *fel3* endosomal phenotype (Table 6). One of the F₂ families of *fel10* crossed to Col-0/YFP-2xFYVE show a segregation of 1:3 ratio, which would support the idea of one single locus of *fel10*, which is inherited in a recessive manner. However, this contradicts the observed segregation of F₂ plants in *fel10* crossed to *Ler*/GFP-2xFYVE and the genetic inheritance shown from outcrossed F₁ progenies. The other F₂ progenies of *fel10* outcrossed to Col-0/YFP-2xFYVE indicate a recessive inheritance for *fel10* mutation (Figure 25; Table 6).

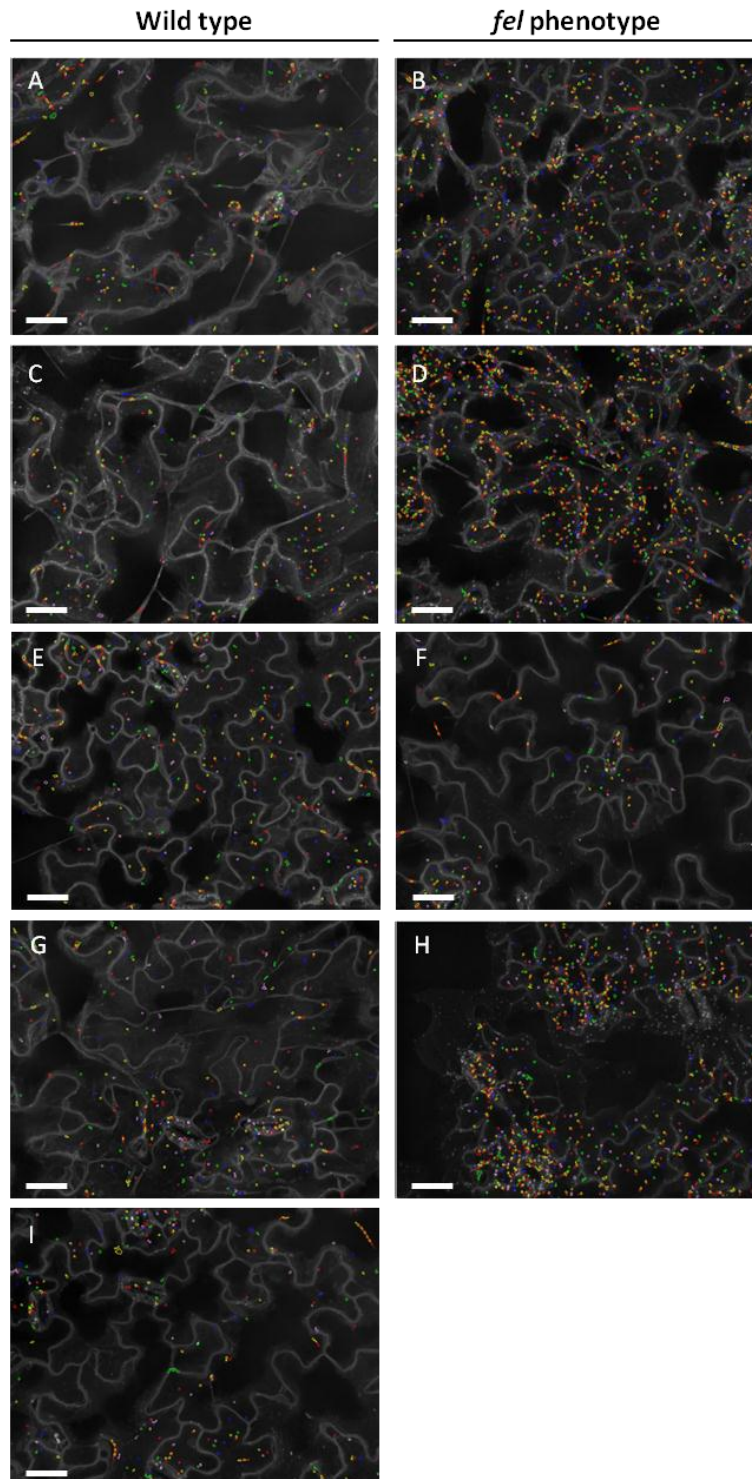


Figure 25. Detection of GFP-2xFYVE compartments in the F₂ of *fel* mutants outcrossed to Col-0/YFP-2FYVE. Merged confocal microscopy images were taken from epidermal cells of Arabidopsis cotyledons expressing GFP/YFP-2xFYVE. Images were taken with the Opera microscope and analyzed with the Endomembrane script (Salomon, 2009). Recognized GFP/YFP-2xFYVE compartments are shown by coloured circles in representative images (scale bar=50 mm). Number of recognized GFP/YFP-2xFYVE FYVE compartments is indicated in brackets. (A), (C), (E), (G), and (I) Outcrossed *fel2*, *fel9*, *fel10*, *fel12* and *fel3* showed wild type endosomal levels. (B), (D), (F), and (H) Outcrossed *fel2*, *fel9*, *fel10* and *fel12* showed increased or reduced endosomal phenotypes.

Plants containing more than 800 GFP/YFP-2xFYVE compartments/image area in the F₂ generation of outcrossed *fel2*, *fel9* and *fel12* were rarely found (Figure 25; Table 6). This data again suggest *fel2*, *fel9* and *fel12* are recessive and multigenic inheritances. This could result from the effect of reduced endosomal level as we observed in progenies of *Ler*/GFP-2xFYVE crossed to *Col-0*/YFP-2xFYVE. In some cases, enlarged GFP/YFP-2xFYVE compartments were found in F₂ outcrossed progenies, regardless of whether they showed *fel* mutant phenotypes or wild type (Supplmentary Figure 1). This reveals that reduced endosomal numbers and large agglomerates existing in *Col-0*/YFP-2xFYVE are still found in outcrossed F₂ progenies. For this reason, phenotypes with increased endosomal levels could be affected. Because outcrossed F₂ progenies contain homozygous or heterozygous or no GFP-2xFYVE transgene, which may determine endosomal levels, phenotypes with enhanced endosomal levels are possibly only detected in plants contain homozygous *FEL*(s) and homozygous GFP-2xFYVE transgene. In summary, the data showed that genetic analysis were hampered by differences between *Ler*/GFP-2xFYVE and to *Col-0*/YFP-2xFYVE parental lines, loss of GFP signal, and multiple loci.

Table 6. Quantification of GFP/YFP-2xFYVE compartments in the F₂ of *fel* mutants crossed to *Col-0*/YFP-2xFYVE. Phenotypic segregation is investigated in the F₂ progenies.

Cross	Number of crosses	Wild type phenotype (200 to 800 compartments)		Mutant phenotype (<200 or >800 compartments)	
		Number of plants	Average Number of endosomes /image area ± SD	Number of plants	Average Number of endosomes /image area ± SD
<i>Col-0</i> /YFP-2xFYVE x <i>fel2</i>	4	930	414 ± 75	25	715 ± 61
<i>fel3</i> x <i>Col-0</i> /YFP-2xFYVE	1	40	342 ± 110	0	N. D. ^a
<i>Col-0</i> /YFP-2xFYVE x <i>fel3</i>	1	40	302 ± 109	0	N. D. ^a
<i>Col-0</i> /YFP-2xFYVE x <i>fel3</i>	1	90	280 ± 112	0	N. D. ^a
<i>Col-0</i> /YFP-2xFYVE x <i>fel9</i>	2	850	390 ± 138	36	995 ± 168
<i>fel10</i> x <i>Col-0</i> /YFP-2xFYVE	1	106	326 ± 94	13	179 ± 12
<i>Col-0</i> /YFP-2xFYVE x <i>fel10</i>	1	87	303 ± 107	32	161 ± 29
<i>fel12</i> x <i>Col-0</i> /YFP-2xFYVE	1	48	436 ± 105	1	980
<i>fel12</i> x <i>Col-0</i> /YFP-2xFYVE	1	55	388 ± 111	1	807
<i>Col-0</i> /YFP-2xFYVE x <i>fel12</i>	1	55	345 ± 136	0	N. D. ^a

^aN. D.=not detected

3.2.6 Genetic characterization of *fel2* and *fel9*

Among most outcrossed F₂ progenies of *fel2*, we found the number of GFP/YFP-2xFYVE compartments ranges from 250-650 per image area (905 plants out of 930 plants, Figure 26 A). This suggests *fel2* phenotypes rarely recover in backcrossed progenies. As we found reduced endosomal levels in reference lines (F₁ of *Ler*/GFP-2xFYVE crossed to *Col-0*/YFP-2xFYVE), the endosomal level of F₂ progenies of *fel2* outcrossed to *Col-0*/YFP-2xFYVE may be affected. Therefore, we decided to change the selection criteria and F₂ with more than 650 were selected as *fel2* mutant phenotypes. With stringent selection criteria for plant with *fel* phenotypes, in F₂ progenies, 25 out of 930 of *fel2* crossed to *Col-0*/YFP-2xFYVE and 37 out of 850 *fel9* crossed to *Col-0*/YFP-2xFYVE carried *fel2* and *fel9* phenotypes could be identified (Figure 26). In order to investigate if *fel2* and *fel9* phenotypes were linked to genetic markers, we genotyped F₂ progenies with *Col-0*/*Ler* single sequence length polymorphism (SSLP) primers (Lukowitz et al., 2000). Rough mapping indicates that *FEL2* co-segregated with marker *ciw7* on chromosome 4. *FEL9* co-segregated with two genetic markers *nga 6* on chromosome 3 and *ciw7* on chromosome 4 (Table 7). To further narrow down the mutation loci, co-segregation of markers upstream and downstream of rough mapping position were tested. As shown in table 6, *FEL2* was presumably located between FCA1 and F18E5 (8.35 to 14.40 Mbp) on chromosome 4. *FEL9* co-segregated with both F24M12 and T20O10 (19.0 to 23.28 Mbp) on chromosome 3 and between FCA0 and F18E5 (8.8 to 14.4 Mbp) on chromosome 4. The rough mapping results reveals *FEL2* and *FEL9* co-segregated on the same position of chromosome 4 (Table 7). This raises the possibility that *FEL2* and *FEL9* could contain the same mutation in the rough mapping region.

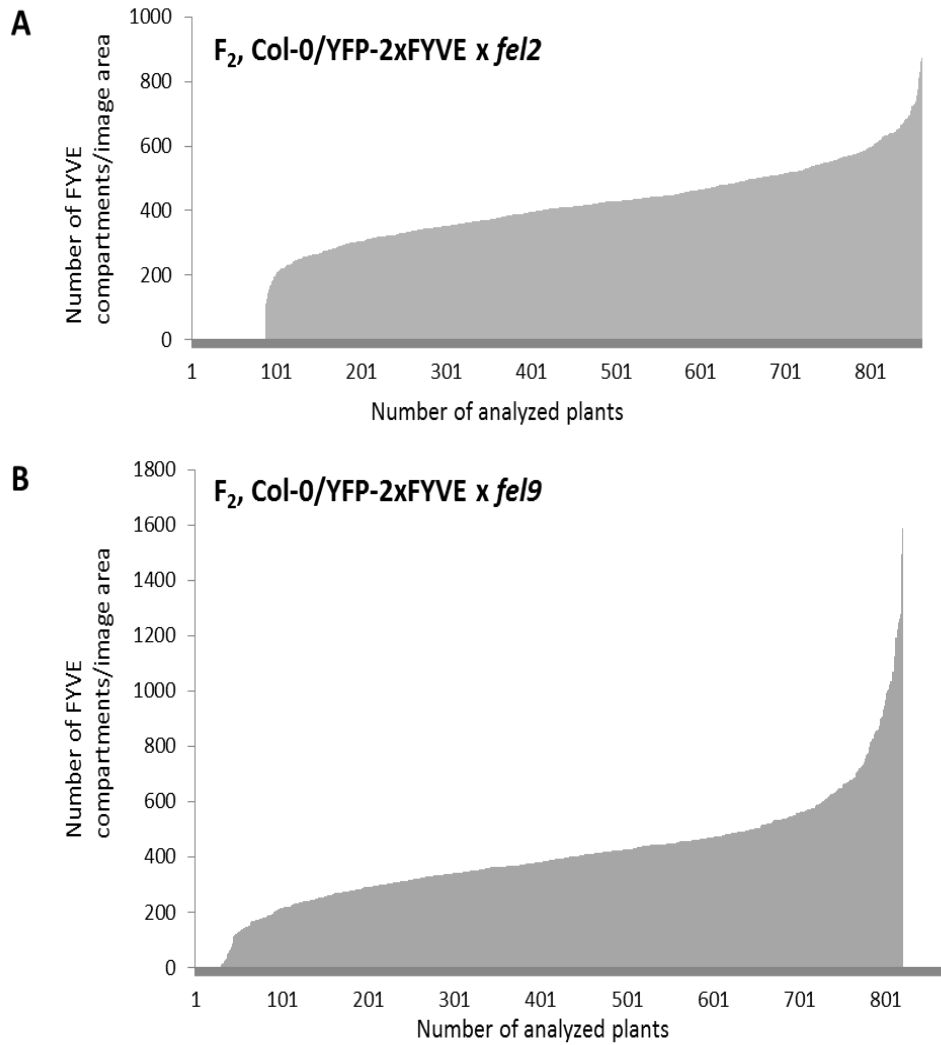


Figure 26. Distribution pattern of average endosomal numbers of F_2 progenies of *fel2* and *fel9* outcrossed to Col-0/YFP-2xFYVE respectively. Cotyledens of two-week-old plants were measured. Bars indicate the average endosomal number in each measured plant. (A) F_2 generation of Col-0/YFP-2xFYVE crossed to *fel2*. (B) F_2 generation of Col-0/YFP-2xFYVE crossed to *fel9*.

Table 7. Genetic mapping of *fel2* and *fel9* mutants.

Tested mutant	Genetic marker	Position (Mbp)	Number of recombinants	Number of analyzed plants
<i>fel2</i> (chromosome 4)				
	FCA1	8.35	1	25
	F28A21	10.28	1	25
	ciw7	11.52	0	25
	F7H19	12.10	2	25
	F27G19	13.69	0	25
	F26K10	14.01	0	25
	F18E5	14.40	5	25
<i>fel9</i> (chromosome 3)				
	F24M12	19.00	8	36
	T209	22.20	0	37
	Nga 6	23.00	4	37
	T20O10	23.28	5	36
<i>fel9</i> (chromosome 4)				
	FCA0	8.12	1	37
	F28A21	10.28	0	36
	F7H19	12.1	0	37
	F18E5	14.40	5	36

In order to identify causal SNPs for *fel2* and *fel9*, we took advantage of deep-sequencing using the Illumina sequence platform. Total DNA isolated from *Ler/GFP-2xFYVE*, M_3 of *fel2* plants and M_3 of *fel9* plants were sequenced with Illumina 76 bp paired-end reads. In total, more than 34.9 million reads were obtained from *Ler/GFP-2xFYVE* leading to an average coverage of 15.6x. More than 29.7 million reads with an average coverage of 16.7x were from *fel2* and more than 39.9 million reads with an average coverage of 44.5x were from *fel9* (Table 8). Subsequently, paired-end reads generated from *Ler/GFP-2xFYVE*, *fel2* and *fel9* were aligned to the Col-0 reference genome. In this study, we focused on SNPs because insertion and deletion are mostly not associated with EMS mutagenesis (Ashelford et al., 2011). There are 394 SNPs in 200 genes shared by *fel2* and *fel9* M_3 plants. Although allelic crosses between *fel2* and *fel9* were not generated, subcellular phenotypes from figure 19 suggests *fel2* and *fel9* may be different mutant plants. Identical SNPs shared by *Ler/GFP-2xFYVE*, *fel2* and *fel9* were filtered out. In *fel2*, 65 SNPs were non-synonymous in coding regions in rough mapping intervals (Table 8; Supplementary Table 6). In *fel9*, there were 24 and 71 non-synonymous SNPs in the coding region on chromosome 3 and chromosome 4 rough mapping positions (Table 8; Supplementary Table 7). Because *fel9* phenotype co-segregated with two genetic loci and made it more difficult to identify genes responsible for *fel9*, we focused on investigation of SNPs in *fel2* mutant plants. From *fel2*, 9 genes contain non-synonymous SNPs and may be linked to membrane trafficking were

further analyzed by classical Sanger sequencing (Table 9). All showed the same nucleotide sequence in *fel2* and *Ler/GFP-2xFYVE*, and thus are likely *Ler* polymorphisms or wrong annotations of the Col-0 reference genome.

Table 8. Whole genome sequencing of *Ler/GFP-2xFYVE*, *fel2* and *fel9*.

Detected lines	Row Paired-read counts	Percent total pairs mapped	Aligned Coverage	SNPs identified in mapping region ^a
<i>Ler/GFP-2xFYVE</i>	34993993	36.76	15.516	Not detected ^b
<i>fel2</i>	29713523	46.70	16.74	65
<i>fel9</i>	39999987	92.29	44.53	24 ^c and 71 ^d

^aNon-synonymous SNPs in coding sequence. ^bSNPs shared with *Ler/GFP-2xFYVE*, *fel2* and *fel9* were removed. ^cSNPs identified in mapping region from chromosome 3. ^dSNPs identified from mapping region from chromosome 4.

Table 9. *In silico* prediction and validation of *fel2* SNPs.

Gene	Description	Chr.	Position	Ref. ^a	SNP	Re-seq.
AT4G14330	phragmoplast-associated kinesin-related protein 2	4	8244771	G	A	<i>Ler</i> SNP
AT4G14370	TIR-NBS-LRR class disease resistance protein	4	8279965	G	A	<i>Ler</i> SNP
AT4G17350	phosphoinositide binding	4	8898535	G	A	<i>Ler</i> SNP
AT4G17850	hypothetical protein	4	9923743	A	G	<i>Ler</i> SNP
AT4G18770	MYB98 (myb domain protein 98)	4	10311404	G	A	<i>Ler</i> SNP
AT4G35380	SEC7-like guanine nucleotide exchange family protein	4	10617931	G	A	<i>Ler</i> SNP
AT4G19490	VPS54	4	10622695	A	C	<i>Ler</i> SNP
AT4G19570	chaperone DnaJ-domain containing protein	4	10665434	A	C	<i>Ler</i> SNP
AT4G35310	calmodulin-domain protein kinase 5	4	16803335	G	A	<i>Ler</i> SNP

^aReference according to Col-0 genome. A = Adenine, C = Cytosine, G = Guanine, T =Thymine

To confirm *fel2* and *fel9* phenotypes in the F₃ families, at least 20 individual F₃ plants from independent F₂ families were inspected. Endosomal numbers in F₃ progenies from outcrossed F₂ plants showing *fel2* and *fel9* phenotypes were measured but endosomal levels varied in each of independent F₃ families (Figure 27; Table 10). *Fel2* phenotype was rarely reproducible in detected F₃ progenies indicating *fel2* mutation is not inherited in the F₃ (Table 10). F₃ families of outcrossed *fel9*, we found *fel9* phenotype is reproducible in one family. *Fel9* phenotype segregated in other investigated F₃ outcrossed lines (Table 10). This suggests endosomal phenotypes are subtle and phenotypes of *fel2* and *fel9* identified in F₂ could be false positive.

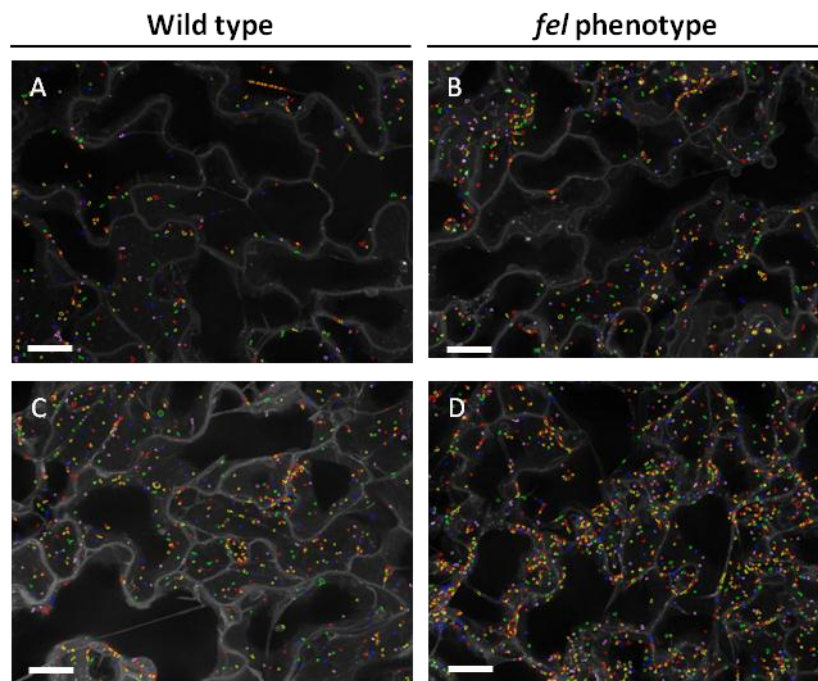


Figure 27. Detection of GFP-2xFYVE compartments in the F₃ of *fel2* and *fel9* outcrossed to Col-0/YFP-2FYVE. Merged confocal microscopy images were taken from epidermal cells of Arabidopsis cotyledons expressing GFP/YFP-2xFYVE. Images were taken with the Opera microscopy and analyzed with the endomembrane script. Recognized GFP/YFP-2xFYVE compartments are shown by coloured circles in representative images (scale bar=50 mm). Number of recognized GFP/YFP-2xFYVE FYVE compartments is indicated in brackets. (A) and (C) Outcrossed *fel2* and *fel9* showed wild type endosomal levels. (B) and (D) Outcrossed *fel2* and *fel9* showed increased endosomal phenotypes

Table 10. Quantification of GFP-2xFYVE compartments in the F₃ of *fel2* and *fel9* outcrossed to Col-0/YFP-2xFYVE. Numbers of GFP/YFP-2xFYVE compartments/image area in individual plants are measured.

F ₃ Col-0/2xFYVE x <i>fel2</i>		F ₃ Col-0/2xFYVE x <i>fel9</i>	
Number of plants displaying a wild type phenotype (200 to 800 compartments)	Number of plants displaying a <i>fel2</i> phenotype (>800 compartments)	Number of plants displaying a wild type phenotype (200 to 800 compartments)	Number of plants displaying a <i>fel9</i> phenotype (>800 compartments)
22	0	0	24
19	8	17	8
18	0	14	11
12	0	7	18
12	0	8	17
21	0	8	17
16	1	6	18
20	3	1	24
15	1	3	13
19	2	0	24
21	0	0	24
19	1	0	23
14	1	21	0
13	1	16	5
22	2	11	5
13	2		

In summary, different numbers of GFP-2xFYVE positive endosomes was found in *Ler*/GFP-2xFYVE and *Col*/YFP-2xFYVE reference lines suggesting the endosomal levels may vary in different ecotypes of Arabidopsis. *Fel1*, *fel2*, *fel3*, *fel6*, *fel9*, and *fel12* revealed genetically recessive mutations while *fel10* was possibly a dominant allele. Two mutants, *fel2* and *fel9* exhibited more GFP-2xFYVE compartments than wild-type reference plants. These two mutants are affected in endosome trafficking and *fel2* is likely tissue specific. The results derived from backcrosses and outcrosses reveal the complexity of genetic screen for these endocytic trafficking mutants. Still, we identified gene loci by classical mapping and whole genome sequencing. Investigation of genes in the rough mapping region will unravel regulators of endocytosis or MVBs biogenesis. *Fel* mutant plants may serve to study molecular mechanisms for membrane trafficking as well as subcellular rearrangements in plant-pathogen interactions.

4. DISCUSSION

4.1 Imaging the *Arabidopsis-Hpa* interaction

Hpa is a widely used pathogen of *Arabidopsis* to study its pathogenicity and ETI; however the subcellular interactions between the plant and the pathogen are fully understood. TEM studies provide high resolution images to describe the ultrastructure of the haustorium and the interface between hosts and pathogens (Mims et al., 2004). Still, the dynamics of subcellular compartments cannot be observed by this method and thus these structural studies must be complemented by live-cell imaging to fully understand the nature of the interactions. During *Hpa* infection, the haustorium is spreading out into the host cell. The EHM serves as the interface between the haustorial body and the plant cell. It is thought to be the site where pathogens and hosts exchange molecular materials including nutrients (O'Connell and Panstruga, 2006). There is little information regarding the biogenesis of the EHM. In order to gain an understanding of the rearrangements of subcellular compartments during haustorial development and the formation of the EHM, this study has used live-cell imaging with CLSM. We compared subcellular localization around the haustorium, the encased haustorium and uninfected cell. Also this work provides information about possible compositions of the EHM and the haustorial encasement (Figure 28).

4.1.1 PM-residing proteins are excluded from the EHM selectively

PM markers including three aquaporins, the syntaxin AtVAMP3 and the brassinosteroid receptor BRI1 are absent from the EHM of *E. cichoracearum* suggesting the EHM contains different components from the plant PM (Koh et al., 2005). In this study, the aquaporin PIP1;4, the PM-localized protein, was not detected at the EHM suggesting that different plant pathogens exclude aquaporins during the formation of their feeding structures. Since aquaporin plays a role in the transport of water or small uncharged solutes (Maurel and Chrispeels, 2001), pathogens may utilize their own aquaporin to conduct water molecular from or to the host cell if the EHM acts as an interface for exchange. The hexose transporter HXT1 (Voegelé et al., 2001) and the sugar transporter SWEET12 (Chen et al., 2010) have both been implicated in the transport of sugars between host and pathogen. In the arbuscular mycorrhizal symbiosis, the fungal symbiont penetrates the cortical cells of the roots and forms differentiated hyphae, arbuscules. As arbuscules develop, subcellular reorganization and formation the periarbuscular membrane which is continuous with the plant plasma membrane occurs in the cortical cell (Pumlin et al., 2009). While arbuscules are enveloped by the periarbuscular membrane, haustoria are surrounded by the EHM. The periarbuscular membrane plays a role in nutrient exchanges between symbionts and host plants (Parniske,

2008). The phosphate transporter MtPT4 localizes specifically to the periarbuscular membrane between arbuscules and the host cell in the symbiotic interaction between arbuscular mycorrhizal fungi and plants (Javot et al., 2011). It is likely that in the *Arabidopsis-Hpa* interactions there are similar host-derived transporters that are found specifically in the EHM and function in nutrient exchange, but these remain to be identified. It is also possible that *Hpa* provides its own aquaporin for water exchange since aquaporins have been identified in filamentous fungi (Tanghe et al., 2006; Aroca et al., 2009).

Another studied aquaporin, PIP2a, is found in vesicular structures close to the PM in the *E. cichoracearum* infected cell at 8 to 14 hours after inoculation when penetration pegs and young haustoria are formed (Koh et al., 2005). In this study, PIP1;4 labelled membrane was not observed around haustorium. This suggests either that the host cells exploit different mechanisms in response to different pathogens or that there is specificity in the rearrangement of compartments labelled by PIP2a and PIP1;4 in response to pathogen invasion.

The Ca²⁺ ATPase ACA8 was not observed at the EHM in this study, consistent with previous reports ATPases are not present in the EHM of obligate biotrophic pathogens (O'Connell and Panstruga, 2006). Again this raises the question of how ion exchange occurs across the EHM. For both PIP1;4 and ACA8 these proteins remained in the PM during *Hpa* infection allowing the conclusion that the PM is distinct from the EHM. PIP1;4 and ACA8 are also absent from the EHM of *Phytophthora infestans* (*Pi*) (Lu et al., 2012) indicating commonalities in the composition of the EHM across two oomycete species.

The PM is continuous with the EHM (Soylu and Soylu, 2003) and therefore there must be a barrier that prevents diffusion of the PM resident proteins into the EHM or there must be a biochemical change in the composition of the membrane such that the EHM is an unfavourable environment for PM proteins. The latter hypothesis is unlikely to occur as the PM resident protein PEN1 was detected at the EHM of *Hpa*. This is consistent with previous work that observed PEN1 at the EHM of young haustoria of *Colletotrichum* but not in mature ones (Shimada et al., 2006). In this study, vesicle-like structures containing GFP-PEN1 appeared in the infected cell, indicating PEN1 was likely secreted to the EHM via vesicles. This suggests that GFP-PEN1 present at the EHM did not originate from diffusion of the GFP-PEN1 pool already present on the PM but was derived from either *de novo* synthesis or endocytic recycling. PEN1 is important for penetration resistance (Collins et al., 2003; Kwon et al., 2008, Meyer et al., 2009). PEN1 is excluded from the EHM during infection of adapted powdery mildew (Collins et al., 2003) but is present in the EHM of *Hpa*. This suggests localization of PEN1 varies between different pathosystems and supports that PEN1 is not necessary for immunity against virulent *Hpa* (Kwon et al., 2008).

Extracellular obstruction of diffusion accompanied by PM composition changes occurs in the root endodermis. The casparian strip domain (CSD) serves as a diffusion barrier. Specific casparian strip membrane domain proteins (CASPs) have been identified that involve the formation of this structure (Roppolo et al., 2011). Since the EHM and CSD both contain electron-dense layer and are continuous from the PM (Mims et al., 2004; Roppolo et al., 2011), it is possible that these two structures share functional and biochemical similarities.

Since RLKs provide a role in immunity when perception of PAMPs/MAMPs, pathogens possibly try to exclude such receptors or to avoid the detection of PAMPs and escape from plant innate immunity. It has been shown that pre-treatment with flg22 or Chitin reduces *Hpa* hyphal colonization in Arabidopsis (Fabro et al., 2011). Moreover, PTI responses are attenuated in host tissues where high numbers of haustoria are established. This again suggests *Hpa* have to overcome or eliminate PTI to successfully infect host cells (Fabro et al., 2011). Recently, the RLK SERK3/BAK1 was shown to contribute to basal resistance against *Pi* in *N. benthamiana* (Chaparro-Garcia et al., 2011) indicating host cells use the similar defence strategies to detect bacteria and oomycetes. The PM resident receptor like kinase, BRI1, is excluded from the EHM of *G. cichoracearum* (Koh et al., 2005). We have shown that another RLK, FLS2 localizes at the EHM of *Hpa*. Recent study reveals FLS2 and EFR are absent around *Pi* haustoria (Lu et al., 2012). This raises the possibility that RLKs are recruited to the EHM selectively (Figure 28). While these studies examined different patho-systems, it is possible that FLS2 is targeted to the EHM because of its defence associated functions, or that gene up-regulation in response to pathogen invasion causes *de novo* synthesis of FLS2 which is targeted non-specifically to the EHM along with other secretory material.

4.1.2 Vesicle trafficking in haustoria containing cells

Secretory vesicles and exocytosis are supposed to contribute to the formation of papillae and the haustorial encasements (Meyer et al., 2009). In this study, accumulation of Golgi around the haustorium was investigated from the epidermal cell and the mesophyll cell. The localization of Golgi bodies around the haustorium implies that secretion is occurring from the host cell to the pathogen. Polarization of secretory vesicles may transport proteins such as PEN1 and FLS2 to the PM as well as the EHM. In contrast to what we observed, Takemoto et al (2003) reported the preferential localization of Golgi stacks at the neck rather than the haustorium of *Hpa* in the epidermal cells of Arabidopsis Col-0. The difference of these two studies might come from the two different pathosystems that were examined. While images were taken in compatible interaction of *Hpa* Waco 9 and Arabidopsis Col-0, Takemoto et al (2003) examined the incompatible *Hpa* isolate Cala 2 applied to *A. thaliana* Col-0. From TEM, small vesicles in the host-cell cytoplasm very near the EHM are observed and some of these vesicles appeared to be in the process of either fusing with or budding off the EHM (Mims et

al., 2004). Therefore, it is possible that in the incompatible interaction, secretory vesicles contribute to build up physical barrier at the penetration site, while in the compatible interaction, secretory vesicles contribute to the biogenesis of the EHM (Figure 28). While YFP-SYP32 and YFP-Got1p were detected in vesicles around *Hpa* haustorium, no accumulation of these two proteins was observed at *Pi* haustoria with exception of encased ones (Lu et al., 2012). The differences in localization of Golgi markers in *Hpa* and *Pi* haustorium infected cells demonstrates specific preference between both oomycetes in the use of secretory vesicles during haustorium development, which may determine the specific exclusion of PM-resident proteins from the EHM that was observed.

The Arabidopsis RPW8.2, provides broad-spectrum resistance against powdery mildew pathogens, and overexpression of *RPW8.2* enhances immunity against *Hpa* (Xiao et al., 2003; Wang et al., 2007). RPW8.2-YFP specifically labels the EHM and is targeted to the EHM by host-derived vesicles in Arabidopsis infected by *G. cichoracearum* UCSC1 and *G. orontii*. This suggests RPW8.2 is involved in the biogenesis of the EHM (Wang et al., 2009; Micali et al., 2011). In Arabidopsis infected by *Hpa*, RPW8.2-YFP containing vesicles could be found around the EHM and at the periphery of infected host cells. RPW8.2-YFP remained punctuate around the haustorium indicating no internalization of this protein into the EHM, consistent with previous reports (Caillaud et al., 2012). RPW8.2-YFP was expressed in plant cells containing haustoria, suggested gene expression was triggered upon pathogen infection or after the formation of the haustorium. Because the penetration sites were not easily to identify during *Hpa* infection, the exact time for *RPW8.2* expression could not be monitored in this study. Evenly distribution of RPW8.2-YFP at the EHM was rarely found in this study as reported by Wang et al (2009). This raises a possibility that plants response to different pathogens in different manners (Wang et al., 2009; Micali et al., 2011; Caillaud et al., 2012).

Accumulation of MVBs around the *Bgh*-induced papillae (An et al., 2006a, b) and clathrin-coated vesicles around the penetration site in *U. vigneae* infected epidermis cells (Xu and Mendgen., 1994) indicates that MVBs and endosomal compartments participate in plant-pathogen interactions. To investigate the behaviour of endosomal compartments after *Hpa* infection, different endosomal markers labelling either TGN, BFA sensitive compartments or MVBs were examined. Interestingly, all tested endocytic vesicles closely localized around the haustorium of *Hpa* suggesting a role in biogenesis of the EHM. In *Pi* infected cells, YFP-VTI12 and GFP-2xFYVE are not associated with the haustoria (Lu et al., 2012). This suggests subcellular rearrangement differs from different pathosystems. We used BFA treatment to test recycling processes in *Hpa* infected cells. It resulted in formation of BFA-bodies in *Hpa* infected cells, which means EEs are trapped and endocytic or recycling pathways are interfered by BFA. These results suggest that endocytic pathways are still functional in infected cell. This further raises the possibility that endocytic vesicles function to the biogenesis of the EHM and selective recruitment of PM-localized proteins.

Time-lapsed images revealed that GFP-2xFYVE compartments moved both towards the haustorial neck and away from the haustorium along cytoplasmic strands. Some vesicles did not move but stayed at the same position. Golgi stacks have previously been observed to show movement via cytoplasmic strands at the penetration site in the interaction between *Hpa* and *Arabidopsis* (Takemoto et al., 2003). Just as Golgi stacks may be recruited to sites for secretion, there could be hot spots for MVBs to stop at certain sites around the haustorium for endocytic recycling. MVBs sort cargo and exosomes, fusing with the PM to release exosomes into paramural space (Meyer et al., 2009). It is possible that accumulation of MVBs around the haustorium facilitates releasing of plant material and helps maturation of the EHM or formation of the haustorial encasement.

TEM images showed that the central vacuole occupied most of the space of the host cell, resulting in limited volume between the EHM and the tonoplast (Mims et al., 2004). In *Hpa* infected cells, the large central vacuole retained its volume and continuous tonoplast surrounded the haustorium. Similar studies reveal that the central vacuole maintains its shape at 4 dpi, but intravacuolar invaginations made of a double tonoplast membrane are found around the haustoria at 6 dpi (Caillaud et al., 2012). This indicates *Hpa* infection may interfere turnover of the vacuolar membrane (Caillaud et al., 2012). Distribution of the cytoplasm marked by GFP is consistent with the previous studies (Mims et al., 2004; Caillaud et al., 2012). Polarity of the plant cell nucleus directed to the haustorium was detected in this study. This is consistent with a close association between the plant cell nucleus and haustoria and the plant cell nucleus is positioned near to the haustorium in infected cells along the growing hyphae (Caillaud et al., 2012). This movement is possibly mediated by the actin skeleton in infected cells (Ketelaar et al., 2002; Iwabuchi et al., 2010). This raises the possibility that the haustorium directly influences nuclear position. Recent evidence suggests that the plant cell nucleus is one of the main targets for pathogen effectors. Oomycete effectors detected from *Pi* reveal that CRINKLER (CRN) effectors target the nucleus (Schornack et al., 2010). In addition, subcellular localization of the *Hpa* effector repertoire shows that the plant nucleus and membrane network are the main targeted compartments (Caillaud et al., 2012).

4.1.3 Membrane compartments around the encasement

Matured haustoria are enveloped by cup-shaped haustorial encasements, a double layered structure containing callose and deposition of plant cell wall material (O'Connell and Panstruga, 2006; Meyer et al., 2009). In *Hpa*, the encasement appears at 4 dpi. This layer provides a second mechanism for defence against the invading pathogen. It is likely that haustorial encasements restrict the uptake of nutrients to the haustorium and transportation of effectors to host cells. At the same time the encasement will also likely prevent the delivery of toxic defence molecules produced from plant cell that cause damage to pathogens (Wang et al., 2009). PEN1, SNAP33 and PEN3 are potentially involved in the

secretion of toxic compound to pathogens via secretory vesicles, being preferentially incorporated to the encasement for this purpose (Meyer et al., 2009).

In this study, localization of membrane compartments around the encasement of *Hpa* was monitored. The PM marker PEN1 labelled the EHM while PIP1;4, NPSN 12 and ACA8 were absent from the EHM. PIP1;4, NPSN 12 and ACA8 were, however, observed in encasements. Proteins that label secretory and endocytic vesicles were accumulated at the encasements (Figure 28). Previous observations suggest that RPW8.2 promotes haustorium encasement (Wang *et al.*, 2009; Micali et al., 2011). RPW8.2 distributes uniformly at the encasements and this is different from vesicular structures observed around the haustoria. These results suggest that components of the plant PM constitute the encasement and also indicate the different natures of the encasement and the EHM of *Hpa*. In this study, secretory and endocytic vesicles localized around the encasements and in some cases, marker proteins were found labelling the encasements. This supports the model that plant secretory vesicles and MVBs are delivered to the haustorial encasement (Micali et al., 2011). Therefore, we can conclude that the processes of secretion and endocytosis are crucial to the formation of haustoria and the encasement. The polarized distribution of vesicles, i.e. that they accumulated at haustoria, indicates that membrane trafficking is a fundamental process required for the biogenesis of the encasement.

Live-cell imaging, together with tagging of membrane compartments with fluorescent markers, has been successfully used in this study to examine subcellular rearrangements in a plant-pathogen interaction. Moreover, this study provides evidence for commonalities and differences between fungal, *Hpa* and *Pi* oomycete EHMs and has established that membrane trafficking plays a role in selective recruitment of PM proteins to the EHM (Figure 28). Future studies are required to provide additional molecular tools to decipher which known or unknown EHM constituents are transported into the EHM/haustoria through the secretory or endocytic pathway. Another challenging question for future studies is to identify how subcellular rearrangements occur. What are the key components and is there a signal that triggers the redirection of trafficking pathways? How do pathogen effectors perturb the accumulation of plant proteins at the EHM and around haustoria? Pathogenicity and development of *Hpa* encasement could be investigated by mutant studies in *Arabidopsis* with disturbed membrane trafficking. Chemical interferences of membrane trafficking would also help to address the role membrane trafficking in encasement biogenesis and *Arabidopsis-Hpa* interactions. New cell biological approaches such as advanced live-cell imaging techniques (Salomon et al., 2010) provide a tool to disclose further secrets of the battle between plant and pathogen and possibly reveal novel aspects of plant cell biology.

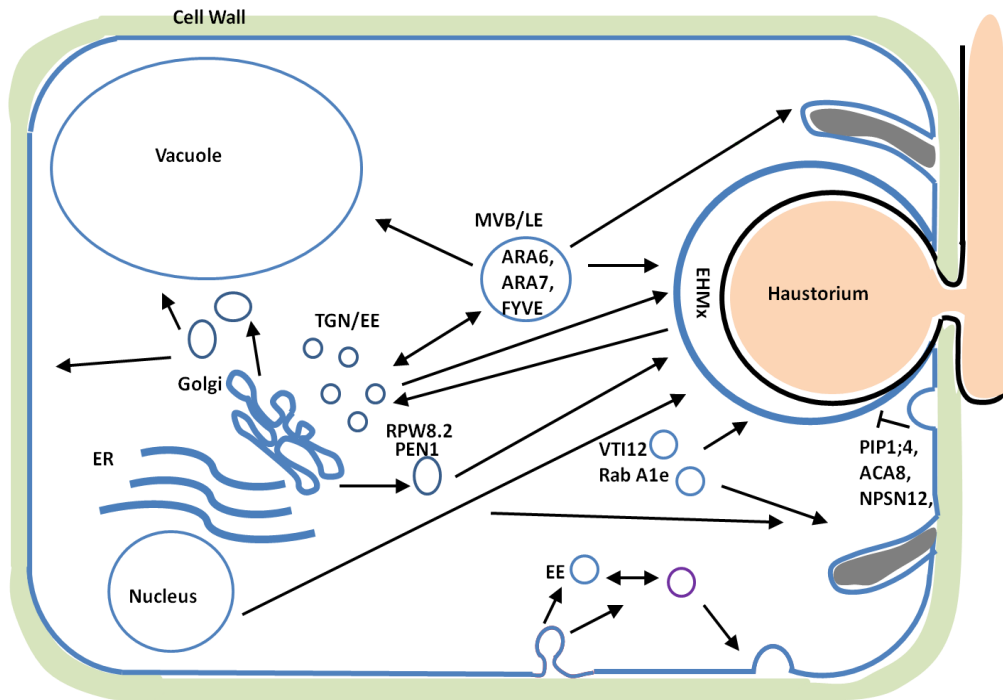


Figure 28. Schematic diagram representing putative vesicle dynamics at the *Arabidopsis*–*Hpa* interface. The PM-resident proteins are selectively excluded from the EHM. Secretory vesicles localize around the haustorium and possibly deliver material to the EHM. A large number of endosomal compartments localize around the haustorium and the encasement suggest their role in the formation of the EHM and the encasement. PM, plasma membrane. EHM, extrahaustorial membrane. EE, early endosomes. MVB/LE, multi vesicular body/late endosome. ER, endoplasmic reticulum.

4.2 A genetic screen to identify membrane trafficking components using a quantitative microscopic platform

4.2.1 Identification of *fel* mutants

To better understand how membrane trafficking machinery functions in plant cells we must identify the subcellular components involved in these pathways. To that aim, imaging-based forward genetic screens have already been shown to be successful (Boulaflous et al., 2008; Takana et al., 2009; Saito et al., 2011). A genetic screen based on the confocal analysis of individual M₂ Arabidopsis plants expressing a Golgi marker was performed for the identification of genes responsible for the morphological and functional integrity of the plant Golgi (Boulaflous et al., 2008). With BFA treatment and fluorescence imaging, *Arabidopsis thaliana* mutants defective in internalization of proteins (*BFA-visualized endocytic trafficking defective1*, *ben1*) were identified (Tanaka et al., 2009). SGR2 (shoot gravitropism) was also identified in a genetic screen as having a function in the formation and/or maintenance of sub-regions of vacuoles or bulbs (Saito et al., 2011). Most fluorescence-based screens in plant cells assessed qualitative phenotypes, i.e. presence or absence of a given fluorescent fusion protein in its expected sub-cellular localization. Without a highthrough-put imaging platform, it is laborious to perform genetic screen by examining qualitative phenotypes and may not allow obtaining informative quantitative properties efficiently. Quantitative imaging using high-resolution, multidimensional confocal imaging and a software tool designed for automated processing of multichannel three dimensional image data was described in *Saccharomyces cerevisiae* (Wolinski et al., 2009). Recently, this automated multichannel imaging has been applied in studying membrane trafficking in plant cells (Salomon et al., 2010).

Such high throughput confocal imaging system makes it possible to examine membrane compartments in a quantitative and automated manner (Salomon et al., 2010). Thus, this technology allows us to perform an unbiased quantitative study of sub-cellular compartments, a type of study which is rarely performed due to its laborious nature. Taking advantage of this automated microscopic platform and the use of a fluorescent marker that labels MVBs, we aimed to dissect the regulatory mechanisms underlying membrane trafficking in plants, and unravel the possible involvement of this process in plant immunity. In a previous study performed in the lab, 12 mutants with altered numbers of GFP-2xFYVE compartments were identified (Salomon, 2009). No additional *fel* mutants could be characterized and confirmed in the M₃ generation although altered endosomal levels were initially detected in a secondary screen performed on additional M₂ plants (this study). This failure to reconfirm these additional *fel* mutant phenotypes is unlikely due to silencing of the GFP-2xFYVE reporter construct, since there was only one case found to have lost the GFP

signal. One plausible explanation would be that, even though there are true mutants in the M₃ populations, the average numbers of endosomes decreased because the phenotype starts to segregate in the M₃. Alternatively, the criteria of the screen may not reflect true quantitative phenotypes. The low rate of phenotype confirmation in the M₃ generation could be due to false positive information that is shown from *fel2* phenotypes. As a mutant with higher endosomal levels, the number of GFP-2xFYVE compartments in *fel2* is higher than the reference *Ler*/GFP-2xFYVE. However, the number of GFP-2xFYVE compartments per cell in *fel2* and *Ler*/GFP-2xFYVE were similar. This suggests *fel2* might be a mutant with altered cell numbers or cell size rather than a true endocytic mutant. To obtain more robust *fel* mutant candidates, we should confirm not only the number of GFP-2xFYVE compartments per image area but also take consideration of how many GFP-2xFYVE compartments per cell.

Among 12 previously identified *fel* mutants, we found that mutants with reduced endosomal levels actually contain more than 200 GFP-2xFYVE compartments per image area. Endosomal levels were in the range of wild type according to the previous definition of “wild type” (Salomon, 2009). Therefore, these mutants were not chosen for genetic studies. Conversely, *fel2* and *fel9* possess an increased number of GFP-2xFYVE compartments, and were selected for further characterization (Figure 17). In both mutants lines, drugs were used to ensure that the nature of these labelled endosomal compartments is unchanged in comparison to the wild type. Upon Wortmannin treatment, *Ler*/GFP-2xFYVE, *fel2* and *fel9* showed an overall reduced number of endosomes in both root cells and cotyledons, presumably associated with an increase of size of these compartments caused by fusion/vacuolation of MVBs. This is in accordance with what has been reported by Vermeer and colleagues (2006). In BY2 cells, GFP-2xFYVE compartment number is reduced upon Wortmannin treatment. The reduced number of GFP-2xFYVE compartments after Wortmannin treatment in all plants tested suggests that the GFP-2xFYVE markers still targets endosomes in *fel2* and in *fel9* that possess a wild-type like membrane composition. After treatment with Wortmannin, large aggregated endosomes, as observed in root hairs of *Medicago truncatula* (Voigt et al., 2005), could be found only in cotyledon of epidermal cells of *Ler*/GFP-2xFYVE and *fel2* but not in root cells. This might indicate a tissue specific response to Wortmannin.

Increased GFP-2xFYVE compartments in *fel2* and *fel9* could result from enhanced endocytosis activity or reduced recycling ability. To discriminate these two hypotheses, BFA was used as application of BFA would recruit all recycling endosomes in a single BFA body. As expected, FM4-64 labelled BFA bodies appeared in the root cells of all three investigated lines but did not co-localize to GFP-2xFYVE compartments. This excludes mis-localization of GFP-2xFYVE to recycling endosomes. Interestingly, different types of small agglomerates of GFP-2xFYVE compartments were present in cotyledons of *Ler*/GFP-2xFYVE, *fel2* and *fel9* lines upon BFA treatment. This indicates that BFA has different effects to *fel2* and *fel9* and

supports the hypothesis that they are, by nature, two different types of mutants. This could be supported by the fact that the number of GFP-2xFYVE compartments/cell was not the same between *fel2* and *fel9*.

4.2.2 FYVE endosomal levels in *Ler* and *Col-0* ecotypes - A fluorescent reporter issue

To clone the *fel2* and *fel9* loci, a map based cloning approach has been tried using *Col-0*/YFP-2xFYVE as an outcross parental line. However, fewer and enlarged FYVE compartments were detected in *Col-0*/YFP-2xFYVE lines (Figure 20). Possible reasons for this variation of endosomal levels in these two reference lines may be: the different transgenes used (GFP-2xFYVE versus YFP-2xFYVE); different transgene insertion sites leading to different expression levels; different copy numbers of transgenes; differences due to the two *Arabidopsis* ecotype backgrounds. In *Col-0*/YFP-2xFYVE, there are fewer YFP-2xFYVE compartments but higher transcript levels of YFP than in *Ler*/GFP-2xFYVE. In tobacco BY-2 cells, overexpression of the YFP-2xFYVE transgene leads to higher levels of PI3P in comparison to YFP only expressing cells (Vermeer et al., 2006). This raises a possibility that PI3P levels vary in different transgenic lines containing either YFP-2xFYVE or GFP-2xFYVE and might explain why more YFP transcripts were detected in *Col-0*/YFP-2xFYVE. In this study, we found there is no correlation between *GFP/YFP-2xFYVE* expression and endosomal levels. Although *Ler*/GFP-2xFYVE and *Col-0*/YFP-2xFYVE contain different transgenes (Vermeer et al., 2006; Voigt et al., 2005), it is still possible that endosomal levels are variable in different *Arabidopsis* ecotypes carrying the same GFP-2xFYVE transgene. To test the hypothesis, we generated introgression of GFP-2xFYVE from *Ler*/GFP-2xFYVE to *Col-0*. No enlarged GFP-2xFYVE compartments appeared in the heterozygous line (Supplementary Figure 2). This suggests that the enlarged FYVE compartment phenotype is not correlated with the differences in *Arabidopsis* ecotypes.

F₁ progenies of *Ler*/GFP-2xFYVE crossed to *Col-0*/YFP-2xFYVE showed reduced numbers of GFP/YFP-2xFYVE compartments but wild type-like endosomal levels in the F₂. Reduction of GFP-2xFYVE compartments was also observed in F₁ progenies as *Ler*/GFP-2xFYVE crossed to *Ler*. This strongly suggests that endosomal levels are decreased because F₁ hybrids are heterozygous for the reporter construct. In accordance with the observation that, in the F₂ progenies of introgression lines, GFP/YFP-2xFYVE labelled compartments number increased again, most likely because the homozygous status of the GFP/YFP-2xFYVE transgenes is restored.

4.2.3 Genetic characterization of *fel* mutants

To investigate the genetic character of *fel* mutants, endosomal levels in F₁ and F₂ progenies of backcrossed and outcrossed *fel* mutants were monitored. *Fel2*, *fel6* and *fel9* mutants phenotypes are inherited in a recessive manner in both backcrossed and outcrossed progenies. Outcrossed *fel12* also demonstrated recessive behaviour. On the contrary, F₁ of backcrossed and outcrossed *fel10* mutant contained endosomal numbers similar to that observed in the M₃ generation suggesting here that the *fel10* mutation is dominant. However, F₂ families revealed recessive characteristics in both backcrossed and outcrossed lines. The numbers of endosomes in the M₃ of *fel10* are low but still in the range of wild type. This suggests *fel10* is too subtle to be mapped or to conclude its genetic inheritance. When *fel* mutants are outcrossed to Col-0/YFP-2xYFVE, it is possible that the progenies contain reduced endosomal levels similar to those detected in *Ler*/GFP-2xYFVE crossed to Col-0/YFP-2xYFVE. This would generate misleading results when investigating genetic inheritances and identifying phenotypes for *fel* mutants. In F₂ progenies of backcrossed and outcrossed *fel* mutants, increased endosomal levels rarely recovered as shown in *fel2*, *fel3*, *fel9* and *fel12*. Gene silencing of GFP/YFP-2xYFVE may be the reason. The GFP has significant advantages over other reporter genes, because expression can be detected in living cells without any substrates. However, stability of transgene expression is also a critical concern, especially in terms of potential epigenetic interactions with host genomes resulting in gene silencing (Martienssen and Colot, 2001).

4.2.4 Map-based cloning of *FEL2* and *FEL9*

To identify *FEL2* and *FEL9* loci, F₂ populations from an outcross using Col-0/YFP-2xYFVE were screened. Mutant plants carrying *fel2* or *fel9* phenotypes were infrequently observed in F₂ progenies suggesting they are recessive mutations. In the M₃ and M₄ generation only a small portion of *fel9* is viable. It has been shown that many mutants in the endocytic pathway are lethal (Tanaka et al., 2009). Mature *fel2* and *fel9* produce short siliques and have low seed production. In F₁ progenies of backcrossed *fel9* to *Ler*/GFP-2xYFVE or *Ler*, most siliques contain no seed inside indicating infertility in *fel9* is a dominant trait. This raises the possibility that viability in F₂ progenies with the *fel9* phenotype is low, and survived F₂ progenies do not contain strikingly increased numbers of GFP-2xYFVE compartments. In successful backcrossed F₂ progenies, plants with *fel2* phenotypes still produce short siliques suggesting that the endosomal phenotype could affect development. Mutants in vesicle trafficking causing developmental defects or lethality have already been reported. For example, the *gnom* mutation disrupts the apical basal pattern of seedlings (Mayer et al., 1993).

Map-based cloning requires outcrossing of the mutant plant with other Arabidopsis ecotypes. Phenotypes and genotypes are scored to identify the rough mapping position of the gene. By stringent phenotyping, a forward genetic screen enabled us to identify rough mapping positions for *FEL2* and *FEL9*. Subsequently, recombination events are measured to narrow down the mapping region. This process is particularly difficult when the phenotype of interest is subtle or when variation of interested phenotypes occurs between parental lines (Alonso-Blanco and Koorneef, 2000). In our cases, *fel2* phenotype did not appear in the F₃ progenies of *fel2* outcrossed lines from 16 individual F₂ families showing increased endosomal levels. Investigation of F₃ families of *fel9* outcrossed to Col-0/YFP-2xFYVE reveals segregation of phenotypes. This raises the possibility that silencing of GFP/YFP-2xFYVE transgenes occurred in the F₃ generation and resulted in reduction of endosomal levels. I encountered difficulties in narrowing down the region containing *fel2* and *fel9* mutations. This suggests low recombination frequencies in certain chromosomes. It has been reported that the genetic recombination rates varied along the chromosome 4 from 0 cM/Mb near the centromere to 20 cM/Mb (Drouaud et al., 2007). This probably leads to low recombination frequency and limits the efficiency of fine mapping.

A powerful approach for determining the biological functions of genes in an organism is to produce mutants with altered phenotypes and physiological responses. EMS induces chemical modification of nucleotides, which results in mispairing and base changes and generates randomly distributed mutations throughout the genome in Arabidopsis (Kim et al., 2006). However, there may still be unassociated polymorphisms segregating with *fel2* and *fel9* phenotypes in mapping populations. Selecting mutants from outcrosses or backcrosses, in combination with whole genome sequencing, could simplify the mapping process and overcome the background noise. Mapping of interesting genes is successful by next generation mapping method. This method quantifies the relative contribution of the parental mutant and mapping families to each SNP in F₂ progenies and requires only small outcrossed F₂ population (Austin et al., 2011). Re-sequencing of multiple backcrossed mutant plants could also help to limit the number of candidate SNPs (Ashelford et al., 2011). Illumina sequencing provided genome information for *fel2*, *fel9* and *Ler/GFP-2xFYVE*. *FEL9* co-segregated with 2 chromosome loci and it is difficult to identify two or more genes that cause the *fel9* mutant phenotype. Due to the low recombination rate of the rough mapping region, there are still many candidate genes for *fel2* mutation. Currently, we are generating *fel2* crossed to *Ler* to eliminate background noise. Confirmed F₃ progenies would be crossed to Col-0/GFP-2xFYVE and re-sequenced to identify possible SNPs. Also to exclude variation caused by different ecotypes, introgression of GFP-2xFYVE from *Ler/GFP-2xFYVE* to Col-0 was generated endosomal levels would be measured in stable homozygous transgenic progenies.

In summary, mutants with altered FYVE-endosome levels were screened and confirmed by high-throughput confocal laser microscopy (Salomon et al., 2010). We revealed different endosomal levels in two reference lines Col-0/YFP-2xFYVE and Ler/GFP-2xFYVE. *Fel2* and *fel9* with increased GFP-2xFYVE compartments are of endocytic nature. Stringent phenotyping enables to locate rough mapping positions for *FEL2* and *FEL9* but the exact SNPs remain to be confirmed. Since whole-genome assemblies of *Ler* were recently released (Cao et al., 2011; Schneeberger et al., 2011) it would also be helpful to identify the causal mutations of *fel2* and *fel9* phenotypes. In parallel to map based cloning, recent study reveals successful identification of a SNP that cause Arabidopsis clock mutant by re-sequencing multiple-backcrossed lines (Ashlford et al., 2011).

To study how *FEL2* and *FEL9* affect plant immunity, further pathogen challenge assays such as *Hpa*, *flg22* and *Pto* DC3000 would be conducted in *fel2* and *fel9* backcrossed lines. Since membrane trafficking seems to contribute in the build up of cellular defence structures in response to filamentous pathogens, it is likely that *fel* mutants will help dissect plant defence responses.

5. REFERENCES

- Alonso-Blanco C, Koornneef M. (2000).** Naturally occurring variation in Arabidopsis: an underexploited resource for plant genetics. *Trends Plant Sci* **1**, 22-29.
- An, Q., Huckelhoven, R., Kogel, K.-H., and van Bel, A.J.E. (2006a).** Multivesicular bodies participate in a cell wall-associated defence response in barley leaves attacked by the pathogenic powdery mildew fungus. *Cellular Microbiology* **8**, 1009-1019.
- An, Q., Ehlers, K., Kogel, K.-H., van Bel, A.J.E., and Huckelhoven, R. (2006b).** Multivesicular compartments proliferate in susceptible and resistant MLA12-barley leaves in response to infection by the biotrophic powdery mildew fungus. *New Phytologist* **172**, 563-576.
- Assaad, F., Qiu, J.-L., Youngs, H., Ehrhardt, D., Zimmerli, L., Kalde, M., Wanner, G., Peck, S., Edwards, H., Ramonell, K., Somerville, C., and Thordal-Christensen, H. (2004).** The PEN1 Syntaxin Defines a Novel Cellular Compartment upon Fungal Attack and Is Required for the Timely Assembly of Papillae. *Mol Biol Cell* **15**, 5118-5129.
- Aroca, R., Bago, A., Sutka, M., Paz, J.A., Cano, C., Amodeo, G., and Ruiz-Lozano, J.M. (2009).** Expression analysis of the first arbuscular mycorrhizal fungi aquaporin described reveals concerted gene expression between salt-stressed and nonstressed mycelium. *Mol Plant Microbe Interact* **22**, 1169–1178.
- Ashelford, K., Eriksson, M.E., Allen, C.M., D'Amore, R., Johansson, M., Gould, P., Kay, S., Millar, A.J., Hall, N., and Hall, A. (2011).** Full genome re-sequencing reveals a novel circadian clock mutation in Arabidopsis. *Genome Biol* **12**, R28.
- Austin, R.S., Vidaurre, D., Stamatiou, G., Breit, R., Provar, N.J., Bonetta, D., Zhang, J., Fung, P., Gong, Y., Wang, P.W., McCourt, P., and Guttman, D.S. (2011).** Next-generation mapping of Arabidopsis genes. *Plant J* **67**, 715-725.
- Bailey BA, Korcak RF, Anderson JD (1993)** Sensitivity to an ethylene biosynthesis-inducing endoxylanase in *Nicotiana* L. cv Xanthi is controlled by a single dominant gene. *Plant Physiol* **101**: 1081–1088.
- Bar, M., and Avni, A. (2009).** EHD2 inhibits ligand-induced endocytosis and signaling of the leucine rich repeat receptor-like protein LeEix2. *Plant J* **59**, 600-611.
- Beck, M., and Robatzek, S. (2011).** “Receptor Trafficking in Plants” in Receptor-like Kinases in Plants. From development to Defense Series: Signaling and Communication in Plants. Springer Verlag **13**.
- Bednarek, P., Pislewska-Bednarek, M., Svatos, A., Schneider, B., Doubek, J., Mansurova, M., Humphry, M., Consonni, C., Panstruga, R., Sanchez-Vallet, A., Molina, A., and Schulze-Lefert, P. (2009).** A glucosinolate metabolism pathway in living plant cells mediates broad-spectrum antifungal defense. *Science* **323**, 101-106.
- Bhat, R.A., Miklis, M., Schmelzer, E., Schulze-Lefert, P., and Panstruga, R. (2005).**

Recruitment and interaction dynamics of plant penetration resistance components in a plasma membrane microdomain. *Proc Natl Acad Sci USA* **102**, 3135-3140.

Böhlenius, H., Mørch, S.M., Godfrey, D., Nielsen, M.E., and Thordal-Christensen, H. (2010). Multivesicular bodylocalized GTPase ARFA1b/1c is important for callose deposition and ROR2 syntaxin-dependent preinvasive basal defense in barley. *Plant Cell* **22**, 3831-3844.

Bolte, S., Talbot, C., Boutte, Y., Catrice, O., Read, N.D., and Satial-Jeunemaitre, B. (2004). FM-dyes as experimental probes for dissecting vesicle trafficking in living plant cells. *J Microscopy* **214**, 159-173.

Boulaflous, A., Faso, C., and Brandizzi, F. (2008). Deciphering the Golgi apparatus: from imaging to genes. *Traffic* **9**, 1613-1617.

Bozkurt, T.O., Schornack, S., Win, J., Shindo, T., Ilyas, M., Oliva, R., Cano, L.M., Jones, A.M., Huitema, E., van der Hoorn, R.A., and Kamoun, S. (2011). Phytophthora infestans effector AVRblb2 prevents secretion of a plant immune protease at the haustorial interface. *Proc Natl Acad Sci U S A.* **108**, 20832-208327.

Cao, J., Schneeberger, K., Ossowski, S., Gunther, T., Bender, S., Fitz, J., Koenig, D., Lanz, C., Stegle, O., Lippert, C., Wang, X., Ott, F., Muller, J., Alonso-Blanco, C., Borgwardt, K., Schmid, K.J., and Weigel, D. (2011). Whole-genome sequencing of multiple Arabidopsis thaliana populations. *Nat Genet* **43**, 956-963.

Caillaud, M.C., Piquerez, S.J., Fabro, G., Steinbrenner, J., Ishaque, N., Beynon, J., and Jones, J.D. (2012). Subcellular localization of the Hpa RxLR effector repertoire identifies a tonoplast-associated protein HaRxL17 that confers enhanced plant susceptibility. *Plant J* **69**, 252-265.

Chen, L.-Q., Hou, B.-H., Lalonde, S., Takanaga, H., Hartung, M.L., Qu, X.-Q., Guo, W.-J., Kim, J.-G., Underwood, W., Chaudhuri, B., Chermak, D., Antony, G., White, F.F., Somerville, S.C., Mudgett, M.B., and Frommer, W.B. (2010). Sugar transporters for intercellular exchange and nutrition of pathogens. *Nature* **468**, 527-532.

Chaparro-Garcia, A., Wilkinson, R.C., Gimenez-Ibanez, S., Findlay, K., Coffey, M.D., Zipfel, C., Rathjen, J.P., Kamoun, S. and Schornack, S. (2011). The receptor-like kinase SERK3/BAK1 is required for basal resistance against the late blight pathogen *Phytophthora infestans* in *Nicotiana benthamiana*. *PLoS One* **6**, e16608.

Chen, X., Irani, N.G., and Friml, J. (2011). Clathrin-mediated endocytosis: the gateway into plant cells. *Curr Opin Plant Biol* **14**, 674-682.

Chinchilla, D., Zipfel, C., Robatzek, S., Kemmerling, B., Nurnberger, T., Jones, J.D., Felix, G., and Boller, T. (2007). A flagellin-induced complex of the receptor FLS2 and BAK1 initiates plant defense. *Nature* **448**, 497-500.

Chisholm, S.T., Coaker, G., Day, B., and Staskawicz, B.J. (2006). Host-Microbe Interactions: Shaping the Evolution of the Plant Immune Response. *Cell* **124**, 803-814.

Coates, M.E., and Beynon, J.L. (2010). *Hyaloperonospora arabidopsidis* as a pathogen model. *Annu Rev Phytopathol* **48**, 329-345.

Collins, N.C., Thordal-Christensen, H., Lipka, V., Bau, S., Kombrink, E., Qiu, J.-L., Huckelhoven, R., Stein, M., Freialdenhoven, A., Somerville, S.C., and Schulze-Lefert, P. (2003). SNARE-protein-mediated disease resistance at the plant cell wall. *Nature* **425**, 973-977.

Cutler, S.R., Ehrhardt, D.W., Griffiths, J.S. and Somerville, C.R. (2000). Random GFP::cDNA fusions enable visualization of subcellular structures in cells of *Arabidopsis* at a high frequency. *Proc Natl Acad Sci USA* **97**, 3718-3723.

van Damme, M., Zeilmaker, T., Elberse, J., Andel, A., de Sain-van der Velden, M., and van den Ackerveken G. (2009). Downy mildew resistance in *Arabidopsis* by mutation of HOMOSERINE KINASE. *Plant Cell* **21**, 2179-89.

Dhonukshe, P., Aniento, F., Hwang, I., Robison, D.G., Mravec, J., Stierhof, Y.D., and Friml, J. (2007). Clathrin-mediated constitutive endocytosis of PIN auxin efflux carriers in *Arabidopsis*. *Curr Biol* **17**, 520-527.

Donofrio, N.M., and Delaney, T.P. (2001). Abnormal callose response phenotype and hypersusceptibility to *Peronospora parasitica* in defense-compromised *Arabidopsis* *nim1-1* and salicylate hydroxylase-expressing plants. *Mol Plant Microbe Interact* **14**, 439-450.

Douchkov, D., Nowara, D., Zierold, U., and Schweizer, P. (2005). A high-throughput gene-silencing system for the functional assessment of defense-related genes in barley epidermal cells. *Mol Plant Microbe Interact* **18**, 755-761.

Drouaud, J., Camilleri, C., Bourguignon, P.Y., Canaguier, A., Berard, A., Vezon, D., Giancola, S., Brunel, D., Colot, V., Prum, B., Quesneville, H., Mezard, C. (2006). Variation in crossing-over rates across Chromosome 4 of *Arabidopsis thaliana* reveals the presence of meiotic recombination hot spots. *Genome Res* **16**, 106-114.

Ehrhardt, D. (2003) GFP technology for live cell imaging. *Curr Opin Plant Biol* **6**, 622-628.

Emans, N., Zimmermann, S., and Fischer, R. (2002). Uptake of a fluorescent marker in plant cells is sensitive to brefeldin A and wortmannin. *Plant Cell* **14**, 71-86.

Fabro G., Steinbrenner, J., Coates, M., Ishaque, N., Baxter, L., Studholem, D. J., Körner, E., Allen, R. L., Piquerez, S.J.M., Rougon-Cardoso, A., Greenshields, D., Lei, R., Badel, J.L., Caillaud, M.-C., Sohn, K.-H., Van den Ackerveken, G., Parker, J.E. Beynon, J and Jones, D.G. (2011). Multiple candidate effectors from the oomycete pathogen *Hyaloperonospora arabidopsidis* suppress host plant immunity. *PLoS Pathog* **7**, e1002348.

Gan, P.H., Rafiqi, M., Ellis, J.G., Jones, D.A., Hardham, A.R., and Dodds, P.N. (2010). Lipid binding activities of flax rust AvrM and AvrL567 effectors. *Plant Signal Behav* **5**, 1272-1275.

Geldner, N., Dénervaud-Tendon, V., Hyman, D.L., Mayer, U., Stierhof, Y.-D. and Chory, J. (2009). Rapid, combinatorial analysis of membrane compartments in intact plants with a multicolor marker set. *Plant J* **59**, 169-178.

Geldner, N., Friml, J., Stierhof, Y.D., Jurgens, G., Palme, K. (2001). Auxin transport inhibitors block PIN1 cycling and vesicle trafficking. *Nature* **413**, 425-428.

Göhre, V., and Robatzek, S. (2008). Breaking the barriers: Microbial effector molecules subvert plant immunity. *Annu Rev Phytopathol* **46**, 189-215.

Gomez, S.K., Javot, H., Deewatthanawong, P., Torres-Jerez, I., Tang, Y., Blancaflor, E.B., Udvardi, M.K., Harrison, M.J. (2009) *Medicago truncatula* and *Glomus intraradices* gene expression in cortical cells harboring arbuscules in the arbuscular mycorrhizal symbiosis. *BMC Plant Biol* **9**: 10.

Gómez-Gómez, L., and Boller, T. (2000). FLS2: An LRR Receptor-like Kinase Involved in the Perception of the Bacterial Elicitor Flagellin in Arabidopsis. *Molecular Cell* **5**, 1003-1011.

Grunewald, W., and Friml, J. (2010). The march of the PINs: developmental plasticity by dynamic polar targeting in plant cells. *EMBO J* **29**, 2700-2714.

Hanton, S.L., Bortolotti, L.E., Renna, L., Stefano, G., and Brandizzi, F. (2005). Crossing the divide transport between the endoplasmic reticulum and Golgi apparatus in plants. *Traffic* **6**, 267-277.

Hanton, S.L., and Brandizzi, F. (2006). Protein transport in the plant secretory pathway. *Can J Bot* **84**, 523-530.

Iwabuchi, K., Minamino, R. and Takagi, S. (2010) Actin reorganization underlies phototropin-dependent positioning of nuclei in Arabidopsis leaf cells. *Plant Physiol* **152**, 1309-1319.

Jacobs, A.K., Lipka, V., Burton, R.A., Panstruga, R., Strizhov, N., Schulze-Lefert, P., and Fincher, G.B. (2003). An Arabidopsis Callose Synthase, GSL5, Is Required for Wound and Papillary Callose Formation. *Plant Cell* **15**, 2503-2513.

Javot, H., Penmetsa, R.V., Breuillin, F., Bhattarai, K.K., Noar, R.D., Gomez, S.K., Zhang, Q., Cook, D.R., and Harrison, M.J. (2011). *Medicago truncatula* mtpt4 mutants reveal a role for nitrogen in the regulation of arbuscule degeneration in arbuscular mycorrhizal symbiosis. *Plant J* **68**, 954-965.

Jones, J.D.G., and Dangl, J.L. (2006). The plant immune system. *Nature* **444**, 323-329.

Jürgens, G. (2004). Membrane trafficking in plants. *Annu Rev Cell Dev Biol* **20**, 481-504.

Ketelaar, T., Faivre-Moskalenko, C., Esseling, J.J., de Ruijter, N.C., Grierson, C.S., Dogterom, M. and Emons, A.M. (2002). Positioning of nuclei in Arabidopsis root hairs: an actin-regulated process of tip growth. *Plant Cell* **14**, 2941-2955.

Keinath, N.F., Kierszniowska, S., Lorekm, J., Bourdais, G., Kessler, S.A., Shimosato-Asano, H., Grossniklaus, U., Schulze, W.X., Robatzek, S., Panstruga, R. (2010). PAMP (pathogen-associated molecular pattern)-induced changes in plasma membrane compartmentalization reveal novel components of plant immunity. *J Bio Chem* **285**, 39140-9.

- Kim, Y., Schumaker, K.S., and Zhu, J.-K.** (2006). EMS mutagenesis of Arabidopsis. *Methods Mol. Biol.* **323**, 101-103.
- Koh, S., André, A., Edwards, H., Ehrhardt, D. and Somerville, S.** (2005), *Arabidopsis thaliana* subcellular responses to compatible *Erysiphe cichoracearum* infections. *Plant J* **44**, 516-529.
- Kwon, C., Neu, C., Pajonk, S., Yun, H.S., Lipka, U., Humphry, M., Bau, S., Straus, M., Kwaaitaal, M., Rampelt, H., Kasmi, F.E., Jurgens, G., Parker, J., Panstruga, R., Lipka, V., and Schulze-Lefert, P.** (2008). Co-option of a default secretory pathway for plant immune responses. *Nature* **451**, 835-840.
- Lee, S.M., Kim, H.S., Han, H.J., Moon, B.C., Kim, C.Y., Harper, J.F., and Chung, W.S.** (2007). Identification of a calmodulin-regulated autoinhibited Ca²⁺-ATPase (ACA11) that is localized to vacuole membranes in Arabidopsis. **581**, 3943-3949.
- Lee, S.W., Han, S.W., Sririyannam, M., Park, C.J., Seo, Y.S., and Ronald, P.C.** (2009) A type I-secreted, sulfated peptide triggers XA21-mediated innate immunity. *Science* **326**, 850-853.
- Leckie, C.P., Callow, J.A., and Green, J.R.** (1995). Reorganisation of the endoplasmic reticulum in pea leaf epidermal cells infected by the powdery mildew fungus *Erysiphe pisi*. *New Phytol* **131**, 211-221.
- Lipka, V., Dittgen, J., Bednarek, P., Bhat, R., Wiermer, M., Stein, M., Landtag, J., Brandt, W., Rosahl, S., Scheel, D., Llorente, F., Molina, A., Parker, J., Somerville, S., and Schulze-Lefert, P.** (2005). Pre- and Postinvasion Defenses Both Contribute to Nonhost Resistance in Arabidopsis. *Science* **310**, 1180-1183.
- Lu, Y.-J., Schornack, S., Spallek, T., Geldner, N., Chory, J., Schellmann, S., Schumacher, K., Kamoun, S., and Robatzek, S.** (2012). Patterns of plant subcellular responses to successful oomycete infections reveal differences in host cell reprogramming and endocytic trafficking. *Cellular Microbiology* doi: 10.1111/j.1462-5822.2012.01751.x.
- Maurel, C. and Chrispeels, M.J.** (2001). Aquaporins. A molecular entry into plant water relations. *Plant Physiol* **125**, 135-138.
- Martienssen, R.A., and Colot, V.** (2001). DNA methylation and epigenetic inheritance in plants and filamentous fungi. *Science* **293**, 1070-1074.
- Mayer, U., Büttner, G., and Jürgens, G.** (1993). Apical-basal pattern formation in the *Arabidopsis* embryo: studies on the role of the *gnom* gene. *Development* **117**, 149-162.
- McMahon, H.T., Boucrot, E.** (2011). Molecular mechanism and physiological functions of clathrin-mediated endocytosis. *Nat Rev Mol Cell Biol* **12**, 517-533.
- Meyer D, Pajonk S, Micali C, O'Connell R, Schulze-Lefert P.** (2009). Extracellular transport and integration of plant secretory proteins into pathogen-induced cell wall compartments. *Plant J* **57**, 986-999.
- Micali, C.O., Neumann, U., Grunewald, D., Panstruga, R. and O'Connell, R.** (2011).

Biogenesis of a specialized plant–fungal interface during host cell internalization of *Golovinomyces orontii* haustoria. *Cellular Microbiology* **13**, 210-226.

Mims, C.W., Richardson, E.A., Holt, B.F III., Dangl, J.L. (2004). Ultrastructure of the host-pathogen interface in *Arabidopsis thaliana* leaves infected by the downy mildew *Hyaloperonospora parasitica*. *Can J Bot* **82**, 1001-1008.

Miya, A., Albert, P., Shinya, T., Desaki, Y., Ichimura, K., Shirasu, K., Narusaka, Y., Kawakami, N., Kaku, H., and Shibuya, N. (2007). CERK1, a LysM receptor kinase, is essential for chitin elicitor signaling in *Arabidopsis*. *Proceedings of the National Academy of Sciences* **104**, 19613-19618.

Nishimura, M.T., Stein, M., Hou, B.-H., Vogel, J.P., Edwards, H. and Somerville, S.C. (2003) Loss of a callose synthase results in salicylic acid-dependent disease resistance. *Science* **301**, 969-972.

Nomura, K., Debroy, S., Lee, Y.H., Pumplin, N., Jones, J., and He, S.Y. (2006). A bacterial virulence protein suppresses host innate immunity to cause plant disease. *Science* **313**, 220-223.

Nomura, K., Mecey, C., Lee, Y N., Imboden, L., Chang, J., and He, S. Y. (2011) Effector-triggered immunity blocks pathogen degradation of an immunity-associated vesicle traffic regulator in *Arabidopsis*. *Proc Natl Acad Sci USA* **108**:10774-10779.

O’Connell, R.J. and Panstruga, R. (2006). Tête à tête inside a plant cell: establishing compatibility between plants and biotrophic fungi and oomycetes. *New Phytol* **171**, 699-718.

Otegui, M.S., and Spitzer, C. (2008). Endosomal functions in plants. *Traffic* **9**, 1589-1598.

Parker, J.E., Szabo, V., Staskawicz, B., Lister, C., Dean, C., Daniels, M.J., and Jones, J.D.G. (1993). Phenotypic characterization and molecular mapping of the *Arabidopsis thaliana* locus RPP5, determining disease resistance to *Peronospora parasitica*. *Plant J* **4**, 821-831.

Parniske M. (2008). Arbuscular mycorrhiza: the mother of plant root endosymbioses. *Nat Rev Microbiol* **6**, 763-75.

Pumplin, N., and Harrison, M.J. (2009). Live-cell imaging reveals periarbuscular membrane domains and organelle location in *Medicago truncatula* roots during arbuscular mycorrhizal symbiosis. *Plant Physiol* **151**, 809-819.

Rafiqi, M., Gan, P.H., Ravensdale, M., Lawrence, G.J., Ellis, J.G., Jones, D.A., Hardham, A.R., and Dodds PN. (2010). Internalization of flax rust avirulence proteins into flax and tobacco cells can occur in the absence of the pathogen. *Plant Cell* **22**, 2017-2032.

Robatzek, S., Chinchilla, D., and Boller, T. (2006). Ligand-induced endocytosis of the pattern recognition receptor FLS2 in *Arabidopsis*. *Genes & Development* **20**, 537-542.

Robinson, D., and Hillmer, S. (1990). Endocytosis in plants. *Plant Physiol* **147**, 1482-1492.

Robinson, D.G., Jiang, L., and Schumacher, K. (2008). The endosomal system of plants:

Charting new and familiar territories. *Plant Physiol* **147**, 1482-1492.

Ron, M., and Avni, A. (2004). The receptor for the fungal elicitor ethyleneinducing xylanase is a member of a resistance-like gene family in tomato. *Plant Cell* **16**, 1604-1615.

Roppolo D., De Rybel, B., Tendon, V.D., Pfister, A., Alassimone, J., Vermeer, J.E., Yamazaki, M., Stierhof, Y.D., Beeckman, T., and Geldner, N. (2011). A novel protein family mediates Casparian strip formation in the endodermis. *Nature* **473**, 380-383.

Salomon, S., and Robatzek, S. (2006). Induced Endocytosis of the Receptor Kinase FLS2. *Plant Signal Behav* **1**, 293-295.

Salomon, S., Grunewald, D., Stüber, K., Schaaf, S., MacLean D., Schulze-Lefert, P. and Robatzek, S. (2010). High-Throughput Confocal Imaging of Intact Live Tissue Enables Quantification of Membrane Trafficking in Arabidopsis. *Plant Physiol* **154**, 1096-1104.

Salomon, S.A. (2009). Linking endosomal traffic and PAMP-triggered immunity in plants. In *Mathematisch-Naturwissenschaftlichen Fakultät der Universität zu Köln (Cologene: Universität zu Köln)*, pp. 106.

Saito, C., Uemura, T., Awai, C., Tominaga, M., Ebine, K., Ito, J., Ueda, T., Abe, H., Morita, M.T., Tasaka, M. and Nakano, A. (2011). The occurrence of 'bulbs', a complex configuration of the vacuolar membrane, is affected by mutations of vacuolar SNARE and phospholipase in Arabidopsis. *Plant J* **68**, 64-73.

Sanderfoot, A.A., Kovaleva, V., Bassham, D.C. and Raikhel, N.V. (2001) Interactions between syntaxins identify at least five SNARE complexes within the Golgi/prevacuolar system of the Arabidopsis cell. *Mol Biol Cell* **12**, 3733-3743.

Scheuring, D., Viotti, C., Krüger, F., Künzl, F., Sturm, S., Bubeck, J., Hillmer, S., Frigerio L., Robinson, D. G., Pimpl, P., and Schmacher K. (2011). Multivesicular Bodies Mature from the Trans-Golgi Network/Early Endosome in Arabidopsis. *Plant cell* **23**, 3463-3481.

Schorneck, S., van Damme, M., Bozkurt, T.O., Cano, L.M., Smoker, M., Thines, M., Gaulin, E., Kamoun, S. and Huitema, E. (2010) Ancient class of translocated oomycete effectors targets the host nucleus. *Proc. Natl Acad. Sci. USA* **107**, 17421-17426.

Shimada, C., Lipka, V., O'Connell, R., Okuno, T., Schulze-Lefert, P., and Takano, Y. (2006). Nonhost resistance in Arabidopsis-Colletotrichum interactions acts at the cell periphery and requires actin filament function. *Mol Plant Microbe Interact* **19**, 270-279.

Schneeberger, K., Ossowski, S., Ott, F., Klein, J.D., Wang, X., Lanz, C., Smith, L.M., Cao, J., Fitz, J., Warthmann, N., Henz, S.R., Huson, D.H., and Weigel, D. (2011). Reference-guided assembly of four diverse Arabidopsis thaliana genomes. *Proc Natl Acad Sci U S A* **108**, 10249-10254.

Soylu, E.M., and Soyly, S. 2003. Light and electron microscopy of the compatible interaction between *Arabidopsis* and the downy mildew pathogen *Peronospora parasitica*. *J Phytopathol* **151**, 300-306.

Stein, M., Dittgen, J., Sanchez-Rodriguez, C., Hou, B.-H., Molina, A., Schulze-Lefert, P., Lipka, V., and Somerville, S. (2006). Arabidopsis PEN3/PDR8, an ATP Binding Cassette Transporter, Contributes to Nonhost Resistance to Inappropriate Pathogens That Enter by Direct Penetration. *Plant Cell* **18**, 731-746.

Takemoto, D., Jones, D.A. and Hardham, A.R. (2003). GFP-tagging of cell components reveals the dynamics of subcellular reorganization in response to infection of Arabidopsis by oomycete pathogens. *Plant J* **33**, 775-792.

Tamura, K., Shimada, T., Kondo, M., Nishimura, M., and Hara-Nishimura, I. (2005). KATAMARI1/MURUS3 Is a novel golgi membrane protein that is required for endomembrane organization in Arabidopsis. *Plant Cell* **17**, 1764-1776.

Tanaka, H., Kitakura, S., De Rycke, R., De Groodt, R., and Friml, J. (2009). Fluorescence imaging based screen identifies ARF GEF component of early endosomal trafficking. *Curr Biol* **19**, 391-397.

Tanghe, A., Dijck, P.V., and Thevelein, J.M. (2006). Why do microorganisms have aquaporins? *Trends Microbiol* **14**, 78-85.

Ueda, T., Uemura, T., Sato, M.H., and Nakano, A. (2004) Functional differentiation of endosomes in Arabidopsis cells. *Plant J* **40**, 783-789.

Vermeer, J.E., van Leeuwen, W., Tobenã-Santamaria, R., Laxalt, A. M., Jones, D.R., Divecha, N., Gadella, T.W. Jr., Munnik, T. (2006). Visualization of PtdIns3P dynamics in living plant cells. *Plant J* **47**, 687-700.

Viotti, C., Bubeck, J., Stierhof, Y.D., Krebs, M., Langhans, M., van den Berg, W., van Dongen, W., Richter, S., Geldner, N., Takano, J., Jurgens, G., de Vries, S.C., Robinson, D.G., and Schumacher, K. (2010). Endocytic and secretory traffic in Arabidopsis merge in the trans-Golgi network/early endosome, an independent and highly dynamic organelle. *Plant Cell* **22**, 1344-1357.

Voegelé, R.T., and Mendgen, K. (2003). Rust haustoria: nutrient uptake and beyond. *New Phytol* **159**, 93-100.

Voegelé, R.T., Struck, C., Hahn, M., and Mendgen, K. (2001). The role of haustoria in sugar supply during infection of broad bean by the rust fungus *Uromyces fabae*. *Proceedings of the National Academy of Sciences, USA* **98**: 8133-8138.

Vogel, J., and Somerville, S. (2000). Isolation and characterization of powdery mildew-resistant Arabidopsis mutants. *Proc. Natl. Acad. Sci. USA* **97**, 1897-1902.

Voigt, B., Timmers, A.C.J, Samaj, J., Hlavacka, A., Ueda, T., Preuss, M., Nielsen, E., Mathur, J., Emans, N., Stenmark, H., Makano, A., Baluška, F., and Menzel D. (2005). Actin-based motility of endosomes is linked to the polar tip growth of root hairs. *Eur J Cell Biol* **84**, 609-621.

Wang, J., Cai, Y., Miao, Y., Lam, S. K., and Jiang, L. (2009a). Wortmannin induces homotypic fusion of plant prevacuolar compartments. *J Exp Bot* **60**, 3075-3083.

Wang, W., Devoto, A., Turner, J.G., and Xiao, S. (2007). Expression of the membrane-associated resistance protein RPW8 enhances basal defense against biotrophic pathogens. *Mol Plant Microbe Interact* **20**, 966-976.

Wang, W., Wen, Y., Berkey, R., and Xiao, S. (2009b). Specific targeting of the Arabidopsis resistance protein RPW8.2 to the interfacial membrane encasing the fungal haustorium renders broad-spectrum resistance to powdery mildew. *Plant Cell* **21**, 2898-2913.

Wolinski, H., Petrovic, U., Mattiazzi, M., Petschnigg, J., Heisem B., Natterm K., and Kohlwein, S.D. (2009). Imaging-based live cell yeast screen identifies novel factors involved in peroxisome assembly. *J Proteome Res* **8**, 20-27.

Xiao, S., Brown, S., Patrick, E., Brearley, C., and Turner, J.G. (2003). Enhanced transcription of the Arabidopsis disease resistance genes RPW8.1 and RPW8.2 via a salicylic acid-dependent amplification circuit is required for hypersensitive cell death. *Plant Cell* **15**, 33-45.

Xu, H., and Mendgen, K. (1994). Targeted Cell Wall Degradation at the Penetration Site of Cowpea Rust Basidiosporelings. *MPMI* **10**, 87-94.

Yaeno, T., Li, H., Chaparro-Garcia, A., Schornack, S., Koshiba, S., Watanabe, S., Kigawa T, Kamoun, S, and Shirasu, K. (2011). Phosphatidylinositol monophosphate-binding interface in the oomycete RXLR effector AVR3a is required for its stability in host cells to modulate plant immunity. *Proc Natl Acad Sci USA* **108**, 14682-14687.

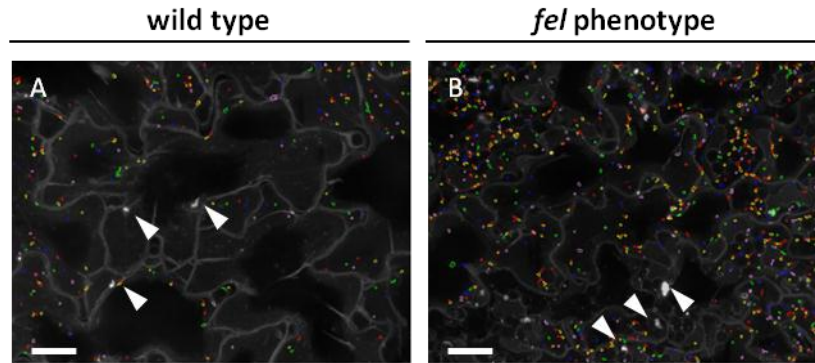
Zheng, H., Bednarek, S.Y., Sanderfoot, A.A., Alonso, J., Ecker, J.R. and Raikhel, N.V. (2002) NPSN11 is a cell plate-associated SNARE protein that interacts with the syntaxin KNOLLE. *Plant Physiol* **129**, 530-539.

Zipfel, C. (2009). Early molecular events in PAMP-triggered immunity. *Curr Opin Plant Biol* **12**, 414-420.

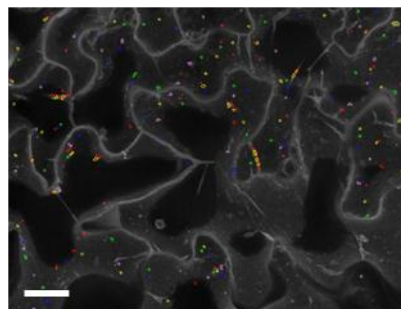
Zipfel, C., Kunze, G., Chinchilla, D., Caniard, A., Jones, J.D.G., Boller, T., and Felix, G. (2006). Perception of the Bacterial PAMP EF-Tu by the Receptor EFR Restricts Agrobacterium-Mediated Transformation. *Cell* **125**, 749-760.

APPENDIX

Appendix A- Supplementary data



Supplementary Figure 1. Detection of GFP-2xFYVE compartments in the F₂ of *fel* mutants outcrossed to Col-0/YFP-2FYVE. Merged confocal microscopy images were taken from epidermal cells of *Arabidopsis cotyledons* expressing GFP/YFP-2xFYVE. Images were taken with the Opera microscopy and analyzed with the endomembrane script. Recognized GFP/YFP-2xFYVE compartments are shown by coloured circles (scale bar=50 mm). Number of recognized GFP/YFP-2xFYVE FYVE compartments is indicated in brackets. (A) Backcrossed *fel19* showed wild type endosomal levels. (B) Backcrossed *fel2* showed increased endosomal phenotype. Arrows indicate enlarged FYVE compartments.



Supplementary Figure 2. Detection of GFP-2xFYVE compartments in the F₈ of *Ler*/GFP-2xFYVE crossed to *Ler*. Merged confocal microscopy images were taken from epidermal cells of *Arabidopsis cotyledons* expressing GFP/YFP-2xFYVE. Images were taken with the Opera microscopy and analyzed with the endomembrane script. Recognized GFP/YFP-2xFYVE compartments are shown by coloured circles (scale bar=50 mm).

Supplementary Table 1. Plant material presented in this study.

Name	Ecotypes	Description and localization	Reference
<i>fel1</i>	Ler/FYVE-GFP	EMS/MVBs	Salomon, 2009
<i>fel2</i>	Ler/FYVE-GFP	EMS/MVBs	Salomon, 2009
<i>fel3</i>	Ler/FYVE-GFP	EMS/MVBs	Salomon, 2009
<i>fel4</i>	Ler/FYVE-GFP	EMS/MVBs	Salomon, 2009
<i>fel5</i>	Ler/FYVE-GFP	EMS/MVBs	Salomon, 2009
<i>fel6</i>	Ler/FYVE-GFP	EMS/MVBs	Salomon, 2009
<i>fel7</i>	Ler/FYVE-GFP	EMS/MVBs	Salomon, 2009
<i>fel8</i>	Ler/FYVE-GFP	EMS/MVBs	Salomon, 2009
<i>fel9</i>	Ler/FYVE-GFP	EMS/MVBs	Salomon, 2009
<i>fel10</i>	Ler/FYVE-GFP	EMS/MVBs	Salomon, 2009
<i>fel11</i>	Ler/FYVE-GFP	EMS/MVBs	Salomon, 2009
<i>fel12</i>	Ler/FYVE-GFP	EMS/MVBs	Salomon, 2009

Supplementary Table 2. Oligonucleotides used in this study.

Chromosome	Position (bp)	Marker	BAC	Forward primer (5'-3')	Reverse primer (5'-3')
I A	3212189	F21M12	F21M12	ggcttctgaaatctgtcc	ttacttttgcctctgtcattg
I B	8322175	MSAT1.3		ggaactgtgtctggtaag	cgattgcactaaaagctctc
I C	18363881	ciw1	F14J22	acatttctcaatccttactc	gagagcttcttatttggat
I D	20873698	nga280	F14J16	ctgatctcacggacaatagtgc	ggctccataaaaaatgcacc
I E	27353212	nga111	F28P22	tgttttttaggacaaatggcg	ctccagttggaagctaaaggg
II A	1194606	ciw2	T18C20	cccaaaagtaattatactgt	ccgggtaataataaatgt
II B	6402864	ciw3	T26I20	gaaactcaatgaaatccactt	tgaactgtgtgagctttga
II C	11461020	MSAT2.21		atttttagcccaatcacgttt	aggtaagtgaaaggtaag
II D	18152580	MSAT2.9		taaaagagtcctcgtaaag	gttgtgtgtggcatt
II E	13831870	MSAT2.4		tgggttttggggtc	gtattattgtctgcctttt
III A	4608277	nga162	MDC16	catgcaattgcatctgagg	ctctgcactctttcctctgg
III B	9774308	ciw11	MF416	ccccgagttgaggatt	gaagaaattcctaagcattc
III C	18890837	ciw4	F18B3	gttcattaacttgcgtgtgt	tacggtcagattgagtgattc
III D	23031050	nga6	T17J13	tggatttctcctctctcac	atggagaagcttacctgatc
IV A	737954	ciw5	T15B16	ggttaaaaattagggttacga	agatttacctggaagcaat
IV B	7892624	ciw6	T6G15	ctcgtagtgcactttcatca	cacatggttagggaacaata
IV C	11524350	ciw7	F17L22	aattggagattagctggaat	ccatgttgatgataagcacia
IV D	18096137	nga1107	T9A14	gcgaaaaaacaaaaatcca	cgacgaatcgacagaattagg
V A	979764	CTR1.2	F17C15	ccactgttctctctctag	tatcaacagaaacgacccgag
V B	7485585	ciw8	MQJ16	tagtgaacctttctcagat	ttatgttttctcaatcagtt
V C	14007897	PHYC.3	MIK22	ctcagagaatcccagaaaaatct	aaactcgagagtttcttagatc
V D	17044001	ciw9	MFO20	cagacgtatcaaatgacaaatg	gactactgctcaactattcgg
V E	24530871	ciw10	MSL3	ccacatttctctttcata	caacatttagcaaatcaact

Supplemental Table 2 (Continued).

Chromosome	Position (bp)	Marker	BAC	Forward primer (5'-3')	Reverse primer (5'-3')
IV	8872074	FCA4		GTGGCAATTACGTGGAAG	TGATCAAATGATGGTTATCT
IV	10288439	F28A21		CATCATTATCACCACACATA	AGTTGGTTTTGAATTGATAG
IV	12108489	F7H19		GCCATTGAAAAACAATAG	AACATAGAAGTGCACAATTA
IV	8121263	FCA0		TGAAGCAACAATGACCTTAG	TGTGAAATCACCTGACTTTA
IV	8358967	FCA1		GTCTACTGGTGGATTGTGTC	CGTGTGGCATGTTAATTACT
IV	8610206	FCA2		TCAAGCGGACATATCAATAA	CCTCGTCTACCATAAA
IV	13023737	M2J2		TTATGATTGCGAGTAATAAC	GACAGGGCTTATGGGTGGT
IV	13664657	M4I22		CATCGGCAAGTGACTTGAG	GTGATCAGGCAAAACCAGTA
III	23031050	T17J13		ATGGAGAAGCTTACTGATC	TGGATTTCTTCTCTCTTAC
III	23281281	T20O10		AAATGCCAGGGGAATAGA	CAAACCATGCAATGATGC
III	1818093	T2J13		CCTCTTACGCCATTGCAT	GTAAGCTCAGTCGCCTTCT
III	2054789	F18B3		GTTCAATAAACTTGC GTGTGT	TACGGTCAGATTGAGTGATTC
IV	AT4G14330			GGTGCTGGAAAGAGTCATAC	CTCCGTTTCTCCACTTTGACA
IV	AT4G14370			AGGACACATAACCACGACTC	GACTTCCACGACAGAGATAG
IV	AT4G17350			TTATGCTACTTATGATTTTG	GCAAATACCTCACAACAGCA
IV	AT4G17850			TTTGTTATTGTAGTTATTGC	AAGAGGTAGATGAAATGCGA
IV	AT4G18770			ATCTTACATCCTTTGCTCA	TCTTCTCAGCAGTCCATTG
IV	AT4G35380			TGACTTCTCTGTTTCTCTCT	ATGTAGGATTTGTAAGCC
IV	AT4G19490			TATTGTTGCTTTACTTTCTT	TGGGATGTCTGATTGATTGG
IV	AT4G19570			ATTCGTGTGATTATTCGTT	CGTATTGTGAGTTTATGAGG

Supplementary Table 3. Quantification of GFP/YFP-2xFYVE compartments in the individual F₁ progenies of *Ler*/GFP-2xFYVE crossed to *Col-0*/YFP-2xFYVE.

Cross (Female x Male)	
<i>Col-0</i> /YFP-2xFYVE x <i>Ler</i> /GFP-2xFYVE	<i>Ler</i> /GFP-2xFYVE x <i>Col-0</i> /YFP-2xFYVE
105	138
118	145
125	159
133	177
137	183
137	198
138	218
150	
156	
178	
182	
184	
216	
219	
234	
243	

Supplementary Table 4. Quantification of GFP/YFP-2xFYVE compartments in individual F₁ progenies of *fel* mutants crossed to *Ler*/GFP-2xFYVE.

Cross (Female x Male)							
<i>Ler</i> /GFP-2xFYVE <i>x fel1</i>	<i>Ler</i> /GFP-2xFYVE <i>x fel2</i>	<i>Ler</i> /GFP-2xFYVE <i>x fel2</i>	<i>fel6</i> x <i>Ler</i> /GFP-2xFYVE	<i>Ler</i> /GFP-2xFYVE <i>x fel9</i>	<i>fel10</i> x <i>Ler</i> /GFP-2xFYVE	<i>Ler</i> /GFP-2xFYVE <i>x fel10</i>	<i>Col-0</i> /YFP-2xFYVE <i>x fel12</i>
Lethal	581	530	398	421	259	256	204
	489	640	467	482	334	421	278
	409	547		578	339	307	162
	524	586		391	314	412	236
	452	698		445	340	272	218
	652	586		539	244	392	236
	458	462		515	322	278	175
	571	458		394	228	238	201
	540	411		471	346	273	247
	558	385		275	318	356	185
	448	412		512	305	296	191
	531	390		518	268	253	161
	554			379	229	333	
	631			504	394		
	496				380		
	663				309		
	552				230		
	635				337		
	449				359		
	424				399		
	309				216		
	759				391		
	662						
	649						
	595						
	624						

Supplementary Table 5. Quantification of GFP/YFP-2xFYVE compartments in individual F₁ progenies of fel mutants crossed to Col-0/YFP-2xFYVE.

Cross (Female x Male)									
Col-0/YFP- 2xFYVE x <i>fel1</i>	Col-0/YFP- 2xFYVE x <i>fel2</i>	<i>fel3</i> x Col-0/YFP- 2xFYVE	Col-0/YFP- 2xFYVE x <i>fel3</i>	<i>fel6</i> x Col-0/YFP- 2xFYVE	Col-0/YFP- 2xFYVE x <i>fel6</i>	Col-0/YFP- 2xFYVE x <i>fel9</i>	<i>fel10</i> x Col-0/YFP- 2xFYVE	<i>fel12</i> x Col-0/YFP- 2xFYVE	Col-0/YFP- 2xFYVE x <i>fel12</i>
368	313	277	235	471	249	313	184	165	204
300	345	200	154	388	221	368	165	151	278
	307		231	324	208		131	155	162
	191			298	326		160	119	236
	220			381	248				218
	226			277	353				236
	283			300	327				175
	314				331				201
	226								247
	240								185
	257								191
	292								161
	218								
	288								
	624								
	432								
	379								
	259								
	265								
	269								
	300								
	266								
	383								
	400								
	343								
	340								

Supplementary Table 6. Prediction of *fel2* SNPs.

Gene	Gene Description	Position	Substitution Type
AT4G13810	receptor like protein 47	8006576	GTT->CTT
		8006898	AAG->AAC
AT4G14070	long-chain acyl-CoA synthetase	8114859	GAG->TAG
AT4G14096	F-box/LRR-repeat protein	8126091	GCA->GCA
AT4G14140	DNA methyltransferase 2	8148347	GAA->GTA
AT4G14140		8150141	CCT->CGT
AT4G14250	structural constituent of ribosome	8209163	AGC->ACC
AT4G14330	phragmoplast-associated kinesin-related protein	8244771	TAC->AAC
AT4G14368	regulator of chromosome condensation repeat-containing protein		CCA->TCA
		8275834	CCA->GCA
AT4G14380	hypothetical protein	8286211	GGG->AGG
AT4G15010	Mitochondrial substrate carrier family protein	8573993	ACA->ATA
AT4G15100	putative serine carboxypeptidase-like 30	8629399	GAT->GAA
AT4G15236	ABC transporter G family member 43	8702117	ATA->GTA
AT4G15280	UDP-glucosyl transferase 71B5	8719894	CAA->CGA
AT4G15396	cytochrome P450, family 702, subfamily A, polypeptide 6	8808960	CAA->CAC
AT4G15650	hypothetical protein	8923505	ACG->ATG
AT4G16045	meprin and TRAF homology domain-containing protein	9091265	AGA->AGT
AT4G16162	Leucine-rich repeat (LRR) family protein	9160420	TGT->TTT
AT4G16215	hypothetical protein	9179773	CTG->ATG
AT4G16220	GDSL esterase/lipase	9183740	ACT->CCT
AT4G16260	catalytic/ cation binding / hydrolase	9201441	CTA->ATA
AT4G16390	pentatricopeptide repeat-containing protein	9259175	TAC->TAA
AT4G16540	Heat shock protein HSP20/alpha crystallin family protein	9316755	TCA->TTA

Supplementary Table 6 (Continued).

Gene	Gene Description	Position	Substitution Type
AT4G16890	protein SUPPRESSOR OF npr1-1, CONSTITUTIVE 1	9500649	GCT->ACT
AT4G16915	hypothetical protein	9518334	AAC->CAC
AT4G16920	TIR-NBS-LRR class disease resistance protein	9520197	AGA->ACA
AT4G16960	TIR-NBS-LRR class disease resistance protein	9547773	TCG->ACG
AT4G16970	cell division control protein 7	9551527	AGC->TGC
AT4G18710	BIN2	10298784	CAT->CAA
AT4G18770	MYB98	10311432	ATT->ACT
AT4G19120	putative methyltransferase PMT21	10461280	AAT->AAG
AT4G19330	putative F-box/kelch-repeat protein	10558602	ACT->ATT
AT4G19570	chaperone DnaJ-domain containing protein	10665687	AAA->TAA
		10665964	AAT->ACT
AT4G20170	hypothetical protein	10897967	TTG->TTC
AT4G20200	terpene cyclase, C1 domain-containing protein	10910292	GAG->GAC
AT4G20450	putative LRR receptor-like serine/threonine-protein kinase	11026864	GTA->GCA
AT4G21080	Dof zinc finger protein DOF4.5	11255144	ATT->GTT
AT4G21640	Subtilase family protein	11497528	GTT->GCT
AT4G21820	binding / calmodulin binding protein	11582448	TAA->AAA
AT4G22190	hypothetical protein	11743159	CAT->CTT
AT4G22320	hypothetical protein	11793657	AAT->AGT
AT4G22510	hypothetical protein	11856910	CGG->TGG
AT4G22517	bifunctional inhibitor/lipid-transfer protein/seed storage 2S albumin-like protein	11856910	TCT->TAT
AT4G23140	cysteine-rich receptor-like protein kinase 6	12121612	GAT->GAG

Supplementary Table 6 (Continued).

Gene	Gene Description	Position	Substitution Type
AT4G23140.1		12122187	CAC->CCC
AT4G23300.1	cysteine-rich receptor-like protein kinase 22	12182631	AGT->AGA
AT4G24890.1	purple acid phosphatase 24	12812160	GTA->GCA
AT4G25515.1	protein SEUSS-like 3	13028624	CAG->AAG
AT4G25850.1	OSBP(oxysterol binding protein)-related protein 4B	13145384	TGT->TGA
AT4G25860.1	OSBP(oxysterol binding protein)-related protein 4A	13149227	GAC->GAG
AT4G25960.1	P-glycoprotein 2	13177533	TTA->TTT
AT4G26090.1	disease resistance protein RPS2	13226035	TTC->TTA
AT4G26600.1	S-adenosyl-L-methionine-dependent methyltransferase-like protein	13419906	ATG->AGG
AT4G26730.1	S-adenosyl-L-methionine-dependent methyltransferase-like protein	13473062	GCT->GTT
AT4G28150.1	hypothetical protein	13978896	GGG->GAG
		13978896	GGG->GAG
AT4G28860.1	protein casein kinase I-like 4	14246918	TCA->TCC
		14246918	TCA->TCC
AT4G29360.1	glucan endo-1,3-beta-glucosidase 12	14452188	TAC->TGC
		14452188	TAC->TGC

Supplementary Table 7. Prediction of *fel9* SNPs.

Gene	Gene Description	Position	Substitution Type
AT3G51640.2	hypothetical protein	19156857	AAG->AAC
AT3G51650.1	hypothetical protein	19159879	GGT->GAT
AT3G51650.1		19162200	ACT->AGT
AT3G52950.1	hypothetical protein	19635806	CAG->CTG
AT3G54100.1	O-fucosyltransferase family protein	20036209	TCC->TAC
AT3G54310.1	hypothetical protein	20112601	ACG->ATG
AT3G55160.1	hypothetical protein	20451558	TGT->TGG
		20452165	
AT3G55254.1	self-incompatibility S1 family protein	20482577	
AT3G55940.1	phosphoinositide phospholipase C 7	20748994	GAT->GGT
		20749014	GAT->TAT
AT3G56860.1	UBP1-associated protein 2A	21051562	GGA->TGA
		21051562	GGA->TGA
		21051562	GGA->TGA
AT3G59180.1	RNI-like/FBD-like domain-containing protein	21882233	TTC->TAC
AT3G59340.1	hypothetical protein	21930175	AGT->ATT
AT3G59455.1	bifunctional inhibitor/lipid-transfer protein/seed storage 2S albumin-like protein	21976891	TGG->CGG
AT3G59550.1	Sister chromatid cohesion 1 protein 3	21999016	ACA->CCA
AT3G61035.1	Cytochrome P450 superfamily protein	22593274	CGT->CAT
		22593284	CGA->TGA
AT3G61520.1	pentatricopeptide repeat-containing protein	22771243	CGG->CAG
AT3G61660.1	hypothetical protein	22816524	GGT->AGT
AT3G63150.1	MIRO-related GTP-ase 2	23331682	CCA->CAA

Supplementary Table 7 (Continued).

Gene	Gene Description	Position	Substitution Type
AT4G14140.1	DNA methyltransferase 2	8150199	AAT->AAG
AT4G14390.1	ankyrin repeat-containing protein	8290830	GGT->GAT
AT4G14940.1	amine oxidase 1	8543534	GAT->GAG
AT4G15050.1	hypothetical protein	8589751	TAT->CAT
AT4G15320.1	cellulose synthase-like protein B6	8744517	TAT->TGT
AT4G15690.1	monothiol glutaredoxin-S5	8934611	TTT->TTA
AT4G15980.1	pectinesterase 43	9058024	GCC->ACC
AT4G16162.3	Leucine-rich repeat (LRR) family protein	9161511	TGC->TCC
AT4G16280.1	RNA binding / abscisic acid binding protein	9207807	CAG->CAT
AT4G16807.1	hypothetical protein	9458292	TTT->GTT
AT4G16845.2	polycomb group protein VERNALIZATION 2	9478206	TGT->TGA
AT4G16850.1	hypothetical protein	9481597	TCT->TGT
AT4G16860.1	TIR-NBS-LRR class disease resistance protein	9491822	AAT->GAT
AT4G16890.1	SNC1	9500538	ATT->GTT
		9501598	CAA->GAA
AT4G16920.1	TIR-NBS-LRR class disease resistance protein	9521794	TTG->TTC
		9521972	GTG->GAG
AT4G16940.1	TIR-NBS-LRR class disease resistance protein	9534428	TGC->AGC
AT4G16960.1	TIR-NBS-LRR class disease resistance protein	9547951	ATG->ATC
		9548105	ATA->ACA
AT4G17680.1	SBP (S-ribonuclease binding protein) family protein	9843682	CCG->TCG
AT4G19120.1	putative methyltransferase PMT21	10461288	TCT->ACT
AT4G19240.1	hypothetical protein	10528314	TGG->TCG
		10528576	GAC->AAC
AT4G19380.1	Long-chain-alcohol oxidase FAO4A	10569067	GAA->GTA
AT4G19460.1	UDP-glycosyltransferase-like protein	10611972	CCC->TCC
AT4G19490.1		10618163	ATA->ATT

Supplementary Table 7 (Continued).

Gene	Gene Description	Position	Substitution Type
		10618163	CTG->CTT
AT4G19512.1	hypothetical protein	10639601	ACT->TCT
AT4G19700.1	SBP (S-ribonuclease binding protein) family protein	10713762	TGT->TGA
AT4G19760.1	Glycosyl hydrolase family protein with chitinase insertion domain	10750706	AGC->ATC
AT4G20200.1	terpene cyclase, C1 domain-containing protein	10910124	GAG->GAC
		10910553	CAC->TAC
		10910617	GAT->GAG
AT4G20340.1	Transcription factor TFIIIE, alpha subunit	10987336	TAC->TCC
AT4G20850.1	tripeptidyl peptidase ii	11161315	AGC->AAC
AT4G21100.1	DNA damage-binding protein 1b	11259791	TGG->GGG
AT4G21400.1	cysteine-rich receptor-like protein kinase 28	11400484	GGT->CGT
		11400687	GTA->GGA
AT4G22120.1	early-responsive to dehydration stress-related protein	11716205	CTC->CGC
		11716205	AAC->AGC
		11716205	AAA->AGA
		11716205	TTC->TGC
		11716205	GCA->GGA
		11716228	AGC->AGA
AT4G22280.1	F-box protein	11777181	TAT->AAT
		11777181	GGT->AGT
AT4G22285.1	ubiquitin carboxyl-terminal hydrolase-like protein	11781873	CAC->CGC
AT4G22410.1	ubiquitin carboxyl-terminal hydrolase-like protein	11818276	ATG->ATA
AT4G23060.1	protein IQ-domain 22	12087294	TTG->TTT

Supplementary Table7 (Continued).

Gene	Gene Description	Position	Substitution Type
AT4G23160.1	cysteine-rich receptor-like protein kinase 8	12133763	ACT->GCT
AT4G23170.1	putative cysteine-rich receptor-like protein kinase 9	12135298	CGA->GGA
		12172974	AAG->AAT
		12173069	GAC->GTC
		12208077	CAA->GAA
AT4G24710.1	P-loop containing nucleoside triphosphate hydrolase-like protein	12748941	GCT->ACT
AT4G25515.1	protein SEUSS-like 3	13028436	CTG->CCG
AT4G25860.1	OSBP(oxysterol binding protein)-related protein 4A	13148832	GGT->AGT
		13148972	TGA->TGT
AT4G26440.1	putative WRKY transcription factor 34	13358969	CGG->CAG
AT4G27360.1	dynein light chain type 1-like protein	13694491	TGC->CGC
AT4G27560.1	UDP-glycosyltransferase-like protein	13760338	TGT->AGT
AT4G27830.1	beta glucosidase 10	13863011	AGT->AAT
AT4G28860.1	protein casein kinase I-like 4	14246966	TGG->TGT
		14246966	TGG->TGT
AT4G28890.1	E3 ubiquitin-protein ligase ATL42	14256445	GAT->AAT

Appendix B – Figure and table lists

List of figures

Figure 1. Membrane compartment and membrane trafficking in plant cells. Secretory.	4
Figure 2. Schematic diagram depicting putative vesicle dynamics at the plant–fungal/ oomycetes interaction site.....	8
Figure 3. The cytoplasm and the nucleus are detected at the haustorium.	27
Figure 4. PM proteins selectively label the <i>Hpa</i> EHM.....	29
Figure 5. Secretory vesicles localize around the <i>Hpa</i> haustoria.	31
Figure 6. Endosomal compartments localize around the <i>Hpa</i> haustoria.	33
Figure 7. MVBs move bi-directional and recycling occurs in the <i>Hpa</i> infected cells.	34
Figure 8. The vacuole envelopes the <i>Hpa</i> haustoria.....	35
Figure 9. The cytoplasm and the nucleus are detected at the encasement.....	36
Figure 10. The PM proteins constitute the encasement..	37
Figure 11. Secretory proteins surround the <i>Hpa</i> encasement.	38
Figure 12. Early endosomal proteins are detected at the <i>Hpa</i> encasement..	38
Figure 13. Proteins marking LEs label the <i>Hpa</i> encasement.....	39
Figure 14. The vacuole envelopes the encased haustoria.	40
Figure 15. Quantification of GFP-2xFYVE compartments <i>fel</i> mutants (M_3).....	42
Figure 16. Detection of GFP-2xFYVE compartments in leaf epidermal tissues.	43
Figure 17. Comparison of GFP-2xFYVE compartments in leaf epidermal tissues.	45
Figure 18. Subcellular phenotypes of <i>Ler</i> /GFP-2xFYVE, M_3 of <i>fel2</i> and M_3 of <i>fel9</i>	46
Figure 19. Transcript levels of GFP in <i>Ler</i> /GFP-2xFYVE, M_3 of <i>fel2</i> and M_3 of <i>fel9</i>	48
Figure 20. Quantification of YFP-2xFYVE and GFP-2xFYVE compartments in reference lines.	49
Figure 21. Transcript levels of GFP and YFP in <i>Ler</i> /GFP-2xFYVE and <i>Col-0</i> /YFP-2xFYVE.....	50
Figure 22. Detection of GFP-2xFYVE compartments in the F_1 <i>fel</i> mutants backcrossed to <i>Ler</i> /GFP-2xFYVE..	52
Figure 23. Detection of GFP-2xFYVE compartments in the F_2 of <i>fel</i> mutants backcrossed to <i>Ler</i> /GFP-2FYVE.	54
Figure 24. Detection of GFP-2xFYVE compartments in the F_1 of <i>fel</i> mutants outcrossed to <i>Col-0</i> /YFP-2FYVE.	56
Figure 25. Detection of GFP-2xFYVE compartments in the F_2 of <i>fel</i> mutants outcrossed to <i>Col-0</i> /YFP-2FYVE.	58
Figure 26. Distribution pattern of average endosomal numbers of F_2 progenies of <i>fel2</i> and <i>fel9</i> outcrossed to <i>Col-0</i> /YFP-2xFYVE respectively.....	61
Figure 27. Detection of GFP-2xFYVE compartments in the F_3 of <i>fel2</i> and <i>fel9</i> outcrossed to <i>Col-0</i> /YFP-2FYVE.	64

Figure 28. Schematic diagram representing putative vesicle dynamics at the Arabidopsis– <i>Hpa</i> interface.....	72
---	----

List of tables

Table 1. Summary of marker lines used in investigation of Arabidopsis– <i>Hpa</i> interaction.....	26
Table 2. Classification of <i>fel</i> candidates in M ₂ plants and endosomal phenotype in M ₃ plants.	44
Table 3. Quantification of GFP-2xFYVE compartments in the F ₁ of <i>fel</i> mutants backcrossed to <i>Ler</i> /GFP-2xFYVE.....	52
Table 4. Quantification of GFP-2xFYVE compartments in the F ₂ of <i>fel</i> mutants crossed to <i>Ler</i> /GFP-2xFYVE.....	55
Table 5. Quantification of GFP-2xFYVE compartments in the F ₁ of <i>fel</i> mutants crossed to <i>Col-0</i> /YFP-2xFYVE.....	57
Table 6. Quantification of GFP/YFP-2xFYVE compartments in the F ₂ of <i>fel</i> mutants crossed to <i>Col-0</i> /YFP-2xFYVE.....	59
Table 7. Genetic mapping of <i>fel2</i> and <i>fel9</i> mutants.	62
Table 8. Whole genome sequencing of <i>Ler</i> /GFP-2xFYVE, <i>fel2</i> and <i>fel9</i>	63
Table 9. <i>In silico</i> prediction and validation of <i>fel2</i> SNPs.....	63
Table 10. Quantification of GFP-2xFYVE compartments in the F ₃ of <i>fel2</i> and <i>fel9</i> outcrossed to <i>Col-0</i> /YFP-2xFYVE.	65

List of supplementary figures

Supplementary Figure 1. Detection of GFP-2xFYVE compartments in the F ₂ of <i>fel</i> mutants outcrossed to <i>Col-0</i> /YFP-2xFYVE.	XV
Supplementary Figure 2. Detection of GFP-2xFYVE compartments in the F ₈ of <i>Ler</i> /GFP-2xFYVE crossed to <i>Ler</i>	XV

List of supplementary tables

Supplementary Table 1. Plant material presented in this study.	XVI
Supplementary Table 2. Oligonucleotides used in this study.	XVII
Supplementary Table 3. Quantification of GFP/YFP-2xFYVE compartments in the individual F ₁ progenies of <i>Ler</i> /GFP-2xFYVE crossed to <i>Col-0</i> /YFP-2xFYVE.	XIX
Supplementary Table 4. Quantification of GFP/YFP-2xFYVE compartments in individual F ₁	

progenies of <i>fel</i> mutants crossed to <i>Ler</i> /GFP-2xFYVE.....	XX
Supplementary Table 5. Quantification of GFP/YFP-2xFYVE compartments in individual F ₁ progenies of <i>fel</i> mutants crossed to <i>Col-0</i> /YFP-2xFYVE.....	XXI
Supplementary Table 6. Prediction of <i>fel2</i> SNPs.....	XXII
Supplementary Table 7. Prediction of <i>fel9</i> SNPs.....	XXV

ACKNOWLEDGEMENTS

I would like to thank my supervisors Dr. Silke Robatzek, Prof. Dr. Jane Parker, and Prof. Dr. Martin Hülskamp for giving me a chance to become a PhD student at MPIZ and patiently providing supervision.

I would also like to thank Prof. Dr. Paul Schulze-Lefert, Dr. Sophien Kamoun, and Dr. Richard O'Connell for giving me helpful advice.

I am sincerely grateful to Dr. Susanne Salomon, who started the *fel* mutant screen project. Also thanks to Heidrun Häweker for lots of technical supporting, and Dr. Dan MacLean for bioinformatic assistance.

I am grateful to everybody from the Robatzek group for daily support and friendship, especially Dr. Nicolas Frei dit Frey for guiding me to cell biology, Dr. Martina Beck, Gildas Bourdais, Dr Christine Faulkner, Rosa Lozano Duran, Dr. Malick Mbengue, Dr. Ji Zhou, and Dr. Thomas Spallek for providing suggestion and discussion to build up my thesis. Special thanks to Dr. Silke Robatzek, for sharing exciting scientific ideas and providing a nice environment to work on science.

I would also like to thank IMPRS for the financial support.

Finally, I would like to express my gratitude to my parents for their encouragement over the last three years: thank you for your consideration and endless support. I would like to express my deepest appreciation to my partner, P. P., without your help, patience, and encouragement, I could not go this far.

ERKLÄRUNG

„Ich versichere, dass ich die von mir vorgelegte Dissertation selbstständig angefertigt, die benutzten Quellen und Hilfsmittel vollständig angegeben und die Stellen der Arbeit – einschließlich Tabellen, Karten und Abbildungen –, die anderen Werken im Wortlaut oder dem Sinn nach entnommen sind, in jedem Einzelfall als Entlehnung kenntlich gemacht habe; dass diese Dissertation noch keiner anderen Fakultät oder Universität zur Prüfung vorgelegen hat; dass sie – abgesehen von den auf Seite II angegebenen Teilpublikationen – noch nicht veröffentlicht worden ist sowie, dass ich eine solche Veröffentlichung vor Abschluss des Promotionsverfahrens nicht vornehmen werde. Die Bestimmungen dieser Promotionsordnung sind mir bekannt. Die von mir vorgelegte Dissertation ist von Prof. Dr. Jane Parker betreut worden.“

LEBENS LAUF

Angaben zur Person

Name: Yi-Ju Lu

Anschrift: 5F, No.7, Aly. 12, Ln. 106, Baojian Rd., Zhongde Dist., New Taipei City
235, Taiwan (R.O.C.)

Telefon: +886-229416787

Geburtsdatum: 16.06.1981

Geburtsort: Taipei

Staatsangehörigkeit: Taiwanesisch

Familienstand: Ledig

Ausbildung

Seit 09/2008 **Promotionsstudium** an der Universität zu Köln am Max-Planck-
Institut für Züchtungsforschung, unter der Leitung von Prof. Dr. Jane
Parker.

01/2008 – 06/2008 **Wissenschaftlicher Mitarbeiter** in der Gruppe für integrative
Pflanzenstresse am Agricultural Biotechnology Research Center
(ABRC), Academia Sinica, Taiwan.

2004 – 2006 **Masterstudium** am Institut für Phytopathologie und Mikrobiologie an
der National Taiwan University, Taipei (Taiwan).

2000 – 2004 **Hochschulstudium** am Institut für Phytopathologie und Mikrobiologie
an der National Taiwan University, Taipei (Taiwan).

1996 – 1999 Zhong Shan Girls High School, Taipei (Taiwan).

Köln, February 2012

Yi-Ju Lu

